

# **DLR-IB-AS-BS-2019-120**

**An initial investigation of solving  
RANS equations in combination  
with two-equation turbulence  
models**

**Forschungsbericht**

Autor  
Stefan Langer



**DLR**

**Deutsches Zentrum  
für Luft- und Raumfahrt**



**DLR-IB-AS-BS-2019-120**

**An initial investigation of solving RANS equations in  
combination with two-equation turbulence models**

**Stefan Langer**

**Herausgeber:**

Deutsches Zentrum für Luft- und Raumfahrt e.V.  
Institut für Aerodynamik und Strömungstechnik  
Lilienthalplatz 7, 38108 Braunschweig

**ISSN 1614-7790**

Stufe der Zugänglichkeit: 1  
Braunschweig, im September 2019

Institutsdirektor:  
Prof. Dr.-Ing. habil. C.-C. Rossow

Verfasser:  
Priv.-Doz. Dr. habil. Stefan Langer

Abteilung: Center of Computer Applications in  
Aerospace Science and Engineering

Abteilungsleiter:  
Prof. Dr.-Ing. N. Kroll

Der Bericht enthält:  
119 Seiten  
56 Bilder  
11 Tabellen  
34 Literaturstellen



# Contents

<b>1</b>	<b>Introduction</b>	<b>3</b>
1.1	Requirements for numerical methods . . . . .	3
1.2	Two equation turbulence models . . . . .	6
<b>2</b>	<b>Governing equations of fluid flow</b>	<b>9</b>
2.1	RANS equations . . . . .	9
2.2	Nondimensionalization of governing equations . . . . .	12
<b>3</b>	<b><math>k\omega</math>-models</b>	<b>15</b>
3.1	Differential form of $k\omega$ -models . . . . .	16
3.1.1	Wilcox $k\omega$ -model of 1988 . . . . .	17
3.1.2	Wilcox $k\omega$ -model of 1998 . . . . .	17
3.1.3	Wilcox $k\omega$ -model of 2006 . . . . .	18
3.1.4	Menter Shear Stress Transport model (1992) . . . . .	19
3.1.5	Menter Shear Stress Transport model (2003) . . . . .	21
3.2	Simplifications of $k\omega$ -models . . . . .	22
3.3	Integral form of $k\omega$ -models . . . . .	24
3.4	Boundary conditions and boundary value problem . . . . .	26
3.4.1	Boundary value problem . . . . .	26
3.4.2	No-slip wall boundary condition . . . . .	27
3.4.3	Farfield boundary condition . . . . .	31
3.5	Nondimensionalization of turbulence flow equations . . . . .	34
3.6	Logarithmic reformulation of $k\omega$ -models . . . . .	39
3.6.1	$\ln(k)$ - and $\ln(\omega)$ -formulation . . . . .	40
3.6.2	Equivalence to original $k\omega$ -models . . . . .	42
3.7	Discussion of SST blending function . . . . .	46
<b>4</b>	<b>Differences of models: Menter-SST vs. Wilcox 2006</b>	<b>49</b>
4.1	Difference in eddy viscosity . . . . .	50
4.2	Production term of $\omega$ -equation . . . . .	54
4.3	Diffusion source term . . . . .	56
4.4	Weighting of viscous flux terms . . . . .	59
4.5	Strain rate and vorticity . . . . .	59

4.6	Summary of differences . . . . .	60
<b>5</b>	<b>Discretization strategy and solution algorithm</b>	<b>67</b>
5.1	Discretization . . . . .	67
5.2	Multistage implicit Runge-Kutta smoother . . . . .	69
5.3	Construction of preconditioner . . . . .	72
5.4	Solving linear systems and truncation criteria . . . . .	73
5.5	Positivity of $k$ and $\omega$ . . . . .	73
<b>6</b>	<b>Numerical examples</b>	<b>77</b>
6.1	RAE 2822 Airfoil . . . . .	78
	6.1.1 Necessity of production limiter . . . . .	80
6.2	NACA 4412 airfoil flow . . . . .	85
	6.2.1 Motivation for NACA 4412 airfoil flow . . . . .	87
	6.2.2 Discussion of results for NACA 4412 airfoil flow . . . . .	91
6.3	Transonic turbulent flow over a common research model . . . . .	106
<b>7</b>	<b>Conclusion and Discussion</b>	<b>109</b>
7.1	Discussion of solution algorithm . . . . .	109
7.2	Discussion of accuracy . . . . .	110
7.3	Boundary value problems . . . . .	112

# Chapter 1

## Introduction

Turbulence modeling is applied in physical applications to represent the effects of turbulence. In the field of **C**omputational **F**luid **D**ynamics (CFD), the origin of modern turbulence theory goes back to Kolmogorov [13, 14]. He introduced the concepts of scale similarity and of a universal inertial cascade. Nevertheless, also before Kolmogorov the description of turbulence was already a subject. It was known for a long time that fluids do not flow smoothly at large scales. This fundamental observation became aware of rivers and clouds. The first quantitative observations of turbulence had been made in the middle of the nineteenth century.

The state of the art turbulence models use either algebraic relations or systems of differential or integral equations to describe mathematically the appearance and dissipation of turbulence in high Reynolds number turbulent flows. In general these turbulence models are used in combination with the **R**eynolds **A**veraged **N**avier-**S**tokes (RANS) equations. Then these turbulence models deliver further parameters required to close the system of equations. Considering Boussinesq' eddy viscosity assumption in which the Reynolds stress tensor is proportional to the mean strain rate tensor, a parameter or function generally called eddy viscosity  $\mu_t$  needs to be determined. Not considering Boussinesq' eddy viscosity assumption a determination of all Reynolds' stresses is necessary.

### 1.1 Requirements for numerical methods

It is ongoing research in the field of computational fluid dynamics to assess data obtained by approximate solutions of RANS equations in combination with some turbulence model. Resilient conclusions about uncertainties and errors of computed numerical data are in general impossible. On the other hand, such assertions are an obvious requirement to use data obtained by numerical simulations in aerodynamic certification process. In case one really wants to plan new aircraft using numerical data, this data must be proven to be trustable.

In particular, trustable data must be given not only for the design point of an aircraft, but also for all edges of the full flight envelope, that is for complex turbulent flows. Typical examples are aircraft at high angle of attack where massively three-dimensional separated flows are observed. Such flows are dominated by compressible and incompressible effects, they show multiple length-scales and are unsteady. To correctly predict such flows the system of RANS equations needs to comprise and resolve at least all dominating turbulent effects. Therefore a turbulence model must be in a position to not only resolve attached boundary layer flow but also, for example, regions with adverse pressure gradient effects and other effects. Roughly speaking, the data required for certification process should be sufficiently accurate together with an assessment of the error.

**Definition 1.1.1** *A numerical method providing both sufficiently accurate data together with a known, assignable bound on the error is called reliable.*

To evaluate the formulation and the accuracy of data obtained by approximate solutions of the RANS equations is not an easy task. From our perspective the following four points are a minimum standard one has to consider:

- a) The full differential or integral formulation of the equations together with the turbulence model equations,
- b) its exact implementation,
- c) a solution algorithm which is able to compute for a given number of degrees of freedom a machine accurate solution and
- d) mesh converged results.

As soon as one of these criteria is not satisfied, certain doubts about the assertions made about the data arise. Unfortunately, throughout the literature about computational fluid dynamics implementation details are often hidden and convincing arguments about convergence are also often missing. In particular, information about the actual formulation of boundary conditions as well as the possible impact of certain limitations of variables to stabilize the solution process is often hidden. Even when all these criteria are satisfied and there is full evidence about the implementation, a strict conclusion about the accuracy of computed results is hard to obtain. Typical validation measures are the comparison with experimental data, which come from a process, which is inaccurate. Moreover, it is generally impossible to replicate the actual experiment one-to-one in a numerical simulation. This introduces a further source of uncertainties.

For example, not only the obvious experimental data such as geometry, velocity of the fluid and angle of attack need to be considered, but also the whole geometry of wind tunnel, possible deformation of geometry and many other effects need to

be incorporated into the numerical setup [15]. The inclusion of such effects may improve accuracy of computed results. More generally, one can say that the main interest is to find the major drivers for errors, to separate the error components from one another and to have a quantitative assertion about each error component. Roughly speaking, the overall objective is to establish a reliable numerical method.

From the four criteria mentioned above, obviously the first two criteria are the simplest to satisfy. Straightforwardly, one simply has to write down the actual implementation of the equations. Nothing should be hidden such as cut-off values for certain variables. On the other hand, though often not mentioned, a lot of implementations use certain strategies to cut-off or to restrict several of the variables. Often, a final solution is not scanned with respect to activity of such limitation processes. But such transparency of solutions is required to assess the data. Since often authors do not discuss or do not even mention these intrusions into the equation, only conjectures about the reasons can be made. One conjecture of relevance is that c) mentioned above is not independent of b). The design of a robust solution method to approximately solve the RANS equations is not straightforward. This assertion is in particular true if the solution process needs to satisfy that

- it works for a large variety of parameters defining the boundary value problem to solve, such as
  - a variety of geometries,
  - a large number of inflow conditions, which includes a range from very low Mach number to hypersonic flows,
  - a broad range of Reynolds numbers,
  - a large number of different boundary conditions,
- it works for a broad range of parameters determining the actual solution method, such as
  - variation in CFL number,
  - inner linear solution methods,
  - linear and nonlinear multigrid as well as cycling strategies
- it always converges to steady-state solution, if a steady state solution exists,
- it does not show significant loss in convergence rates with systematic mesh refinement studies, i.e., an increase in the number of degrees of freedom are considered.

These conditions might be viewed minimum for a method such that it can be used on routine basis in industrial processes. Since up to now the design of a solution method for the RANS equations satisfying all these conditions is an open problem,

it can be assumed that various interventions into several solution methods have been incorporated to be in a position to compute steady-state solutions, at least for a small number of problems with a specific choice of parameters.

## 1.2 Two equation turbulence models

Over the last several years some progress has been made for the RANS equations in combination with a one-equation Spalart-Allmaras turbulence model [25, 1]. It can be shown that at least for a variety of flow cases machine accurate solutions can be obtained. On the other hand, it is often argued that the one-equation turbulence model is applicable for attached smooth flow, but it is not suited for flows with adverse pressure gradient and flows with massive separation. Throughout the literature there does not exist a profound argument supporting this hypothesis. Data obtained with such turbulence model can only be investigated case dependent and compared with noisy measurements. General assertions about the possible range of applications of a turbulence model should be expressed with care.

Due to possible shortcomings of algebraic and one-equation turbulence models, an important example representing an algebraic turbulence model is the one of Baldwin and Lomax [2], two equation turbulence models are established and widely used in the world of computational fluid dynamics. The two differential or integral equations describe quantities for the turbulence kinetic energy and the length scale or dissipation rate. There exist many variants of these models.

A rather complete overview of the number of possible models as well as their relationship can be found in the report by Bredberg [5]. In general, they can be classified in the  $k\varepsilon$ -type and  $k\omega$ -type models. The dimensional transport variables  $k = k(x, t)$ ,  $\varepsilon = \varepsilon(x, t)$  and  $\omega = \omega(x, t)$  resp. describe the turbulence kinetic energy and the rate of dissipation of the turbulence kinetic energy. Given the functions  $k$ ,  $\varepsilon$  and  $\omega$  resp. the required eddy viscosity is then computed either, for example, by

$$\mu_t = C_\mu \rho \frac{k^2}{\varepsilon}, \quad C_\mu := \frac{9}{100},$$

or

$$\mu_t = \rho \frac{k}{\omega}. \tag{1.1}$$

Early two equation models rely on the work of Rodi and Spalding [23] and Jones and Launder [11]. Another established two equation model is Menter's Shear-Stress Transport (SST) model [18, 21]. It combines  $k\varepsilon$ -type and  $k\omega$ -type models using an intermediate function such that it behaves in the neighborhood of a no-slip wall like a  $k\omega$ -type and in the region far away from the wall like a  $k\varepsilon$ -type model. Also, for the original  $k\omega$ -type model of Wilcox published in 1988 [31] there has been an update in 2008 [34] where several additional source terms have been introduced.

Besides this general classifications two equation type models possibly differ in their actual formulation. For example:

- a) One finds in the literature that the production term in the equation for the turbulence kinetic energy may be formulated using the strain rate or the vorticity.
- b) Often one finds that the production term in the equation for the turbulence kinetic energy is limited with respect to the destruction term.
- c) Several limitation techniques directly related to the variables  $k$  and  $\omega$  are established.
- d) Limitations of the resulting eddy viscosity can be found.
- e) Boundary conditions are often not described or different.
- f) Parameter choices are different.

With respect to all the variations that can be found, to the author's opinion it can be assumed that there do not exist two computer codes implementing the same two equation turbulence models. And the reason for all these variations is an interesting question on its own.

One answer possibly is that within the context of the compressible RANS equations in combination with a two equation model a robust approximation of a steady state solution is not straightforward. However, being aware of the fact that physical modeling of turbulence is an ongoing task in the field of computational fluid dynamics and that the number of possible two equation models which have been published is large, within this article we follow the approach to present some well established and frequently used two equation models. These are

- a) The original  $k\omega$ -model of Wilcox published in 1988 [31].
- b) Menter's Shear-Stress Transport (SST) model [18, 21].
- c)  $k\omega$ -model of Wilcox of 2006 [33, 34].

Based upon these models this article has three principal objectives:

- a) It is the first goal to face the challenge for identifying possible numerical issues for approximately solving the RANS equations in combination with a two equation model.
- b) It is the second goal to understand possible differences and similarities in the models and their impact on solutions.

- c) It is the third goal to give a complete picture of the corresponding boundary value problems.

It turned out that when one tries to find a reliable way for solving transport equations including turbulence models, a thorough understanding of these equations is necessary. One cannot assume that one can withdraw to the pure implementation of these equations into a code and make it work. The complexity of these equations seems to be so large and the understanding so little that basic work is required to make such models run. In particular this holds true if one needs to be in a position where these equations need to be solved in general and not only for some basic test cases. To emphasize this again, the objective is to develop methods which can be used on routine basis in industrial processes.

The present report is structured as follows. In Chapter 2 we shortly present the governing equations of fluid flow. Chapter 3 is dedicated to the presentation of two equation turbulence models, together with a discussion of the boundary conditions and reformulations. A comparison on an analytic level of two equation turbulence models is given in Chapter 4, and Chapter 5 deals with the topic of a numerical realization. Selected test cases and applicability are presented in Chapter 6. This report closes with a final discussion in Chapter 7.

# Chapter 2

## Governing equations of fluid flow

We shortly present the governing equations of fluid flow which are in our interest.

### 2.1 RANS equations

To describe flow effects we consider for the domain  $D \subset \mathbb{R}^m$ ,  $m = 2, 3$ , i.e., an open and connected set, and an interval  $[0, T) \subset \mathbb{R}$ ,  $T > 0$ , the RANS equations in conservative form. These are a system of non-linear conservation laws which results naturally from the fundamental laws of conservation of mass, momentum and energy. The dimensional form of the governing equations can be expressed in integral form by

$$0 = \frac{d}{dt} V_D(W)(t) + R_{\partial D}(W)(t), \quad t \in (0, T), \quad (2.1a)$$

where the integral operators  $V_D$  and  $R_{\partial D}$  are given by

$$V_D(W)(t) := \int_D W(x, t) dx \quad (2.1b)$$

$$R_{c, \partial D}(W)(t) := \int_{\partial D} \langle f_c(W(y, t)), n(y) \rangle ds(y), \quad (2.1c)$$

$$R_{v, \partial D}(W)(t) := \int_{\partial D} \langle f_v(W(y, t)), n(y) \rangle ds(y), \quad (2.1d)$$

$$R_{\partial D} := R_{c, \partial D} - R_{v, \partial D}, \quad (2.1e)$$

and  $W : D \times [0, T) \rightarrow \mathbb{R}^{m+2}$ ,

$$W(x, t) := (\rho(x, t), \rho(x, t)u(x, t), \rho(x, t)E(x, t))^T,$$

denotes the vector field of conserved variables and  $n$  is the unit outward normal on  $\partial D$ . The terms  $f_c$  and  $f_v$  describe the convective and viscous contribution

$$f_c(W) := \begin{pmatrix} \rho u \\ \rho u_1 u + p e_1 \\ \vdots \\ \rho u_m u + p e_m \\ \rho H u \end{pmatrix}, \quad f_v(W) := \begin{pmatrix} 0 \\ \tau_1(W) \\ \vdots \\ \tau_m(W) \\ \theta(W) \end{pmatrix}, \quad m = 2, 3.$$

The expression

$$\langle x, y \rangle := \sum_{j=1}^m x_j y_j, \quad x, y \in \mathbb{R}^m,$$

denotes the standard  $l^2$  scalar product in  $\mathbb{R}^m$ . The dimensional quantities  $\rho$ ,  $u = (u_1, \dots, u_m)^T$ ,  $E$  and

$$H := E + p/\rho \quad (2.2)$$

are the density, velocity, the specific total energy, and the enthalpy of the fluid. The equation of state

$$p(W(x, t)) := (\gamma - 1)\rho(x, t) \left( E(x, t) - \frac{\|u(x, t)\|_2^2}{2} \right) \quad (2.3)$$

defines the pressure  $p$ , and  $\gamma$  is the gas dependent ratio of specific heats, which is given by 1.4 for air. Assuming that an effective viscosity

$$\mu_{\text{eff}} := \mu_{\text{eff}}(W) = \mu_{\text{eff}}(W(x, t))$$

is given and, using Stoke's hypothesis, that the bulk viscosity satisfies  $\lambda = -2/3\mu_{\text{eff}}$ , the viscous stress tensor  $\tau = \tau(W) = \tau(W(x, t))$  is given by

$$\tau(W) := \mu_{\text{eff}} \mathcal{S} + \lambda \operatorname{div}(u) \operatorname{Id} = 2\mu_{\text{eff}} \left( \mathcal{S} - \frac{1}{3} \operatorname{div}(u) \operatorname{Id} \right) = 2\mu_{\text{eff}} \bar{\mathcal{S}}, \quad (2.4)$$

$$\bar{\mathcal{S}} := \mathcal{S} - \frac{1}{3} \operatorname{div}(u) \operatorname{Id}, \quad (2.5)$$

and  $\mathcal{S}$  denotes the strain rate, which is given by the symmetric part of the total derivative of flow velocity  $u$ ,

$$\mathcal{S} := \frac{1}{2} \left( \frac{du}{dx} + \left( \frac{du}{dx} \right)^T \right), \quad \text{i.e.} \quad \mathcal{S}_{ij} = \frac{1}{2} \left( \frac{\partial u_i}{\partial x_j} + \frac{\partial u_j}{\partial x_i} \right). \quad (2.6)$$

Hence,  $\tau$  is symmetric and can be explicitly expressed by

$$\begin{aligned} \tau_{ii}(W) &= 2\mu_{\text{eff}} \frac{\partial u_i}{\partial x_i} + \lambda \operatorname{div}(u) = \frac{2}{3}\mu_{\text{eff}} \left( 2\frac{\partial u_i}{\partial x_i} - \sum_{j=1, j \neq i}^m \frac{\partial u_j}{\partial x_j} \right), \quad i = 1, \dots, m, \\ \tau_{ij}(W) &= 2\mu_{\text{eff}} \mathcal{S}_{ij} = \mu_{\text{eff}} \left( \frac{\partial u_i}{\partial x_j} + \frac{\partial u_j}{\partial x_i} \right), \quad \tau_{ji} = \tau_{ij}, \quad 1 \leq i < j \leq m. \end{aligned}$$

The missing viscous flux term for the energy equation is given by

$$\theta(W) := \tau(W)u + q(W), \quad (2.7a)$$

$$q(W) := \kappa_{\text{eff}} \text{grad } T. \quad (2.7b)$$

The effective viscosity  $\mu_{\text{eff}}$  and effective conductivity  $\kappa_{\text{eff}}$  are computed by

$$\mu_{\text{eff}} := \mu_l + \mu_t, \quad \kappa_{\text{eff}} := \kappa_l + \kappa_t, \quad (2.8)$$

and the laminar viscosity is given by Sutherland's law

$$\mu_l(W) := \mu_{l,\infty} \left( \frac{T}{T_\infty} \right)^{3/2} \frac{T_\infty + \bar{T}}{T + \bar{T}}, \quad \mu_{l,\infty} := \frac{\rho_\infty u_\infty L}{Re}, \quad (2.9)$$

$$\kappa_l(W) := \frac{c_p \mu_l(W)}{Pr_l} \quad \text{and} \quad c_p := \Re \frac{\gamma}{\gamma - 1}, \quad (2.10)$$

whereby  $\rho_\infty > 0$  and  $u_\infty > 0$  denote some constant reference density and velocity,  $L > 0$  is some constant reference length scale,  $Re > 0$  is the corresponding Reynolds number,

$$\bar{T} := 110.4K \quad (2.11)$$

is Sutherland's constant,  $\Re$  is the universal gas constant and the laminar Prandtl number is given by  $Pr_l := 0.72$ .

In this report we restrict ourselves to linear turbulence models represented by differential or integral equations. The solutions of these equations reveal additional quantities in the considered fluid. These occurring variables extend the degrees of freedom given by the conservative variables  $W$  by a further unknown function

$$W_t : D \times [0, T) \rightarrow \mathbb{R}^{N_t}.$$

Here  $N_t \in \mathbb{N}$  depends on the turbulence model. In this report we have

$$\begin{aligned} N_t &= 1 && \text{for the Spalart-Allmaras model,} \\ N_t &= 2 && \text{for the Wilcox } k\omega\text{-model and the SST-model.} \end{aligned}$$

Since we mainly deal with two equation turbulence models, throughout this whole report one can assume  $N_t = 2$ . The Spalart-Allmaras model is mentioned here for completeness and since results used for comparisons are presented in Chapter 6. Note, when for example using an algebraic model  $N_t = 0$  and no additional unknowns need to be considered.

The additional variables required for the turbulence model are then used to determine the eddy viscosity,

$$\mu_t = \mu_t(W_t(x, t), W(x, t)) \geq 0 \quad \text{for all } (x, t) \in D \times [0, T),$$

which is required for (2.8). Given the eddy viscosity  $\mu_t$  the turbulent thermal conductivity is described by the algebraic relation

$$\kappa_t := c_p \frac{\mu_t}{Pr_t}, \quad Pr_t := 0.92. \quad (2.12)$$

Formula (2.12) is also required for (2.8). The determination of  $\mu_t$  closes the system of the Reynolds averaged Navier-Stokes equations (2.1a).

## 2.2 Nondimensionalization of governing equations

Throughout this section we denote dimensional variables using the sign  $\hat{\cdot}$ , for example dimensional density is denoted by  $\hat{\rho}$ .

In the code environment we use the governing equations (2.1) are implemented in nondimensional form. Given reference states with dimensions  $\rho_{\text{ref}}, p_{\text{ref}}, T_{\text{ref}}$ , and using relations

$$\Re_{\text{ref}} = \frac{p_{\text{ref}}}{\rho_{\text{ref}} T_{\text{ref}}} \quad \text{and} \quad u_{\text{ref}} = \sqrt{T_{\text{ref}} \Re_{\text{ref}}} = \sqrt{\frac{p_{\text{ref}}}{\rho_{\text{ref}}}}. \quad (2.13)$$

non-dimensionalized variables, free stream values, and additionally the length scale and time may be obtained by

$$\begin{aligned} \rho &:= \hat{\rho} / \rho_{\text{ref}}, & \rho_{\infty} &:= \hat{\rho}_{\infty} / \rho_{\text{ref}}, \\ p &:= \hat{p} / p_{\text{ref}}, & p_{\infty} &:= \hat{p}_{\infty} / p_{\text{ref}}, \\ T &:= \hat{T} / T_{\text{ref}}, & T_{\infty} &:= \hat{T}_{\infty} / T_{\text{ref}}, \\ L &:= \hat{L} / L_{\text{ref}}, & t &:= L / u. \end{aligned} \quad (2.14a)$$

For simplicity we choose  $\rho_{\text{ref}} = \hat{\rho}_{\infty}$ ,  $p_{\text{ref}} = \hat{p}_{\infty}$ , and  $T_{\text{ref}} = \hat{T}_{\infty}$ . Due to this choice the reference kinematic and laminar viscosity are given by

$$\nu_{l,\text{ref}} = u_{\text{ref}} L_{\text{ref}}, \quad \mu_{l,\text{ref}} = \rho_{\text{ref}} \nu_{l,\text{ref}}. \quad (2.15)$$

As a consequence, we obtain the following normalized nondimensionalized relations

$$\rho_{\infty} = 1, \quad p_{\infty} = 1, \quad T_{\infty} = 1, \quad \Re = 1, \quad (2.16a)$$

$$u_{\infty} = \frac{\hat{u}_{\infty}}{\sqrt{\frac{p_{\text{ref}}}{\rho_{\text{ref}}}}} = \frac{M_{\infty} \hat{a}_{\infty}}{\sqrt{\frac{p_{\text{ref}}}{\rho_{\text{ref}}}}} = \frac{M_{\infty} \sqrt{\gamma \frac{\hat{p}_{\infty}}{\hat{\rho}_{\infty}}}}{\sqrt{\frac{p_{\text{ref}}}{\rho_{\text{ref}}}}} = M_{\infty} \sqrt{\gamma}, \quad (2.16b)$$

$$\begin{aligned} a_{\infty} &= \sqrt{\frac{\gamma p_{\infty}}{\rho_{\infty}}} = \sqrt{\gamma}, \\ \mu_{l,\infty} &= \frac{\rho_{\infty} u_{\infty} L}{Re} = \frac{\sqrt{\gamma} M_{\infty} L}{Re}. \end{aligned} \quad (2.16c)$$

To this end Sutherland's law (2.9) in its nondimensionalized version is implemented by

$$\mu_l = \frac{\sqrt{\gamma} M_\infty L}{Re} \left( \frac{\hat{T}}{T_{\text{ref}}} \right)^{3/2} \left( \frac{\frac{\hat{T}_\infty}{T_{\text{ref}}} + \frac{\hat{T}}{T_{\text{ref}}}}{\frac{\hat{T}}{T_{\text{ref}}} + \frac{\hat{T}}{T_{\text{ref}}}} \right) = \frac{\sqrt{\gamma} M_\infty L}{Re} \Gamma(T), \quad (2.17a)$$

$$\Gamma(T) := T^{3/2} \left( \frac{1 + C_{\text{suth}}}{T + C_{\text{suth}}} \right), \quad C_{\text{suth}} := \frac{\hat{T}}{T_{\text{ref}}}. \quad (2.17b)$$



# Chapter 3

## $k\omega$ -models

In this section we describe the two families of two-equation  $k\omega$ -models, which are often used for aerodynamic applications:

- a) A family of models originally introduced by Wilcox 1988:
  - 1) The original model version of 1988
  - 2) A modified version of 1998
  - 3) A modified version from 2006
- a) A family of models introduced by Menter 1992:
  - 1) The original model version of 1992
  - 2) A modified version from 2003

Throughout the literature these models are most often stated and formulated in differential and compressible form. To formulate these models two variables  $(\rho k, \rho\omega)$  are introduced.

In finite-volume and finite-element codes these equations are often used and implemented in their incompressible, which is derived and discussed below in Section 3.3. In this form, instead of solving for  $(\rho k, \rho\omega)$  one directly solves for  $(k, \omega)$ . Discretization of these equations may depend on the underlying data structure. Computer codes restricted to purely structured meshes, where directions of interest can be used, one finds that directly the differential form of the equations is exploited. In computer codes based on hybrid meshing strategies this is in general not possible. Here discretization is based on the integral form of the equations.

Both,

$$k = k(x, t) > 0 \quad \text{and} \quad \omega = \omega(x, t) > 0 \quad \text{for all } (x, t) \in D \times (0, T) \quad (3.1)$$

describe positive functions, namely  $k$  the turbulence kinetic energy per unit mass and  $\omega$  the dissipation rate of turbulence kinetic energy. It has become popular

to include this assumption about positivity directly into the formulation of the equations considering variable substitution. Several authors (see e.g. [10, 4]) use for example substitution for  $\omega$ ,

$$\omega = e^\Omega, \quad \text{that is} \quad \Omega = \ln(\omega).$$

Instead of solving for  $\omega$  one now tries to approximate  $\Omega$ . Originally, also  $k$  was substituted by

$$k = e^\mathcal{K}, \quad \text{that is} \quad \ln(k) = \mathcal{K},$$

and one solves for  $\mathcal{K}$ . Such substitutions are discussed more detailed in Section 3.6. Both substitutions assume that  $k$  and  $\omega$  are nondimensional variables. Nondimensionalization of the equations is described in Section 3.5.

Before we state the two transport equations for  $k$  and  $\omega$ , we define using the strain rate tensor  $\mathcal{S}$  and  $\overline{\mathcal{S}}$  given in (2.6) and (2.5) the mean-molecular-stress sensor,  $t = (t_{ij})_{1 \leq i, j \leq m}$ , and the Reynolds stress tensor  $\tau = (\tau_{ij})_{1 \leq i, j \leq m}$ ,

$$t = 2\mu_{\text{eff}}\overline{\mathcal{S}}, \quad \rho\tau = 2\mu_t\overline{\mathcal{S}} - \frac{2}{3}\rho k\text{Id}. \quad (3.2)$$

Additionally, according to  $\mathcal{S}$  we define the vorticity  $\Omega$  as skew-symmetric part of the total derivative of flow velocity  $u$ ,

$$\Omega := \frac{1}{2} \left( \frac{du}{dx} - \left( \frac{du}{dx} \right)^T \right), \quad \text{i.e.} \quad \Omega_{ij} = \frac{1}{2} \left( \frac{\partial u_i}{\partial x_j} - \frac{\partial u_j}{\partial x_i} \right). \quad (3.3)$$

### 3.1 Differential form of $k\omega$ -models

Throughout the literature two-equation turbulence models are typically presented in their differential form. In general these equations are used in the context of conservation laws, for example Navier-Stokes equations, and the variables used in these equations describe quantities of conservation. With respect to this statement we follow in our presentation the same ideas.

In Sections 3.1.1, 3.1.2 and 3.1.3 we present the several forms of the Wilcox  $k\omega$ -model. Sections 3.1.4 and 3.1.5 introduce the Shear-Stress-Transport model suggested by Menter.

Based on such presentations of these models we consider certain simplifications of the original formulations in Section 3.2. Such considerations yield certain forms of such models. By integration of the simplified forms we finally obtain the integral form of two-equation  $k\omega$ -type models in Section 3.3.

### 3.1.1 Wilcox $k\omega$ -model of 1988

The  $k\omega$ -model of Wilcox (1988) has the form

$$\frac{\partial(\rho k)}{\partial t} + \operatorname{div}(\rho k u) = \operatorname{div}((\mu_l + \sigma_k \mu_t) \operatorname{grad} k) + \rho Q_{k,(k,\omega)}^{(88)}, \quad (3.4a)$$

$$\frac{\partial(\rho \omega)}{\partial t} + \operatorname{div}(\rho \omega u) = \operatorname{div}((\mu_l + \sigma_\omega \mu_t) \operatorname{grad} \omega) + \rho Q_{\omega,(k,\omega)}^{(88)}. \quad (3.4b)$$

The eddy viscosity also called turbulent viscosity is computed by

$$\mu_t = \rho \frac{k}{\omega}. \quad (3.5)$$

The source terms for  $k$ -equation and  $\omega$ -equation have a production and destruction term,

$$Q_{k,(k,\omega)}^{(88)} := Pr_{k,(k,\omega)}^{(88)} - De_{k,(k,\omega)}^{(88)}, \quad Q_{\omega,(k,\omega)}^{(88)} := Pr_{\omega,(k,\omega)}^{(88)} - De_{\omega,(k,\omega)}^{(88)},$$

which are given by

$$Pr_{k,(k,\omega)}^{(88)} := \tau \otimes \frac{du}{dx}, \quad De_{k,(k,\omega)}^{(88)} := \beta^* k \omega \quad (3.6a)$$

$$Pr_{\omega,(k,\omega)}^{(88)} := \alpha \frac{\omega}{k} \tau \otimes \frac{du}{dx}, \quad De_{\omega,(k,\omega)}^{(88)} := \beta \omega^2. \quad (3.6b)$$

Here and throughout the rest of this report symbol  $\otimes$  denotes for  $A, B \in \mathbb{R}^{n \times n}$ ,  $A = (a_{ij})$ ,  $B = (b_{i,j})$  the product

$$A \otimes B = \sum_{i,j=1}^n a_{ij} b_{ij}.$$

The constants of the model are

$$\sigma_k = \frac{1}{2}, \quad \sigma_\omega = \frac{1}{2}, \quad \alpha = \frac{5}{9}, \quad \beta = \frac{3}{40}, \quad \beta^* = \frac{9}{100}.$$

Before we go on formulating the advancements of the  $k\omega$ -models of Wilcox, it is emphasized that the production term in the  $\omega$  equation is directly formulated using a weighting of  $\omega/k$ . Because it is exactly this term which generates a major difference of the  $k\omega$ -models when compared with the SST-model.

### 3.1.2 Wilcox $k\omega$ -model of 1998

For the  $k\omega$ -model of Wilcox in 1998 several of the constants have been supplemented and some of them are prescribed by additional functions. For completeness, the constants of the model are

$$\sigma_k = \frac{1}{2}, \quad \sigma_\omega = \frac{1}{2}, \quad \alpha^{(98)} = \frac{13}{25}, \quad \beta_o = \frac{9}{125}, \quad \beta_o^* = \frac{9}{100}.$$

Now, functions describing the missing elements of the model are

$$\begin{aligned} f_\beta &= \frac{1 + 70\chi_\omega}{1 + 80\chi_\omega}, & \chi_\omega &= \left| \frac{\Omega_{ij}\Omega_{jk}\hat{S}_{ki}}{(\beta_o^*\omega)^3} \right|, & \hat{S}_{ki} &= S_{ki} - \frac{1}{2} \frac{\partial u}{\partial x_m} \delta_{ik} \\ \beta^{*,(98)} &= \beta_o^* f_{\beta^*}, & \beta^{(98)} &= \beta_o f_\beta, & \chi_k &= \frac{1}{\omega^3} \langle \text{grad } k, \text{grad } \omega \rangle, \\ f_{\beta^*} &= \begin{cases} \frac{1+680\chi_k^2}{1+400\chi_k^2}, & \chi_k \geq 0, \\ 1, & \chi_k \leq 0. \end{cases} \end{aligned}$$

The source terms are defined by

$$Q_{k,(k,\omega)}^{(98)} := Pr_{k,(k,\omega)}^{(88)} - De_{k,(k,\omega)}^{(98)}, \quad Q_{\omega,(k,\omega)}^{(88)} := Pr_{\omega,(k,\omega)}^{(98)} - De_{\omega,(k,\omega)}^{(98)},$$

where

$$Pr_{\omega,(k,\omega)}^{(98)} := \alpha^{(98)} \frac{\omega}{k} \tau \otimes \frac{du}{dx}, \quad De_{k,(k,\omega)}^{(98)} := \beta^{*,(98)} k \omega, \quad De_{\omega,(k,\omega)}^{(98)} := \beta^{(98)} \omega^2.$$

Hence, compared to the version of 1988 the main difference is the formulation of the scalar weighting the destruction terms in the  $k$ -equation and the  $\omega$ -equation. In the 1988 version of the model these terms are simply weighted by some fixed scalar values, in the 1998 version these terms are weighted by functions involving flow variables. Supplementing  $\alpha$  by  $\alpha^{(98)}$  seems to be a minor change in the model.

For what follows, it is interesting to note that both models presented below, namely the 2006 version of Wilcox and the SST model of Menter modify the  $\omega$ -equation significantly and the  $k$ -equation only moderately.

### 3.1.3 Wilcox $k\omega$ -model of 2006

For the  $k\omega$ -model of Wilcox in 2006 the source terms for production and destruction of the  $k$ -equation agree with the 1988 version,

$$Q_{k,(k,\omega)}^{(2006)} := Pr_{k,(k,\omega)}^{(2006)} - De_{k,(k,\omega)}^{(2006)}, \quad Pr_{k,(k,\omega)}^{(2006)} = Pr_{k,(k,\omega)}^{(88)}, \quad De_{k,(k,\omega)}^{(2006)} = De_{k,(k,\omega)}^{(88)}.$$

Note that this is not absolutely true, because the definition of eddy viscosity is changed in this model and hence the stress tensor  $\tau$  is influenced. The consequences are discussed more detailed in Section 4.2. For the  $\omega$ -equation an additional cross-diffusion term has been added to the source terms when compared with the  $k\omega$ -model of 1988. Hence, the difference is

$$Q_{\omega,(k,\omega)}^{(2006)} = Pr_{\omega,(k,\omega)}^{(2006)} - De_{\omega,(k,\omega)}^{(2006)} + Di_{\omega,(k,\omega)}^{(2006)},$$

where

$$Di_{\omega,(k,\omega)}^{(2006)} := \frac{\sigma_d}{\omega} \langle \text{grad } k, \text{grad } \omega \rangle. \quad (3.7)$$

$$\sigma_k = \frac{3}{5}, \quad \sigma_\omega = \frac{1}{2}, \quad \alpha = \frac{13}{25}, \quad \beta_o = 0.0708, \quad \beta = \beta_o f_\beta, \quad \beta^* = \frac{9}{100}.$$

The constants and functions describing the missing elements of the model are

$$f_\beta = \frac{1 + 85\chi_\omega}{1 + 100\chi_\omega}, \quad \chi_\omega = \left| \frac{\Omega_{ij}\Omega_{jk}\hat{S}_{ki}}{(\beta^*\omega)^3} \right|, \quad \hat{S}_{ki} = S_{ki} - \frac{1}{2} \frac{\partial u}{\partial x_m} \delta_{ik},$$

$$\sigma_d = \begin{cases} 0, & \langle \text{grad } k, \text{grad } \omega \rangle \leq 0, \\ \sigma_{do}, & \langle \text{grad } k, \text{grad } \omega \rangle > 0, \end{cases} \quad \sigma_{do} = \frac{1}{8}.$$

Additionally, for the implementation of the eddy viscosity a so-called stress limiter is introduced, and the eddy viscosity is computed by

$$\mu_t = \rho \frac{k}{\tilde{\omega}}, \quad \tilde{\omega} = \max \left\{ \omega, C_{\text{lim}} \sqrt{\frac{2\Omega \otimes \Omega}{\beta^*}} \right\}. \quad (3.8)$$

Maybe it is important to note that the change in the eddy viscosity is only applied in the source terms, for the diffusion terms

$$\text{div}((\mu_l + \sigma_k \mu_t) \text{grad } k) \quad \text{and} \quad \text{div}((\mu_l + \sigma_\omega \mu_t) \text{grad } \omega)$$

the eddy viscosity is computed using (3.5).

**Notation 3.1.1** *Due to the similarity of the models and to shorten notation, for the rest of this report the superscript for the actual version is neglected and not mentioned. In case the precise formulation of the model is of importance, there will be a corresponding note.*

### 3.1.4 Menter Shear Stress Transport model (1992)

The SST-model in differential form has similar shape. Suggested by Menter this model modifies the formula for eddy viscosity  $\mu_t$ , diffuse term  $f_v$  and the source term  $Q$  when compared with the  $k\omega$ -model,

$$\frac{\partial(\rho k)}{\partial t} + \text{div}(\rho k u) = \text{div}((\mu_l + \Phi_k \mu_t) \text{grad } k) + \rho Q_{k,\text{SST}} \quad (3.9a)$$

$$\frac{\partial(\rho \omega)}{\partial t} + \text{div}(\rho \omega u) = \text{div}((\mu_l + \Phi_\omega \mu_t) \text{grad } \omega) + \rho Q_{\omega,\text{SST}} \quad (3.9b)$$

For the SST-model there does not exist one preferred recommended version, but slight modifications and adaptations are suggested. The original version of the model was suggested in [18, 20, 21], and an update was given in [22]. In the shear-stress transport model the eddy viscosity is defined via

$$\mu_t = \rho k \min \left\{ \frac{1}{\omega}, \frac{a_1}{F_2 \sqrt{2\Omega \otimes \Omega}} \right\} \quad (1992 \text{ version}). \quad (3.10)$$

Here  $F_2$  is a blending function defined by

$$F_2 := \tanh \left( (\max \{\Gamma_1, 2\Gamma_3\})^2 \right) \quad (3.11)$$

where

$$\Gamma_1 := \frac{C_{\Gamma_1} \nu_l}{d^2 \omega}, \quad \Gamma_3 := \frac{\sqrt{k}}{\beta^* \omega d}, \quad \beta^* := 0.09, \quad (3.12)$$

and  $d$  is the distance to the closest no-slip wall. The constants  $C_{\Gamma_1}$  and  $a_1$  are not uniquely defined. In the article [18] these constants are given in formulae A-10 and A-12, and their values are

$$a_1 = 0.3 \quad \text{and} \quad C_{\Gamma_1} = 400,$$

another article listing these constants is [21] and here the values in formulae A-13 and A-16 are

$$a_1 = 0.31 \quad \text{and} \quad C_{\Gamma_1} = 500.$$

The first of these mentioned articles is a NASA Technical Memorandum whereas the second is an AIAA Journal article. The NASA Technical Memorandum is released with the note "to quickly provide the research community with important information". With respect to this information we assume that the second mentioned data set is the one to use, and what has been used for the results presented in this document.

The source terms for  $k$ -equation has a production and destruction term, the  $\omega$ -equation has an additional diffusion term,

$$Q_{k,\text{SST}} = Pr_{k,\text{SST}} - De_{k,\text{SST}}, \quad Q_{\omega,\text{SST}} = Pr_{\omega,\text{SST}} - De_{\omega,\text{SST}} + Di_{\omega,\text{SST}}.$$

Before we state the source terms, note that the SST-model involves a blending of a  $k\omega$ - and a  $k\varepsilon$ -model. This blending is controlled by a function  $\Phi = \Phi(x; \varepsilon_1, \varepsilon_2)$ . This function is designed to detect the edge of the boundary layer, such that the SST-model behaves inside the boundary layer like a  $k\omega$ -model and outside like a  $k\varepsilon$ -model. Such detection works using a convex combination of an additional function  $F_1$  together with a scalar weighting of the terms,

$$\begin{aligned} \Phi & : [0, 1] \rightarrow [\varepsilon_1, \varepsilon_2] \\ \Phi(F_1; \varepsilon_1, \varepsilon_2) & := F_1 \varepsilon_1 + (1 - F_1) \varepsilon_2. \end{aligned} \quad (3.13)$$

The fixed, given values  $\varepsilon_1$  and  $\varepsilon_2$  are additional parameters which are different for the blending in the diffusive terms and source terms.

To realize smooth blending, the function  $F_1$  is modeled using the hyperbolic tangent,

$$F_1 : [0, \infty) \rightarrow [0, 1], \quad (3.14a)$$

$$F_1 = F_1(\Gamma_{F_1}) = \tanh(\Gamma_{F_1}^4). \quad (3.14b)$$

Finally, the term  $\Gamma_{F_1}$  determines, using actual flow conditions, the position in the flow field,

$$\Gamma_{F_1} := \min \{ \max \{ \Gamma_1, \Gamma_3 \}, \Gamma_2 \}, \quad (3.15)$$

$$\Gamma_2 := \frac{4\sigma_{\omega_2}\rho k}{d^2 C_D}, \quad (3.16)$$

$$C_D := \max \left\{ \frac{2\sigma_{\omega_2}\rho}{\omega} \langle \text{grad } k, \text{grad } \omega \rangle, \delta \right\}, \quad \delta = 10^{-20}. \quad (3.17)$$

The consequence of these definitions are discussed in Section 3.7. Using the function  $\Phi$  functions  $\Phi_k$  and  $\Phi_\omega$  required for viscous flux in (3.9) are given by

$$\Phi_k := \Phi(F_1; \sigma_{k_1}, \sigma_{k_2}), \quad \sigma_{k_1} = 0.85, \quad \sigma_{k_2} = 1, \quad (3.18a)$$

$$\Phi_\omega := \Phi(F_1; \sigma_{\omega_1}, \sigma_{\omega_2}), \quad \sigma_{\omega_1} = 0.5, \quad \sigma_{\omega_2} = 0.856. \quad (3.18b)$$

The source terms for the  $k$ -equation of the SST-model are identical with the source terms (3.6a) of the  $k\omega$ -model, the source terms for the  $\omega$ -equation introduce a further diffusion term combining  $k$  and  $\omega$  as well as some blending,

$$Pr_{k,\text{SST}} := \tau \otimes \frac{du}{dx}, \quad De_{k,\text{SST}} := \beta^* k \omega, \quad (3.19a)$$

$$Pr_{\omega,\text{SST}} := \Phi_\gamma \frac{1}{\nu_t} \tau \otimes \frac{du}{dx}, \quad De_{\omega,\text{SST}} := \Phi_\beta \omega^2, \quad (3.19b)$$

$$Di_{\omega,\text{SST}} := 2(1 - F_1) \sigma_{\omega_2} \frac{1}{\omega} \langle \text{grad } k, \text{grad } \omega \rangle, \quad (3.19c)$$

where

$$\Phi_\gamma := \Phi(F_1; \gamma_1, \gamma_2), \quad \Phi_\beta := \Phi(F_1; \beta_1, \beta_2) \quad (3.20)$$

and the constants are

$$\begin{aligned} \beta_1 &= 3/40, & \beta_2 &= 0.0828, & \beta^* &= \frac{9}{100}, \\ \gamma_1 &= \frac{\beta_1}{\beta^*} - \sigma_{\omega_1} \frac{v_k^2}{\sqrt{\beta^*}}, & \gamma_2 &= \frac{\beta_2}{\beta^*} - \sigma_{\omega_2} \frac{v_k^2}{\sqrt{\beta^*}}, & v_k &= 0.41. \end{aligned}$$

The last constant  $v_k$  is well known as the *von Karman* constant in the literature. The values of the constants  $\gamma_i$ ,  $i = 1, 2$  can be explicitly computed and are approximately

$$\gamma_1 \approx 0.55317 \quad \text{and} \quad \gamma_2 \approx 0.44035. \quad (3.21)$$

### 3.1.5 Menter Shear Stress Transport model (2003)

The definition of eddy viscosity was modified in the version of 2003. The magnitude of vorticity was supplemented by magnitude of strain rate,

$$\mu_t = \rho k \min \left\{ \frac{1}{\omega}, \frac{a_1}{F_2 \sqrt{2\mathcal{S} \otimes \mathcal{S}}} \right\} \quad (2003 \text{ version}). \quad (3.22)$$

The constant is given by  $a_1 := 0.31$ . The constant  $\delta$  required for (3.17) differs for the different versions of the model, and in the 2003 version it was exchanged by

$$\delta := 10^{-10}.$$

Furthermore, the definitions of  $\gamma_1$  and  $\gamma_2$  have changed in the 2003 version. Here the constants are explicitly defined by

$$\gamma_1 = \frac{5}{9} \quad \text{and} \quad \gamma_2 = 0.44, \quad (3.23)$$

which are close to the original values given in (3.21) but not the same. A reason for this change is not given by the author, nor are the effects discussed.

## 3.2 Simplifications of $k\omega$ -models

Though these models are often formulated like (3.4) and (3.9) their actual implementation and usage is often based on their incompressible version, even when they are used with respect to compressible flow. To simplify these models, one assumes

$$\operatorname{div}(u) = 0, \quad (3.24)$$

$$\frac{2}{3}\rho k \approx 0. \quad (3.25)$$

As a direct consequence of (3.24), an application of the differential form of the equation of mass gives

$$\begin{aligned} 0 &= \frac{\partial \rho}{\partial t} + \operatorname{div}(\rho u) = \frac{\partial \rho}{\partial t} + \langle \operatorname{grad} \rho, u \rangle + \rho \operatorname{div}(u) \\ &= \frac{\partial \rho}{\partial t} + \langle \operatorname{grad} \rho, u \rangle, \end{aligned}$$

and consequently

$$\begin{aligned} \frac{\partial(\rho k)}{\partial t} + \operatorname{div}(\rho k u) &= k \frac{\partial \rho}{\partial t} + \rho \frac{\partial k}{\partial t} + \langle \operatorname{grad} \rho, k u \rangle + \rho \operatorname{div}(k u) \\ &= k \left( \frac{\partial \rho}{\partial t} + \langle \operatorname{grad} \rho, u \rangle \right) + \rho \left( \frac{\partial k}{\partial t} + \operatorname{div}(k u) \right) \\ &= \rho \left( \frac{\partial k}{\partial t} + \operatorname{div}(k u) \right), \end{aligned} \quad (3.26)$$

and equivalently

$$\frac{\partial(\rho \omega)}{\partial t} + \operatorname{div}(\rho \omega u) = \rho \left( \frac{\partial \omega}{\partial t} + \operatorname{div}(\omega u) \right). \quad (3.27)$$

Inserting (3.26) and (3.27) into either (3.4) or (3.9) and division by  $\rho > 0$  yields either (in the following we neglect the superscripts for the different  $k\omega$ -models)

$$\frac{\partial k}{\partial t} + \operatorname{div}(ku) = \frac{1}{\rho} \operatorname{div}((\mu_l + \sigma_k \mu_t) \operatorname{grad} k) + Q_{k,(k,\omega)}, \quad (3.28a)$$

$$\frac{\partial \omega}{\partial t} + \operatorname{div}(\omega u) = \frac{1}{\rho} \operatorname{div}((\mu_l + \sigma_\omega \mu_t) \operatorname{grad} \omega) + Q_{\omega,(k,\omega)}, \quad (3.28b)$$

or

$$\frac{\partial k}{\partial t} + \operatorname{div}(ku) = \frac{1}{\rho} \operatorname{div}((\mu_l + \Phi_k \mu_t) \operatorname{grad} k) + Q_{k,\text{SST}}, \quad (3.29a)$$

$$\frac{\partial \omega}{\partial t} + \operatorname{div}(\omega u) = \frac{1}{\rho} \operatorname{div}((\mu_l + \Phi_\omega \mu_t) \operatorname{grad} \omega) + Q_{\omega,\text{SST}}. \quad (3.29b)$$

Consequently, the independent variables  $(\rho k, \rho \omega)$  are now replaced by  $(k, \omega)$ . To be consistent using assumption (3.25) we have

$$\rho \tau = 2\mu_t \bar{\mathcal{S}}. \quad (3.30)$$

In a second step, assumption (3.24) can be integrated into (3.30). This yields  $\bar{\mathcal{S}} = \mathcal{S}$  and finally

$$\rho \tau = 2\mu_t \mathcal{S}. \quad (3.31)$$

**Remark 3.2.1** *One rarely finds information if assumptions (3.24) and (3.25) are included into the formulation of the turbulence model, if (3.30) or (3.31) is used for the formulation of the production terms. For the implementation considered here we chose (3.30), though being not consistent with (3.24).*

Using these simplifications the source terms for the  $k\omega$ -model given in (3.6a) and (3.6b) are implemented by

$$\begin{aligned} Pr_{k,(k,\omega)}^{(88)} &= \tau \otimes \frac{du}{dx} = 2\nu_t \bar{\mathcal{S}} \otimes \frac{du}{dx} = 2\frac{k}{\omega} \bar{\mathcal{S}} \otimes \frac{du}{dx}, \\ Pr_{\omega,(k,\omega)}^{(88)} &= \alpha \frac{\omega}{k} \tau \otimes \frac{du}{dx} = 2\alpha \bar{\mathcal{S}} \otimes \frac{du}{dx}. \end{aligned}$$

Due to the change in eddy viscosity these consideration do not carry over for the SST and the 2006 model (see Section 4.2 and the discussion for the SST-model below). The tensor product  $\bar{\mathcal{S}} \otimes \frac{du}{dx}$  is explicitly computed for the 3D case by (see e.g. [17])

$$\bar{\mathcal{S}} \otimes \frac{du}{dx} = \frac{2}{3} \left\{ \sum_{i=1}^3 \left( \frac{\partial u_i}{\partial x_i} \right)^2 - \sum_{1 \leq i < j \leq 3} \left( \frac{\partial u_i}{\partial x_i} \frac{\partial u_j}{\partial x_j} \right) \right\} + \frac{1}{2} \sum_{1 \leq i < j \leq 3} \left( \frac{\partial u_i}{\partial x_j} + \frac{\partial u_j}{\partial x_i} \right)^2.$$

Since

$$\sum_{i=1}^3 \left( \frac{\partial u_i}{\partial x_i} \right)^2 - \sum_{1 \leq i < j \leq 3} \left( \frac{\partial u_i}{\partial x_i} \frac{\partial u_j}{\partial x_j} \right) = \frac{1}{2} \sum_{1 \leq i < j \leq 3} \left( \frac{\partial u_i}{\partial x_i} - \frac{\partial u_j}{\partial x_j} \right)^2$$

we conclude

$$\bar{\mathcal{S}} \otimes \frac{du}{dx} = \frac{1}{3} \sum_{1 \leq i < j \leq 3} \left( \frac{\partial u_i}{\partial x_i} - \frac{\partial u_j}{\partial x_j} \right)^2 + \frac{1}{2} \sum_{1 \leq i < j \leq 3} \left( \frac{\partial u_i}{\partial x_j} + \frac{\partial u_j}{\partial x_i} \right)^2 \geq 0. \quad (3.32)$$

For the SST-model the eddy viscosity in the source terms cannot be simply replaced by expressions including  $\rho$ , and  $k$  and  $\omega$ . Due to its definition in (3.10) or (3.22), obviously one needs to take care of the limitation. The source terms for the SST-model given in (3.19a) and (3.19b) and (3.19c) are implemented by

$$\begin{aligned} Pr_{k,\text{SST}} &= \tau \otimes \frac{du}{dx} = 2\nu_t \bar{\mathcal{S}} \otimes \frac{du}{dx}, \\ Pr_{\omega,\text{SST}} &= \Phi_\gamma \frac{1}{\nu_t} \tau \otimes \frac{du}{dx} = 2\Phi_\gamma \bar{\mathcal{S}} \otimes \frac{du}{dx}. \end{aligned}$$

Additionally, for both models we also do not use the clean production term stated above, but the analytic representation is replaced by

$$\tilde{Pr}_{k,(k,\omega)} := \min \{ Pr_{k,(k,\omega)}, 20De_{k,(k,\omega)} \}, \quad (3.33a)$$

$$\tilde{Pr}_{k,\text{SST}} := \min \{ Pr_{k,\text{SST}}, 20De_{k,\text{SST}} \}. \quad (3.33b)$$

We will show in example in Section 6.1.1 the necessity for (3.33a) in combination with the  $k\omega$ -model. For the  $k\omega$ -model this limitation actually means a reduction of production of turbulence kinetic energy. For the SST-model limitation (3.33b) is not that obvious. Since eddy viscosity is already bounded, the additional limitation actually means a double limitation

$$\begin{aligned} \tilde{Pr}_{k,\text{SST}} &= \min \left\{ 2\nu_t \bar{\mathcal{S}} \otimes \frac{du}{dx}, 20\beta^* k\omega \right\} \\ &= 2k \min \left\{ \min \left\{ \frac{1}{\omega}, \frac{a_1}{F_2 \sqrt{2\mathcal{S} \otimes \mathcal{S}}} \right\} \bar{\mathcal{S}} \otimes \frac{du}{dx}, 10\beta^* \omega \right\}. \end{aligned}$$

The impact of such double limitation on the production of turbulence kinetic energy has not been discussed in detail in literature, and about its effect can only be speculated.

### 3.3 Integral form of $k\omega$ -models

Unfortunately, when integrating the diffusive terms in (3.28) and (3.29) over a control volume, they cannot be rewritten as a surface integral because of division

with density  $\rho$ . Hence, a further approximation is introduced assuming either for the  $k\omega$ -model

$$\frac{1}{\rho} \operatorname{div}((\mu_l + \sigma_k \mu_t) \operatorname{grad} k) \approx \operatorname{div}((\nu_l + \sigma_k \nu_t) \operatorname{grad} k), \quad (3.34a)$$

$$\frac{1}{\rho} \operatorname{div}((\mu_l + \sigma_\omega \mu_t) \operatorname{grad} \omega) \approx \operatorname{div}((\nu_l + \sigma_\omega \nu_t) \operatorname{grad} \omega), \quad (3.34b)$$

or for the SST-model

$$\frac{1}{\rho} \operatorname{div}((\mu_l + \Phi_k \mu_t) \operatorname{grad} k) \approx \operatorname{div}((\nu_l + \Phi_k \nu_t) \operatorname{grad} k), \quad (3.35a)$$

$$\frac{1}{\rho} \operatorname{div}((\mu_l + \Phi_\omega \mu_t) \operatorname{grad} \omega) \approx \operatorname{div}((\nu_l + \Phi_\omega \nu_t) \operatorname{grad} \omega). \quad (3.35b)$$

Integration of (3.28) using approximation (3.34) gives the integral equation

$$V_D(Q_{(k,\omega)}(W_t, W))(t) = \frac{d}{dt} V_D(W_t)(t) + R_{\partial D, (k,\omega)}(W_t, W)(t), \quad (3.36)$$

where the integral operators are

$$\begin{aligned} R_{c, \partial D, (k,\omega)}(W_t, W)(t) &:= \int_{\partial D} \langle f_{c, (k,\omega)}(W_t(y, t), W(y, t)), n(y) \rangle ds(y), \\ R_{v, \partial D, (k,\omega)}(W_t, W)(t) &:= \int_{\partial D} \langle f_{v, (k,\omega)}(W_t(y, t), W(y, t)), n(y) \rangle ds(y), \\ R_{\partial D, (k,\omega)} &:= R_{c, \partial D, (k,\omega)} - R_{v, \partial D, (k,\omega)}. \end{aligned}$$

Here the convective  $f_{c, (k,\omega)}$  and viscous  $f_{v, (k,\omega)}$  contributions as well as the source terms  $Q_{(k,\omega)}$  are summarized by

$$\begin{aligned} f_{c, (k,\omega)}(W_t, W) &:= \begin{pmatrix} ku \\ \omega u \end{pmatrix}, \\ f_{v, (k,\omega)}(W_t, W) &:= \begin{pmatrix} (\nu_l + \sigma_k \frac{k}{\omega}) \operatorname{grad} k \\ (\nu_l + \sigma_\omega \frac{k}{\omega}) \operatorname{grad} \omega \end{pmatrix}, \\ Q_{(k,\omega)}(W_t, W) &:= \begin{pmatrix} Pr_{k, (k,\omega)}(W_t, W) - De_{k, (k,\omega)}(W_t, W) \\ Pr_{\omega, (k,\omega)}(W_t, W) - De_{\omega, (k,\omega)}(W_t, W) \end{pmatrix}. \end{aligned}$$

Equivalently, for the SST-model (3.29) together with (3.35) give integral equation

$$V_D(Q_{\text{SST}}(W_t, W))(t) = \frac{d}{dt} V_D(W_t)(t) + R_{\partial D, \text{SST}}(W_t, W)(t), \quad (3.37)$$

where

$$Q_{\text{SST}} := \begin{pmatrix} Pr_{k, \text{SST}} - De_{k, \text{SST}} \\ Pr_{\omega, \text{SST}} - De_{\omega, \text{SST}} + Di_{\omega, \text{SST}} \end{pmatrix},$$

and the integral operators are

$$\begin{aligned} R_{c,\partial D,\text{SST}}(W_t, W)(t) &:= \int_{\partial D} \langle f_{c,(k,\omega)}(W_t(y, t), W(y, t)), n(y) \rangle ds(y), \\ R_{v,\partial D,\text{SST}}(W_t, W)(t) &:= \int_{\partial D} \langle f_{v,\text{SST}}(W_t(y, t), W(y, t)), n(y) \rangle ds(y), \\ R_{\partial D,\text{SST}} &:= R_{c,\partial D,\text{SST}} - R_{v,\partial D,\text{SST}}. \end{aligned}$$

The convective and diffusive flux for the SST model are given by

$$f_{c,\text{SST}} := f_{c,(k,\omega)}, \quad f_{v,\text{SST}}(W_t, W) := \begin{pmatrix} (\nu_l + \Phi_k \nu_t) \text{grad } k \\ (\nu_l + \Phi_\omega \nu_t) \text{grad } \omega \end{pmatrix}. \quad (3.38)$$

## 3.4 Boundary conditions and boundary value problem

So far, we have only stated the integral equations of interest. That is, the mean flow equations (2.1) together with a system of equations describing the required eddy viscosity  $\mu_t$ , for example (3.4) or (3.9). Naturally, for a closed representation we need to formulate a corresponding boundary value problem.

### 3.4.1 Boundary value problem

The boundary value problems of interest in this report model the motion of a rigid body through a viscous fluid. We formulate this as a flow past an obstacle, where the center of mass is held in place by appropriate forces and the fluid flow past the obstacle tends to a uniform velocity field at large distances from the obstacle. This consideration corresponds to a wind tunnel experiment. Mathematically, the domain of interest is then an exterior region and the boundary value problems are formulated as exterior flow problems.

Due to a lack of theoretical understanding of both mean flow and turbulence flow equations, the definition of boundary values and conditions at infinity are not straightforward. For example, for a complete and closed formulation the decay behavior at infinity for  $\rho$ ,  $u$ ,  $p$ , and additionally even for  $k$  and  $\omega$ , is required. Since this is in general unknown, we prescribe these values formally. For the representation of the exterior boundary value problems of interest we introduce the formal setting,

$$\begin{aligned} W_\infty &:= (\rho_\infty, \rho_\infty u_\infty, \rho_\infty E_\infty), \\ W_{t,\infty} &:= (k_\infty, \omega_\infty). \end{aligned}$$

The actual choice of these values for realization is given in (3.56) below. Furthermore, in the sequel let  $D \subset \mathbb{R}^m$  be a bounded domain and for the sake of simplicity,

we assume that the boundary of  $\partial D$  is connected and that  $\partial D$  is an orientable submanifold of  $\mathbb{R}^m$  of dimension  $m - 1$ .

Though we have stated the RANS equations in their unsteady form, we are only interested in approximating a steady state solution. Hence, we formulate the boundary value problems only for the steady state.

**Exterior turbulent flow problem:**

Find a function  $W$  that satisfies the steady RANS equations in  $\mathbb{R}^m \setminus \overline{D}$ , that is

$$\frac{d}{dt}W^\dagger(x, t) = 0 \quad \text{for all } x \in \mathbb{R}^m \setminus \overline{D}, \quad t \geq T^\dagger > 0,$$

and satisfies the (adiabatic) no-slip wall boundary conditions

$$u = 0 \quad \text{and} \quad \frac{\partial T}{\partial n} = 0 \quad \text{on} \quad \partial D$$

in the sense of a trace operator, and  $\lim_{\|x\|_2 \rightarrow \infty} W(x, t) = W_\infty$  uniformly for all directions. Additionally, find a function  $W_t$  that satisfies the  $k\omega$ -turbulence model in  $\mathbb{R}^m \setminus \overline{D}$ , and satisfies the boundary conditions

$$(k, \omega) = (0, \infty) \quad \text{on} \quad \partial D$$

in the sense that

$$\lim_{h \rightarrow 0^+} \omega(x - hn(x)) \rightarrow \infty, \quad x \in \partial D, \quad (3.39)$$

and  $\lim_{\|x\| \rightarrow \infty} W_t(x, t) = W_{t, \infty}$  uniformly for all directions.

### 3.4.2 No-slip wall boundary condition

To realize boundary conditions for  $k$  and  $\omega$  is not straightforward. The only simple boundary condition corresponding to vanishing velocity  $u_{\partial D_{\text{no-slip}}} = 0$  is

$$k_{\partial D_{\text{no-slip}}} = 0. \quad (3.40)$$

To derive a boundary condition on no-slip wall for  $\omega$  we follow the presentation in [31, 32]. We assume that near a no-slip wall a solution to Navier-Stokes equations is incompressible and pressure is constant, and as a consequence convective terms are negligible. Maybe, it is important to note that these assumptions correspond to the considerations of Section 3.2. Then the equations for  $k$  and  $\omega$  simplify to

$$\begin{aligned} 0 &= \operatorname{div}((\nu_l + \sigma_k \nu_t) \operatorname{grad} k) + 2 \frac{k}{\omega} \overline{\mathcal{S}} \otimes \frac{du}{dx} - \beta^* \omega k, \\ 0 &= \operatorname{div}((\nu_l + \sigma_\omega \nu_t) \operatorname{grad} \omega) + 2\alpha \overline{\mathcal{S}} \otimes \frac{du}{dx} - \beta \omega^2. \end{aligned}$$

In a next step it is assumed that only the velocity gradient in direction normal to the no-slip wall is dominant. If this direction is identified with  $y$ -coordinate, we obtain

$$\frac{du}{dx} = \begin{pmatrix} \frac{\partial u_1}{\partial x} & \frac{\partial u_1}{\partial y} & \frac{\partial u_1}{\partial z} \\ \frac{\partial u_2}{\partial x} & \frac{\partial u_2}{\partial y} & \frac{\partial u_2}{\partial z} \\ \frac{\partial u_3}{\partial x} & \frac{\partial u_3}{\partial y} & \frac{\partial u_3}{\partial z} \end{pmatrix} \approx \begin{pmatrix} 0 & 0 & 0 \\ 0 & \frac{\partial u_2}{\partial y} & 0 \\ 0 & 0 & 0 \end{pmatrix},$$

and as a consequence we have

$$\begin{aligned} 0 &= \frac{\partial}{\partial y} \left( (\nu_l + \sigma_k \nu_t) \frac{\partial k}{\partial y} \right) + 2 \frac{k}{\omega} \left( \frac{\partial u}{\partial y} \right)^2 - \beta^* \omega k, \\ 0 &= \frac{\partial}{\partial y} \left( (\nu_l + \sigma_\omega \nu_t) \frac{\partial \omega}{\partial y} \right) + 2\alpha \left( \frac{\partial u}{\partial y} \right)^2 - \beta \omega^2. \end{aligned}$$

Finally, it is assumed that the production terms are negligible compared to the remaining terms. Then, using (3.40) to conclude that  $\nu_t$  vanishes on the no-slip wall, all what is left of the  $\omega$ -equation is the ordinary differential equation

$$\beta \omega^2 = \nu_l \frac{\partial^2 \omega}{\partial y^2} \quad \Leftrightarrow \quad \frac{\beta}{\nu_l} \omega^2 = \frac{\partial^2 \omega}{\partial y^2},$$

which has the solution

$$\omega(y) = \frac{6\nu_l}{\beta y^2}.$$

Generalization of this procedure for normal direction  $n$ , we formally derived under the assumptions mentioned above for  $\omega$  the boundary condition

$$\lim_{h \rightarrow 0^+} \omega(x - hn(x)) h^2 = \frac{6\nu_l}{\beta}, \quad x \in \partial D_{\text{no-slip}}. \quad (3.41)$$

To investigate the behavior of  $k$  in a neighborhood of a no-slip wall, as a direct consequence, we can apply the same assumptions to the equation for  $k$  to obtain

$$\beta^* \omega k = \beta^* \frac{6\nu_l}{\beta y^2} k = \nu_l \frac{\partial^2 k}{\partial y^2} \quad \Leftrightarrow \quad \frac{6\beta^*}{\beta} \frac{k}{y^2} = \frac{\partial^2 k}{\partial y^2}.$$

Searching for a solution of the form  $k(y) = y^\alpha$ , a comparison of left and right hand side gives

$$\lambda y^{\alpha-2} = \alpha(\alpha-1) y^{\alpha-2}, \quad \lambda = \frac{6\beta^*}{\beta},$$

and therefore

$$\begin{aligned} \alpha_{1/2} &= \frac{1}{2} \pm \sqrt{\frac{1}{4} + \lambda} = \frac{1}{2} \pm \sqrt{\frac{1}{4} + \frac{6\beta^*}{\beta}} = \frac{1}{2} \pm \sqrt{\frac{1}{4} + \frac{6 \cdot 9 \cdot 40}{3 \cdot 100}}, \\ \alpha_1 &\approx \frac{1}{2} + 2.73 = 3.23, \quad \alpha_2 \approx \frac{1}{2} - 2.73 = -2.23. \end{aligned}$$

Assuming that the second solution  $\alpha_2$  is non-physical, otherwise  $k$  would have singular behavior at a no-slip wall, a contradiction to (3.40), we obtain

$$k(y) = C_k y^{\alpha_1} \approx y^{3.23},$$

which corresponds exactly to the behavior figured out in [31, 12]. Here  $C_k > 0$  denotes some constant, which cannot be determined in general. In contrast to  $\omega$  the behavior of function  $k$  is identified in a neighborhood of a no-slip wall only up to some scaling  $C_k$ . On the other hand, under the assumptions formulated above we do not only have the boundary condition  $k_{\partial D_{\text{no-slip}}} = 0$ , but also in a neighborhood of a no-slip wall we have the quantitative behavior

$$\lim_{h \rightarrow 0^+} \frac{k(x - hn(x))}{h^{\alpha_1 - \varepsilon}} = 0, \quad x \in \partial D_{\text{no-slip}}, \quad \varepsilon > 0. \quad (3.42)$$

**Remark 3.4.1** *Under the assumptions mentioned above, and imposing boundary condition (3.41) for  $\omega$ , in a neighborhood of a no-slip wall  $k$  satisfies condition (3.42), and the value  $\alpha$  is determined by the relation of  $\beta^*$  and  $\beta$ .*

Furthermore, since  $k$  represents turbulence kinetic energy, i.e.

$$k = \frac{1}{2} (u_1'^2 + u_2'^2 + u_3'^2),$$

this observation also determines the behavior of the fluctuating part of velocity  $u'$  in a neighborhood of a no-slip wall. In a neighborhood of a no-slip wall velocity  $u'$  satisfies approximately the quantitative behavior

$$u'(y) = \sqrt{y^{\alpha_1}} \approx y^{1.615},$$

that is

$$\lim_{h \rightarrow 0^+} \frac{u'(x - hn(x))}{h^{\alpha_1/2 - \varepsilon}} = 0, \quad x \in \partial D_{\text{no-slip}}, \quad \varepsilon > 0. \quad (3.43)$$

**Remark 3.4.2** *Under the assumptions mentioned above, and imposing boundary condition (3.41) for  $\omega$ , in a neighborhood of a no-slip wall both the behavior of  $k$  and the behavior of  $u'$  are determined and need to satisfy conditions (3.42) and (3.43). To say it more direct, the specification of no-slip wall boundary condition and near wall behavior for  $\omega$  controls the near wall behavior of  $k$  and  $u'$ . Hence, physical situations which do not follow conditions (3.43), (3.42) and (3.41) can in general not be simulated using the above boundary condition for  $\omega$ .*

To implement this quadratic singular behavior (3.41) for  $\omega$  is not straightforward. In our environment we followed the idea given in [18, 21]. Note, when approaching a smooth no-slip wall, the asymptotic behavior is determined by (3.41), which can be reformulated by

$$\lim_{h \rightarrow 0^+} \omega(x - hn(x)) = \lim_{h \rightarrow 0^+} \frac{6\nu_l (W(x - hn(x)))}{\beta \|hn(x)\|_2^2} = \lim_{h \rightarrow 0^+} \frac{6\nu_l (W(x - hn(x)))}{\beta h^2}.$$

Since  $h$  represents the distance to closest no-slip wall in normal direction, it was suggested to represent this expression numerically by

$$\|hn(x)\|_2 = h \approx d_i \approx \|p_{i,bdry} - p_{i,n}\|_2,$$

where  $p_{i,bdry}$  denotes the point on the no-slip wall and  $p_{i,n}$  the closest, next discrete point in direction  $-n(p_{i,bdry})$ . Then  $d_i$  is the distance to the closest no-slip wall of the next discrete point into anti normal direction. To take care of the quadratic singular behavior, it was suggested to multiply this value with an additional order of magnitude, hence the no-slip boundary value for  $\omega$  is realized by

$$\omega_{\text{no-slip}}(p_{i,bdry}) = \frac{60\nu_l (W(p_{i,bdry}))}{\beta \|p_{i,bdry} - p_{i,n}\|_2^2}, \quad p_{i,bdry} \in \partial D_{\text{no-slip}}. \quad (3.44)$$

Now, to obtain the value for  $\omega$  required to evaluate the boundary flux, a linear extrapolation is done. The increase, i.e. the gradient into normal direction of  $\omega$  for the boundary edge  $e_{i,bdry}$  is approximated by

$$\left(\frac{\partial\omega}{\partial x_k}\right)_{e_{i,bdry}}^{\text{TSL,app}} \approx \frac{(n_{i,bdry})_k (\omega_{\text{no-slip}} - \omega_{i,bdry})}{\|p_{i,bdry} - p_{i,n}\|_2}.$$

Then, in a small neighborhood of  $p_{i,bdry}$ , the function  $\omega$  is approximated by

$$\begin{aligned} \omega(p_{i,bdry} + hn_{i,bdry}) &\approx \omega(p_{i,bdry}) + \langle \text{grad } \omega(p_{i,bdry}), hn_{i,bdry} \rangle \\ &\approx \omega(p_{i,bdry}) + h \frac{(\omega_{\text{no-slip}} - \omega_{i,bdry})}{\|p_{i,bdry} - p_{i,n}\|_2} \langle n_{i,bdry}, n_{i,bdry} \rangle \\ &= \omega(p_{i,bdry}) + h \frac{(\omega_{\text{no-slip}} - \omega_{i,bdry})}{\|p_{i,bdry} - p_{i,n}\|_2}. \end{aligned}$$

Now, a suitable choice for  $h$  is required. For the computations presented in this report the choice  $h = 2 \|p_{i,bdry} - p_{i,n}\|_2$  was done, and as a consequence one obtains

$$\omega(p_{i,bdry} + 2 \|p_{i,bdry} - p_{i,n}\|_2 n_{i,bdry}) \approx 2\omega_{\text{no-slip}} - \omega_{i,bdry}. \quad (3.45)$$

The right hand side of (3.45) is used to evaluate the boundary flux for a no-slip wall. The construction for  $k$  is significantly simpler. Given a value for  $k$  on the no-slip wall, i.e.  $k_{i,bdry}$  we define as the state for the no-slip wall

$$k_{\text{no-slip}}(p_{i,bdry}) := -k_{i,bdry}.$$

To evaluate the boundary flux for a no-slip wall these values are averaged, and hence  $k = 0$  is enforced in the flux, which realizes the boundary condition for  $k$ .

### 3.4.3 Farfield boundary condition

To determine farfield boundary conditions  $(k_\infty, \omega_\infty)$  we assume for  $\|x\|_2 \rightarrow \infty$  constant velocity  $u_\infty$ , and constant density  $\rho_\infty > 0$ . Mathematically, this translates into

$$\lim_{\|x\|_2 \rightarrow \infty} \begin{pmatrix} u_1(x) \\ u_2(x) \\ u_3(x) \end{pmatrix} = \begin{pmatrix} u_{1,\infty} \\ u_{2,\infty} \\ u_{3,\infty} \end{pmatrix}, \quad \text{hence} \quad \lim_{\|x\|_2 \rightarrow \infty} \frac{du}{dx} = 0, \quad (3.46)$$

where

$$\begin{pmatrix} u_{1,\infty} \\ u_{2,\infty} \\ u_{3,\infty} \end{pmatrix} = \begin{pmatrix} u_\infty \sin \varphi \cos \theta \\ u_\infty \sin \varphi \sin \theta \\ u_\infty \cos \theta \end{pmatrix}, \quad 0 \leq \varphi \leq \pi, \quad 0 \leq \theta < 2\pi.$$

Then, for sufficiently large  $\|x\|_2$  we get from (3.4b) and assumption (3.46)

$$-\beta \rho_\infty \omega^2 = \operatorname{div}(\rho_\infty \omega u_\infty) - \operatorname{div}((\mu_l + \sigma_\omega \mu_t) \operatorname{grad} \omega).$$

Additionally, it seems reasonable to postulate that in the free-stream, far away from the obstacle, variations in  $k$  and  $\omega$  become small, that is

$$\lim_{\|x\|_2 \rightarrow \infty} \operatorname{grad} \omega = \lim_{\|x\|_2 \rightarrow \infty} \operatorname{grad} k = 0.$$

Then we obtain

$$-\beta \rho_\infty \omega^2 = \operatorname{div}(\rho_\infty \omega u_\infty) = u_\infty \rho_\infty \left( \sum_{i=1}^3 n_i \frac{\partial \omega}{\partial x_i} \right) = u_\infty \rho_\infty \langle \operatorname{grad} \omega, n \rangle, \quad (3.47)$$

where

$$n = \begin{pmatrix} n_1 \\ n_2 \\ n_3 \end{pmatrix} = \begin{pmatrix} \sin \varphi \cos \theta \\ \sin \varphi \sin \theta \\ \cos \theta \end{pmatrix}.$$

Division by  $\rho_\infty u_\infty$  gives the differential equation

$$\langle \operatorname{grad} \omega, n \rangle = -\frac{\beta}{u_\infty} \omega^2. \quad (3.48)$$

A solution of (3.48) is given by

$$\omega(y) = \frac{u_\infty}{\beta} \frac{(n_1 + n_2 + n_3)}{y_1 + y_2 + y_3}. \quad (3.49)$$

This can be easily verified. Straightforward differentiation yields

$$\frac{\partial \omega}{\partial y_i} = -\frac{u_\infty}{\beta} \frac{(n_1 + n_2 + n_3)}{(y_1 + y_2 + y_3)^2},$$

and therefore

$$\begin{aligned}
\langle \text{grad } \omega, n \rangle &= -\frac{u_\infty}{\beta} \left( \sum_{i=1}^3 n_i \frac{(n_1 + n_2 + n_3)}{(y_1 + y_2 + y_3)^2} \right) \\
&= -\frac{u_\infty (n_1 + n_2 + n_3)^2}{\beta (y_1 + y_2 + y_3)^2} \\
&= -\frac{\beta}{u_\infty} \left( \frac{u_\infty}{\beta} \right)^2 \frac{(n_1 + n_2 + n_3)^2}{(y_1 + y_2 + y_3)^2} \\
&= -\frac{\beta}{u_\infty} \omega^2(y).
\end{aligned}$$

Under the assumption formulated above we conclude that  $\omega$  decays at infinity as

$$\lim_{\|x\|_2 \rightarrow \infty} \omega(x) = O\left(\frac{1}{\|x\|_2}\right). \quad (3.50)$$

Inserting the assumptions mentioned above and the representation of  $\omega$  at infinity into (3.4a) we have

$$\text{div}(\rho_\infty k(y) u_\infty) = -\beta^* \rho_\infty k \omega = -\beta^* \rho_\infty k(y) \frac{u_\infty (n_1 + n_2 + n_3)}{\beta (y_1 + y_2 + y_3)},$$

which yields

$$\langle \text{grad } k, n \rangle = -\frac{\beta^* (n_1 + n_2 + n_3) k(y)}{\beta (y_1 + y_2 + y_3)}. \quad (3.51)$$

A solution of this differential equation is given by

$$k(y) = \frac{1}{(y_1 + y_2 + y_3)^{\beta^*/\beta}}, \quad (3.52)$$

which is confirmed by the computation

$$\frac{\partial k}{\partial y_i} = -\frac{\beta^*}{\beta} \frac{1}{(y_1 + y_2 + y_3)^{1+\beta^*/\beta}}$$

and

$$\langle \text{grad } k, n \rangle = -\frac{\beta^* (n_1 + n_2 + n_3)}{\beta (y_1 + y_2 + y_3)^{1+\beta^*/\beta}} = -\frac{\beta^* (n_1 + n_2 + n_3) k(y)}{\beta (y_1 + y_2 + y_3)}.$$

Under the assumptions formulated above we have shown that  $k$  decays at infinity as

$$\lim_{\|x\|_2 \rightarrow \infty} k(x) = O\left(\frac{1}{\|x\|_2^{\beta^*/\beta}}\right). \quad (3.53)$$

For the  $k\omega$ -model of Wilcox 1988 we have

$$\beta^*/\beta = \frac{\frac{9}{100}}{\frac{3}{40}} = \frac{9 \cdot 40}{3 \cdot 100} = \frac{360}{300} = \frac{6}{5} = 1.2,$$

and for the SST-model we approximately get

$$\lim_{\|x\|_2 \rightarrow \infty} \beta^*/\Phi_\beta = \frac{\frac{9}{100}}{\frac{828}{10000}} = \frac{90000}{100 \cdot 828} = \frac{900}{828} \approx 1.086$$

since

$$\lim_{\|x\|_2 \rightarrow \infty} \Phi_\beta = \lim_{\|x\|_2 \rightarrow \infty} (F_1\beta_1 + (1 - F_1)\beta_2) = \beta_2.$$

As a direct result we obtain for the eddy viscosity

$$\lim_{\|x\|_2 \rightarrow \infty} \frac{\rho k}{\omega} = O\left(\frac{1}{\|x\|_2^{\beta^*/\beta - 1}}\right), \quad \text{hence} \quad \lim_{\|x\|_2 \rightarrow \infty} \mu_t = 0. \quad (3.54)$$

In practice we only have a finite domain, and we need to prescribe values for  $k_\infty$  and  $\omega_\infty$ . Because of representations (3.49) and (3.52) we conclude that  $k_\infty$  and  $\omega_\infty$  need to be chosen small, in practice. However, note that a mathematical reasonable choice of such values is an open problem. The clear recommendation is to design the mesh in such a way that the outer boundary is sufficiently far away from the considered body such that appropriate values close to 0 can be chosen. To satisfy (3.54) values for  $k_\infty$  need to include the relation of decay behavior between  $k$  and  $\omega$  at infinity. In particular  $k_\infty$  needs to be smaller than  $\omega_\infty$ .

**Remark 3.4.3** *One often finds in implementations the possibility to define a certain relation of eddy viscosity to laminar viscosity, i.e., it is possible to prescribe*

$$\text{Input parameter at farfield} = \frac{\mu_{t,\infty}}{\mu_{l,\infty}}.$$

*Such an input parameter defines only one condition for determining either  $k_\infty$  or  $\omega_\infty$  and hence a second condition is required. Moreover, due to the analysis presented we have*

$$\lim_{\|x\|_2 \rightarrow \infty} \frac{\mu_{t,\infty}}{\mu_{l,\infty}} = 0, \quad (3.55)$$

*and therefore the prescription of such relation does in general not include information to satisfy condition (3.54). Hence, it is the recommendation to directly define  $k_\infty$  and  $\omega_\infty$  and to conclude from this the relation  $\mu_{t,\infty}/\mu_{l,\infty}$ .*

**Remark 3.4.4** *The decay behavior for the eddy viscosity (3.54) was not formulated in assumptions of this Section 3.4.3, but it is a consequence. The constants  $\beta^*$  and  $\beta$  determine the decay behavior at infinity. For any reasonable model these constants need to be chosen such that  $\mu_t$  vanishes at infinity.*

Finally, we still need to define free-stream values for  $k_\infty$  and  $\omega_\infty$ . Obviously, due to the decay behavior of  $k$  and  $\omega$  these values should depend on the maximum value  $k_{\max}$  and  $\omega_{\max}$  in the field and the distance of the outer boundary to these values. In particular  $k_{\max}$  and  $\omega_{\max}$  are unknown and cannot be used. Hence, we simply choose

$$k_\infty = 9 \cdot 10^{-9} u_\infty^2 \quad \text{and} \quad \omega_\infty = 10^{-6} \left( \frac{u_\infty^2}{\nu_{l,\infty}} \right). \quad (3.56)$$

As a consequence we get

$$\frac{\mu_{t,\infty}}{\mu_{l,\infty}} = \frac{k_\infty}{\omega_\infty} \frac{1}{\nu_{l,\infty}} = \frac{9 \cdot 10^{-9}}{10^{-6}} = 9 \cdot 10^{-3}.$$

Nevertheless, this fixed value in general contradicts (3.55). Assuming the derived decay behavior of  $k$  and  $\omega$  at infinity is correct, the fixed choice (3.56) is in general wrong and boundary value problems formulated using (3.56) do not have a solution.

### 3.5 Nondimensionalization of turbulence flow equations

Throughout this section we denote dimensional variables using the sign  $\hat{\cdot}$ , for example dimensional density is denote by  $\hat{\rho}$ .

With respect to the knowledge that  $\hat{k}$  represents the turbulence kinetic energy and  $\hat{\omega}$  a length scale, the dimensions of these variables are

$$[k] = \frac{\text{m}^2}{\text{sec}^2} \quad \text{and hence} \quad [\omega] = \frac{1}{\text{sec}}.$$

For a complete nondimensionalization of the  $k\omega$ -model of Wilcox (1988) presented in Section 3.1.1 we refer to [17].

Here we present nondimensionalization of the SST-model in integral form documented in Section 3.3. To nondimensionalize  $\hat{k}$  and  $\hat{\omega}$  we choose as reference values

$$k_{\text{ref}} = u_{\text{ref}}^2 \quad \text{and} \quad \omega_{\text{ref}} = \frac{u_{\text{ref}}}{L_{\text{ref}}}. \quad (3.57)$$

Then nondimensional variables may be given by

$$k = \frac{\hat{k}}{u_{\text{ref}}^2} \quad \text{and} \quad \omega = \frac{\hat{\omega}}{\omega_{sc} \omega_{\text{ref}}}, \quad \omega_{sc} = \frac{Re}{\sqrt{\gamma} M_\infty L}, \quad (3.58)$$

where  $\omega_{sc}$  denotes an additional scaling for  $\omega$ .

Note that the functions  $\Gamma_1$ ,  $\Gamma_2$  and  $\Gamma_3$  given in (3.12) and (3.16) are nondimensional by construction. This, for example follows by a straightforward dimensional analysis,

$$\begin{aligned} [\Gamma_1] &= \frac{[\hat{\nu}_l]}{[\hat{d}^2][\hat{\omega}]} = \frac{\frac{\text{m}}{\text{sec}}\text{m}}{\text{m}^2\frac{1}{\text{sec}}} = 1, \\ [\Gamma_3] &= \frac{[\sqrt{\hat{k}}]}{[\hat{\omega}][\hat{d}]} = \frac{\frac{\text{m}}{\text{sec}}}{\frac{1}{\text{sec}}\text{m}} = 1. \end{aligned}$$

Since we have introduced the scaling parameter  $\omega_{sc}$  in (3.58) for proper scaling of  $\omega$  this factor needs to be included in the implementation. Inserting this setting into the definition of  $\Gamma_1$  given in (3.12) we obtain using (3.57) and (3.58)

$$\Gamma_1 = \frac{C_{\Gamma_1}\hat{\nu}_l}{\hat{d}^2\hat{\omega}} = \frac{C_{\Gamma_1}u_{\text{ref}}L_{\text{ref}}\nu_l}{L_{\text{ref}}^2d^2\omega_{sc}\omega_{\text{ref}}\omega} = \frac{C_{\Gamma_1}}{\omega_{sc}}\frac{\nu_l}{d^2\omega}, \quad (3.59)$$

which is a nondimensional value and used for the implementation. For  $\Gamma_3$  we obtain

$$\Gamma_3 = \frac{u_{\text{ref}}\sqrt{k}}{\beta^*\omega_{sc}\frac{u_{\text{ref}}}{L_{\text{ref}}}\omega L_{\text{ref}}d} = \frac{\sqrt{k}}{\beta^*\omega_{sc}\omega d}. \quad (3.60)$$

The dimensional analysis for  $\Gamma_2$  is more complicated, since it involves the analysis for  $C_D$  given in (3.17),

$$\begin{aligned} [C_D] &= \max \left\{ \frac{2\sigma_{\omega_2}[\hat{\rho}]}{[\hat{\omega}]} \left\langle [\text{grad } \hat{k}], [\text{grad } \hat{\omega}] \right\rangle, [\delta] \right\} \\ &= \max \left\{ \frac{\text{kg}}{\text{m}^3}\text{sec} \frac{\text{m}^2}{\text{sec}^2} \frac{1}{\text{m}} \frac{1}{\text{sec}} \frac{1}{\text{m}}, [\delta] \right\} = \max \left\{ \frac{\text{kg}}{\text{m}^3} \frac{1}{\text{sec}^2}, [\delta] \right\}. \end{aligned}$$

This short analysis offers a dilemma in the formulation of the SST-model. The constant  $\delta$ , which is given for example in publications [18, 21, 22] as a fixed value only (see also Sections 3.1.4 and 3.1.5), needs to correspond to the correct physical dimensional quantities. Hence, this constant needs to fit to certain quantities used for nondimensionalization of the variables. Or, vice versa, in a dimensional implementation this constant needs to be chosen with respect to other physical quantities determining the actual problem.

Hence, a choice of  $\delta$  independent of physical quantities required for nondimensionalization yields results depending on the value of  $\delta$ , and these results are in general only reproducible in such code environment. In other words, it cannot be expected that two implementations using different nondimensionalization strategies are in a position to produce comparable results unless  $\delta$  carries information about

nondimensionalization. To choose  $\delta$  such that it takes care of physical relations is discussed below.

To find out a nondimensional form of  $\Gamma_2$ , as a first step, we neglect the constant  $\delta$  in the definition of  $C_D$  in (3.17), that is, we assume

$$\max \left\{ \frac{2\sigma_{\omega_2}\hat{\rho}}{\hat{\omega}} \langle \text{grad } \hat{k}, \text{grad } \hat{\omega} \rangle, \delta \right\} = \frac{2\sigma_{\omega_2}\hat{\rho}}{\hat{\omega}} \langle \text{grad } \hat{k}, \text{grad } \hat{\omega} \rangle.$$

Then we have

$$\begin{aligned} C_D &= \frac{2\sigma_{\omega_2}\rho_{\text{ref}}\rho}{\omega_{sc}\omega_{\text{ref}}\omega} \frac{k_{\text{ref}}\omega_{sc}\omega_{\text{ref}}}{L_{\text{ref}}^2} \langle \text{grad } k, \text{grad } \omega \rangle \\ &= \frac{\rho_{\text{ref}}k_{\text{ref}}}{L_{\text{ref}}^2} \frac{2\sigma_{\omega_2}\rho}{\omega} \langle \text{grad } k, \text{grad } \omega \rangle. \end{aligned} \quad (3.61)$$

Now, for  $C_D$  in nondimensional form we obtain

$$\begin{aligned} C_D &= \max \left\{ \frac{2\sigma_{\omega_2}\rho}{\omega} \langle \text{grad } k, \text{grad } \omega \rangle, \delta \right\} \\ &= \frac{\rho_{\text{ref}}k_{\text{ref}}}{L_{\text{ref}}^2} \max \left\{ \frac{2\sigma_{\omega_2}\rho}{\omega} \langle \text{grad } k, \text{grad } \omega \rangle, \frac{L_{\text{ref}}^2}{\rho_{\text{ref}}k_{\text{ref}}} \delta \right\}. \end{aligned} \quad (3.62)$$

As mentioned above, this short computation shows, that in the nondimensional form of  $C_D$  the constant  $\delta$  needs to include the reference state

$$\delta_{\text{nd}} := \frac{L_{\text{ref}}^2}{\rho_{\text{ref}}k_{\text{ref}}} \delta, \quad (3.63)$$

to ensure that the nondimensional form of the equations is in agreement with its dimensional form. Hence, the constant  $\delta$  needs to be supplemented by  $\delta_{\text{nd}}$  given in (3.63). Using this analysis we conclude that  $\Gamma_2$  is nondimensional,

$$[\Gamma_2] = \frac{4\sigma_{\omega_2} [\hat{\rho}] [\hat{k}]}{[\hat{d}^2] [C_D]} = \frac{\frac{\text{kg}}{\text{m}^3} \frac{\text{m}^2}{\text{sec}^2}}{\text{m}^2 \frac{\text{kg}}{\text{m}^3} \frac{1}{\text{sec}^2}} = 1.$$

More general we can say that any fixed constant introduced in a turbulence model equation needs to be chosen with respect to nondimensionalization of the other variables. Otherwise, such constants act differently with respect to different nondimensionalization strategies. To this author it was interesting to note that in the original publication of the SST-model there were no indications how to treat such constant.

Moreover, such investigation shows up a further effect. In practice, for the application of a nondimensional code, neither the reference values for density  $\rho_{\text{ref}}$ , for

kinetic energy  $k_{\text{ref}} = u_{\text{ref}}^2$  or for reference length  $L_{\text{ref}}$  are known nor are they required (see Section 2.2). In this sense, the SST-model can be only applied this additional data is given. In an environment, where one can get these data in principle, this is not an issue. In case this data is not available and for test purposes one wants to apply the methodology to some artificial test case, additional care needs to be taken to include this data consistently.

Going on with actual implementation of the SST-model we insert expression (3.62) for  $C_D$  into the definition of  $\Gamma_2$  given in (3.16),

$$\begin{aligned}\Gamma_2 &= \frac{4\sigma_{\omega_2}\hat{\rho}\hat{k}}{\hat{d}^2C_D} = \frac{4\sigma_{\omega_2}\rho_{\text{ref}}\rho k_{\text{ref}}k}{L_{\text{ref}}^2 d^2 \frac{\rho_{\text{ref}}k_{\text{ref}}}{L_{\text{ref}}^2} \max\left\{\frac{2\sigma_{\omega_2}\rho}{\omega} \langle \text{grad } k, \text{grad } \omega \rangle, \frac{L_{\text{ref}}^2}{\rho_{\text{ref}}k_{\text{ref}}}\delta\right\}} \\ &= \frac{4\sigma_{\omega_2}\rho k}{d^2 \max\left\{\frac{2\sigma_{\omega_2}\rho}{\omega} \langle \text{grad } k, \text{grad } \omega \rangle, \frac{L_{\text{ref}}^2}{\rho_{\text{ref}}k_{\text{ref}}}\delta\right\}}.\end{aligned}\quad (3.64)$$

Formula (3.64) represents the implemented form for  $\Gamma_2$ . These forms for  $\Gamma_1$ ,  $\Gamma_2$  and  $\Gamma_3$  are used for evaluation of functions  $\Phi_k$ ,  $\Phi_\omega$ ,  $\Phi_\gamma$  and  $\Phi_\beta$  given in (3.18a), (3.18b) and (3.20).

For example, from (3.59), (3.64) and (3.60) we can implement (3.15) by

$$\Gamma_{F_1} = \min \left\{ \frac{1}{\omega_{sc}} \max \left\{ \frac{C_{\Gamma_1}}{\omega_{sc}} \frac{\nu_l}{d^2\omega}, \frac{\sqrt{k}}{\beta^*\omega d} \right\}, \frac{4\sigma_{\omega_2}\rho k}{d^2 \max\left\{\frac{2\sigma_{\omega_2}\rho}{\omega} \langle \text{grad } k, \text{grad } \omega \rangle, \delta_{\text{nd}}\right\}} \right\}.$$

To obtain the nondimensional version of eddy viscosity (3.10) or (3.22) we compute

$$\begin{aligned}\mu_t &= \frac{\hat{\rho}}{\rho_{\text{ref}}} \frac{\hat{k}}{k_{\text{ref}}} \min \left\{ \frac{\omega_{\text{ref}}}{\hat{\omega}}, \frac{\omega_{\text{ref}} a_1}{F_2 \sqrt{2\hat{\Omega} \otimes \hat{\Omega}}} \right\} = \rho k \min \left\{ \frac{\omega_{\text{ref}}}{\hat{\omega}}, \frac{a_1}{F_2 \frac{L_{\text{ref}}}{u_{\text{ref}}} \sqrt{2\hat{\Omega} \otimes \hat{\Omega}}} \right\} \\ &= \frac{1}{\omega_{sc}} \rho k \min \left\{ \frac{1}{\omega}, \frac{\omega_{sc} a_1}{F_2 \sqrt{2\hat{\Omega} \otimes \hat{\Omega}}} \right\}.\end{aligned}$$

The function

$$\nu_t = \frac{1}{\omega_{sc}} k \min \left\{ \frac{1}{\omega}, \frac{\omega_{sc} a_1}{F_2 \sqrt{2\hat{\Omega} \otimes \hat{\Omega}}} \right\}$$

denotes the turbulent kinematic viscosity for the SST-model. Naturally, for the version of 2003 the magnitude of vorticity needs to be supplemented by magnitude of strain rate, that is

$$\mu_t = \rho \nu_t, \quad \nu_t = \frac{1}{\omega_{sc}} k \min \left\{ \frac{1}{\omega}, \frac{\omega_{sc} a_1}{F_2 \sqrt{2\mathcal{S} \otimes \mathcal{S}}} \right\}.$$

As a consequence we obtain that the convective flux and the diffusive flux (3.38) of the SST model can be expressed via

$$f_{c,\text{SST}}(\hat{W}_t, \hat{W}) = u_{\text{ref}} \begin{pmatrix} k_{\text{ref}} & 0 \\ 0 & \omega_{\text{ref}}\omega_{sc} \end{pmatrix} f_{c,\text{SST}}(W_t, W). \quad (3.65)$$

and

$$f_{v,\text{SST}}(\hat{W}_t, \hat{W}) = u_{\text{ref}} \begin{pmatrix} \frac{k_{\text{ref}}}{\omega_{sc}} & 0 \\ 0 & \omega_{\text{ref}} \end{pmatrix} \tilde{f}_{v,\text{SST}}(W_t, W), \quad (3.66)$$

where

$$\tilde{f}_{v,\text{SST}}(W_t, W) := \begin{pmatrix} (\Gamma(T) + \Phi_k \nu_t) \text{grad } k \\ (\Gamma(T) + \Phi_\omega \nu_t) \text{grad } \omega \end{pmatrix},$$

Additionally, for the source terms we obtain

$$Pr_{k,\text{SST}}(\hat{W}_t, \hat{W}) = \frac{u_{\text{ref}}^3}{L_{\text{ref}}\omega_{sc}} 2\nu_t \overline{\mathcal{S}}(u) \otimes \frac{du}{dx} = \frac{u_{\text{ref}}^3}{L_{\text{ref}}\omega_{sc}} Pr_{k,\text{SST}}(W_t, W), \quad (3.67a)$$

$$De_{k,\text{SST}}(\hat{W}_t, \hat{W}) = \frac{u_{\text{ref}}^3 \omega_{sc}}{L_{\text{ref}}} \beta^* k \omega = \frac{u_{\text{ref}}^3 \omega_{sc}}{L_{\text{ref}}} De_{k,\text{SST}}(W_t, W), \quad (3.67b)$$

$$Pr_{\omega,\text{SST}}(\hat{W}_t, \hat{W}) = \frac{u_{\text{ref}}^2}{L_{\text{ref}}^2} 2\Phi_\gamma \overline{\mathcal{S}}(u) \otimes \frac{du}{dx} = \frac{u_{\text{ref}}^2}{L_{\text{ref}}^2} Pr_{\omega,\text{SST}}(W_t, W), \quad (3.67c)$$

$$De_{\omega,\text{SST}}(\hat{W}_t, \hat{W}) = \frac{u_{\text{ref}}^2 \omega_{sc}^2}{L_{\text{ref}}^2} \Phi_\beta \omega^2 = \frac{u_{\text{ref}}^2 \omega_{sc}^2}{L_{\text{ref}}^2} De_{\omega,\text{SST}}(W_t, W), \quad (3.67d)$$

$$\begin{aligned} Di_{\omega,\text{SST}}(\hat{W}_t, \hat{W}) &= \frac{u_{\text{ref}}^2}{L_{\text{ref}}^2} 2(1 - F_1) \sigma_{\omega_2} \frac{1}{\omega} \langle \text{grad } k, \text{grad } \omega \rangle \\ &= \frac{u_{\text{ref}}^2}{L_{\text{ref}}^2} Di_{\omega,\text{SST}}(W_t, W). \end{aligned} \quad (3.67e)$$

Introducing the mapping

$$\begin{aligned} g : D &\rightarrow \hat{D}, \\ x &\mapsto L_{\text{ref}} x, \end{aligned}$$

which maps the computational domain  $D$  to its physical domain  $\hat{D}$ , we have by an application of substitution formula

$$\int_{\hat{D}} v(x) dx = L_{\text{ref}}^m \int_D v(g(y)) dy, \quad (3.68a)$$

$$\int_{\partial \hat{D}} \langle v(y), n(y) \rangle ds(y) = L_{\text{ref}}^{m-1} \int_{\partial D} \langle v(g(y)), n(y) \rangle ds(y). \quad (3.68b)$$

Application of (3.68) to (3.37) using (3.65), (3.66) and (3.67a)–(3.67e) gives

$$\begin{aligned} & \left( \begin{array}{c} \frac{L_{\text{ref}}^2 u_{\text{ref}}^3}{\omega_{sc}} \int_D Pr_{k,\text{SST}} dy - L_{\text{ref}}^2 u_{\text{ref}}^3 \omega_{sc} \int_D De_{k,\text{SST}} dy \\ L_{\text{ref}} u_{\text{ref}}^2 \int_D Pr_{\omega,\text{SST}} dy - L_{\text{ref}} u_{\text{ref}}^2 \omega_{sc}^2 \int_D De_{\omega,\text{SST}} dy + L_{\text{ref}} u_{\text{ref}}^2 \int_D Di_{\omega,\text{SST}} dy \end{array} \right) \\ = & \left( \begin{array}{cc} L_{\text{ref}}^2 u_{\text{ref}}^3 & 0 \\ 0 & \omega_{sc} L_{\text{ref}} u_{\text{ref}}^2 \end{array} \right) \left\{ \frac{d}{dt} V_D(W_t)(t) + R_{c,\partial D,(k,\omega)}(W_t, W)(t) \right\} \\ - & \left( \begin{array}{cc} \frac{1}{\omega_{sc}} L_{\text{ref}}^2 u_{\text{ref}}^3 & 0 \\ 0 & L_{\text{ref}} u_{\text{ref}}^2 \end{array} \right) \int_{\partial D} \langle \tilde{f}_{v,\text{SST}}(W_t, W), n \rangle ds(y). \end{aligned}$$

Multiplication of the whole system with the diagonal matrix

$$\left( \begin{array}{cc} \frac{1}{L_{\text{ref}}^2 u_{\text{ref}}^3} & 0 \\ 0 & \frac{1}{\omega_{sc}} \frac{1}{L_{\text{ref}} u_{\text{ref}}^2} \end{array} \right)$$

gives the mathematically equivalent system of equations

$$\begin{aligned} & \left( \begin{array}{c} \omega_{sc}^{-1} \int_D Pr_{k,\text{SST}} dy - \omega_{sc} \int_D De_{k,\text{SST}} dy \\ \omega_{sc}^{-1} \int_D Pr_{\omega,\text{SST}} dy - \omega_{sc} \int_D De_{\omega,\text{SST}} dy + \omega_{sc}^{-1} \int_D Di_{\omega,\text{SST}} dy \end{array} \right) \\ = & \frac{d}{dt} V_D(W_t)(t) + R_{c,\partial D,(k,\omega)}(W_t, W)(t) \\ - & \left( \begin{array}{cc} \omega_{sc}^{-1} & 0 \\ 0 & \omega_{sc}^{-1} \end{array} \right) \int_{\partial D} \langle \tilde{f}_{v,\text{SST}}(W_t, W), n \rangle ds(y). \end{aligned} \quad (3.69)$$

The system of equations (3.69) is the actual system of equations which is implemented. The scaling parameter  $\omega_{sc}$  is introduced for numerical stability only, and it can also be chosen in different way; for example,  $\omega_{sc} = 1$  is also possible. Then the whole analysis simplifies significantly. The nondimensionalization of the turbulence flow equations was investigated because the system of equations is not one-to-one compared with the original dimensional equations. In particular, when the scaling coefficient  $\omega_{sc}$  is introduced, careful analysis is required to understand in which term this scaling coefficient needs to be incorporated into the nondimensional form.

### 3.6 Logarithmic reformulation of $k\omega$ -models

When solving two equation  $k\omega$ -type or  $k\varepsilon$ -type models one typically runs into the problem of ensuring that turbulence variables remain positive during the iterations. In general, negative values of  $k$  and / or  $\omega$  directly yield a breakdown of the iteration resulting in "Not a number". To avoid such problems, it was suggested in [10] to substitute variables  $k$  and  $\varepsilon$  or  $\omega$  by

$$k = e^{\mathcal{K}}, \quad \varepsilon = e^{\mathcal{E}}, \quad \omega = e^{\Omega}. \quad (3.70)$$

In particular, the sole substitution for  $\omega$  found its way into several implementations, most often in the background of discontinuous Galerkin methods. Here, the idea has been picked up originally by Bassi et al. [4] and reused in [8]. Recently, a further application of such substitution was used in [26].

Naturally, substitutions (3.70) only make sense for nondimensional  $k$ ,  $\varepsilon$  and  $\omega$ . This is not a severe restriction, but depending on the implementation care must be taken. For example, typically implementations want to support flexible restart options. Then knowledge about the output variable such as its kind of nondimensionalization and scaling is necessary to convert the variable.

### 3.6.1 $\ln(k)$ - and $\ln(\omega)$ -formulation

To better understand the logarithmic reformulation and its consequences we present a possible derivation. Starting with equation (3.4b) we substitute  $\omega = e^\Omega$  and apply the chain rule to obtain

$$\begin{aligned}
\frac{\partial(\rho\omega)}{\partial t} + \operatorname{div}(\rho\omega u) &= \frac{\partial(\rho e^\Omega)}{\partial t} + \operatorname{div}(\rho e^\Omega u) \\
&= e^\Omega \frac{\partial\rho}{\partial t} + \rho \frac{\partial e^\Omega}{\partial t} + e^\Omega \operatorname{div}(\rho u) + \langle \operatorname{grad} e^\Omega, \rho u \rangle \\
&= e^\Omega \left( \frac{\partial\rho}{\partial t} + \operatorname{div}(\rho u) \right) + e^\Omega \left( \rho \frac{\partial\Omega}{\partial t} + \langle \operatorname{grad} \Omega, \rho u \rangle \right) \\
&= e^\Omega \left( \frac{\partial\rho}{\partial t} + \operatorname{div}(\rho u) \right) \\
&\quad + e^\Omega \left( \frac{\partial(\rho\Omega)}{\partial t} - \Omega \frac{\partial\rho}{\partial t} + \operatorname{div}(\rho\Omega u) - \Omega \operatorname{div}(\rho u) \right) \\
&= e^\Omega \left( \frac{\partial\rho}{\partial t} + \operatorname{div}(\rho u) \right) \\
&\quad + e^\Omega \left( \frac{\partial(\rho\Omega)}{\partial t} + \operatorname{div}(\rho\Omega u) - \Omega \left( \frac{\partial\rho}{\partial t} + \operatorname{div}(\rho u) \right) \right) \\
&= e^\Omega (1 - \Omega) \left( \frac{\partial\rho}{\partial t} + \operatorname{div}(\rho u) \right) \\
&\quad + e^\Omega \left( \frac{\partial(\rho\Omega)}{\partial t} + \operatorname{div}(\rho\Omega u) \right) \\
&= e^\Omega \left( \frac{\partial(\rho\Omega)}{\partial t} + \operatorname{div}(\rho\Omega u) \right). \tag{3.71}
\end{aligned}$$

The last equality is a consequence of conservation of mass

$$\frac{\partial\rho}{\partial t} + \operatorname{div}(\rho u) = 0. \tag{3.72}$$

For the diffusive term one computes in a similar manner

$$\begin{aligned}
\operatorname{div} [(\mu_l + \sigma_\omega \mu_t) \operatorname{grad} e^\Omega] &= e^\Omega \langle \operatorname{grad} (\mu_l + \sigma_\omega \mu_t), \operatorname{grad} \Omega \rangle \\
&\quad + (\mu_l + \sigma_\omega \mu_t) \operatorname{div} (\operatorname{grad} e^\Omega) \\
&= e^\Omega [\langle \operatorname{grad} (\mu_l + \sigma_\omega \mu_t), \operatorname{grad} \Omega \rangle \\
&\quad + (\mu_l + \sigma_\omega \mu_t) (\|\operatorname{grad} \Omega\|_2^2 + \Delta \Omega)] \\
&= e^\Omega [\operatorname{div} ((\mu_l + \sigma_\omega \mu_t) \operatorname{grad} \Omega) \\
&\quad + (\mu_l + \sigma_\omega \mu_t) \|\operatorname{grad} \Omega\|_2^2],
\end{aligned}$$

where we have used the relation

$$\begin{aligned}
\operatorname{div} (\operatorname{grad} e^\Omega) &= \operatorname{div} (e^\Omega \operatorname{grad} \Omega) \\
&= \langle \operatorname{grad} e^\Omega, \operatorname{grad} \Omega \rangle + e^\Omega \operatorname{div} (\operatorname{grad} \Omega) \\
&= e^\Omega (\|\operatorname{grad} \Omega\|_2^2 + \Delta \Omega).
\end{aligned}$$

Therefore, formally we obtain from (3.4b) and using the substitution for  $\omega$ , the equation for  $\Omega$ ,

$$\begin{aligned}
e^\Omega \left( \frac{\partial (\rho \Omega)}{\partial t} + \operatorname{div} (\rho \Omega u) \right) &= e^\Omega (\operatorname{div} ((\mu_l + \sigma_\omega \mu_t) \operatorname{grad} \Omega)) + \rho Q_{\omega, (k, \omega)} \\
&\quad + e^\Omega (\mu_l + \sigma_\omega \mu_t) \|\operatorname{grad} \Omega\|_2^2.
\end{aligned} \tag{3.73}$$

Division by  $e^\Omega$  yields the equation

$$\begin{aligned}
\frac{\partial (\rho \Omega)}{\partial t} + \operatorname{div} (\rho \Omega u) &= \operatorname{div} ((\mu_l + \sigma_\omega \mu_t) \operatorname{grad} \Omega) + \frac{\rho}{e^\Omega} Q_{\omega, (k, \omega)} \\
&\quad + (\mu_l + \sigma_\omega \mu_t) \|\operatorname{grad} \Omega\|_2^2.
\end{aligned} \tag{3.74}$$

Using (3.6b) the source terms are explicitly given by

$$\frac{\rho}{e^\Omega} Q_{\omega, (k, \omega)} = \rho \left( \alpha \frac{1}{k} \tau \otimes \frac{du}{dx} - \beta e^\Omega \right).$$

Integration and application of Gauss' theorem gives us the integral equation

$$\begin{aligned}
\frac{d}{dt} \int_D \rho \Omega dx &+ \int_{\partial D} \langle \rho \Omega u, n \rangle ds = \int_{\partial D} \langle (\mu_l + \sigma_\omega \mu_t) \operatorname{grad} \Omega, n \rangle ds \\
&+ \int_D \frac{\rho}{e^\Omega} Q_{\omega, (k, \omega)} dx + \int_D (\mu_l + \sigma_\omega \mu_t) \|\operatorname{grad} \Omega\|_2^2 dx.
\end{aligned} \tag{3.75}$$

Using the substitution  $k = e^\mathcal{K}$  in the same way the integral equation

$$\begin{aligned}
\frac{d}{dt} \int_D \rho \mathcal{K} dx &+ \int_{\partial D} \langle \rho \mathcal{K} u, n \rangle ds = \int_{\partial D} \langle (\mu_l + \sigma_k \mu_t) \operatorname{grad} \mathcal{K}, n \rangle ds \\
&+ \int_D \frac{\rho}{e^\mathcal{K}} Q_{k, (k, \omega)} dx + \int_D (\mu_l + \sigma_k \mu_t) \|\operatorname{grad} \mathcal{K}\|_2^2 dx,
\end{aligned} \tag{3.76}$$

for  $\mathcal{K}$  can be derived and the source terms are explicitly given by

$$\frac{\rho}{e^{\mathcal{K}}} Q_{k,(k,\omega)} = \frac{\rho}{e^{\mathcal{K}}} \left( \tau \otimes \frac{du}{dx} - \beta^* e^{\mathcal{K}} e^{\Omega} \right) = \rho \left( \frac{1}{e^{\mathcal{K}}} \tau \otimes \frac{du}{dx} - \beta^* e^{\Omega} \right).$$

In this context we may also assume (3.24), (3.25) and (3.34) to obtain from (3.75) the simplified equation

$$\begin{aligned} \frac{d}{dt} \int_D \Omega dx + \int_{\partial D} \langle \Omega u, n \rangle ds &= \int_{\partial D} \langle (\nu_l + \sigma_\omega \nu_t) \text{grad } \Omega, n \rangle ds \\ &+ \int_D \frac{1}{e^\Omega} Q_{\omega,(k,\omega)} dx + \int_D (\nu_l + \sigma_\omega \nu_t) \|\text{grad } \Omega\|_2^2 dx, \end{aligned} \quad (3.77)$$

and from (3.76)

$$\begin{aligned} \frac{d}{dt} \int_D \mathcal{K} dx + \int_{\partial D} \langle \mathcal{K} u, n \rangle ds &= \int_{\partial D} \langle (\nu_l + \sigma_k \nu_t) \text{grad } \mathcal{K}, n \rangle ds \\ &+ \int_D \frac{1}{e^{\mathcal{K}}} Q_{k,(k,\omega)} dx + \int_D (\nu_l + \sigma_k \nu_t) \|\text{grad } \mathcal{K}\|_2^2 dx. \end{aligned} \quad (3.78)$$

### 3.6.2 Equivalence to original $k\omega$ -models

Now the following questions need to be answered. Consider we supplement in the system of equations (3.36)

- a) either the equation for  $\omega$  by (3.77),
- b) or the equation of  $k$  by (3.78),
- c) or both the equations for  $k$  and  $\omega$  by (3.77) and (3.78):

Is the obtained system of equations equivalent to the original system of equations, that is assume that  $\Omega$ , or  $\mathcal{K}$  or  $(\Omega, \mathcal{K})$  is a solution of the modified system of equations, does the follow that  $\omega$ , or  $k$  or  $(k, \omega)$  is a solution of the original system of equations (3.36)?

Before we go into a more detailed analysis, we first note that the equations (3.75) and (3.76) are derived from (3.4a) and (3.4b), but not from a set of integral equations which are typically implemented and approximately solved. A direct derivation of (3.75) and (3.76) in integral form is generally not possible. Using a representative integral form instead of (3.73), we obtain the integral equation

$$\begin{aligned} \int_D e^\Omega \left( \frac{\partial(\rho\Omega)}{\partial t} + \text{div}(\rho\Omega u) \right) dx &= \int_D e^\Omega (\text{div}((\mu_l + \sigma_\omega \mu_t) \text{grad } \Omega)) dx \\ &+ \int_D (\rho Q_{\omega,(k,\omega)} + e^\Omega (\mu_l + \sigma_\omega \mu_t) \|\text{grad } \Omega\|_2^2) dx. \end{aligned} \quad (3.79)$$

Obviously, a division by  $e^\Omega$  is not possible for (3.79). Hence, the relation between (3.75) and (3.79) is not clear.

A further concern about using substitutions (3.70) is based on the derivation of equations (3.75) and (3.76). To obtain the convective part we assumed that conservation of mass (3.72) holds. Analytically this is correct. On the other hand, in numerical simulations often an early stopping of the iteration is performed or even worse a steady state cannot be reached. In both cases (3.72) is not satisfied. Then, instead of (3.71) we have

$$\begin{aligned} \frac{\partial(\rho\Omega)}{\partial t} + \operatorname{div}(\rho\Omega u) &= e^{-\Omega} \left( \frac{\partial(\rho\omega)}{\partial t} + \operatorname{div}(\rho\omega u) \right) - (1 - \Omega) \left( \frac{\partial\rho}{\partial t} + \operatorname{div}(\rho u) \right) \\ &= \frac{1}{\omega} \left( \frac{\partial(\rho\omega)}{\partial t} + \operatorname{div}(\rho\omega u) \right) - (1 - \ln \omega) \left( \frac{\partial\rho}{\partial t} + \operatorname{div}(\rho u) \right). \end{aligned}$$

This shows that as long as states  $\rho$  and  $\rho u$  do not satisfy (3.72), state  $\Omega$  is smeared by an additional portion of  $\rho u$  introducing a further unknown error component. This statement has at least two effects.

- a) In case the system of equations is not solved to machine accuracy for a given mesh, the equation for conservation of mass is not even solved on discrete level yielding an additional error.
- b) Even if the system of equations is solved to machine accuracy, the equation for conservation of mass is solved only with respect to some discretization error. Such an error component is part of the substitute equation associated with change of variable.

Hence, to get an idea of this additional error component, a reference solution without substitution is required. This consideration questions the whole substitution procedure.

After such global view on substitutions (3.70) we consider a more detailed analysis. The answer for equivalence of  $k$ -equation is straightforward. Since  $k$  represents turbulence kinetic energy, no-slip wall boundary condition is

$$k|_{\partial D_{\text{no-slip}}} = 0.$$

But the consequence of substituting  $e^{\mathcal{K}}$  for  $k$  is

$$k > 0,$$

rather than 0 at the no-slip wall boundary. Therefore, equation (3.78) does not allow for solutions of  $k$ , which need to satisfy no-slip wall boundary condition. Hence, for boundary value problems which relies on such boundary conditions, substituting  $e^{\mathcal{K}}$  for  $k$  cannot be realized equivalently.

To illustrate this fact and to go along with the derivation above, consider the following initial value problem in differential form

$$\frac{df(x)}{dx} = 2x, \quad f(0) = 0,$$

with the unique solution  $f(x) = x^2$ . Now, substituting  $f(x) = e^{g(x)}$  we obtain

$$e^{g(x)}g'(x) = 2x, \quad \text{hence} \quad g'(x) = \frac{2x}{e^{g(x)}},$$

which has the solution

$$g(x) = \ln(x^2 + c), \quad g(x) \neq 0 \quad \text{for all } x,$$

where  $c \geq 0$  is some constant. Hence, the representation  $f(x) = e^{g(x)}$  cannot satisfy condition  $f(0) = 0$ , and therefore, this substitution is too restrictive for the space of solutions required to solve this simple problem. However, in general, we do not solve the differential equation but the corresponding integral equation. Integration of the differential problem, including the initial value, we have the integral equation

$$f(0) + \int_0^x f'(y)dy = f(x), \quad \text{and thus} \quad f(0) + \int_0^x 2ydy = f(x).$$

Again, the solution of this problem is  $f(x) = x^2$ . Introducing the substitution into the integral equation above, one obtains

$$f(0) + \int_0^x e^{g(y)}g'(y)dy = x^2, \tag{3.80}$$

with the general solution  $g(x) = \ln(x^2 + c)$ . To determine the constant  $c$  we transform

$$1 = f(0) + f(1) - f(0) = f(1) = e^{g(1)} = 1 + c, \quad \text{hence} \quad c = 0.$$

So, the integral equation (3.80) has the smooth solution

$$g(x) = \ln x^2, \quad x \in (0, 1],$$

whereas the initial value problem in differential form for  $g$  has no solution. Moreover, for the integral equation we have

$$f(x) = e^{g(x)} = e^{\ln(x^2)} = x^2.$$

**Remark 3.6.1** *Substitution of  $k$  by  $e^k$  cannot be equivalently implemented considering a boundary condition  $k_{\partial D} = 0$ . Such substitution might be considered when all functions are used. However, due to the discussion above, we do not support that substitution of  $k$  is a general and successful way to deal with problems involving  $k\omega$ -models.*

Considerations about substitution of  $\omega = e^\Omega$  are more interesting. To realize the boundary condition for  $\omega$  given by (3.41), one needs to realize a quadratic singularity, i.e.

$$\lim_{h \rightarrow 0^+} \omega(x - hn(x)) = O\left(\frac{1}{h^2}\right), \quad x \in \partial D_{\text{no-slip}}.$$

Using substitution (3.70) for  $\omega$  one obtains for  $\Omega$

$$\lim_{h \rightarrow 0^+} \Omega(x - hn(x)) = \lim_{h \rightarrow 0^+} \ln \omega(x - hn(x)) = -O(\ln h). \quad (3.81)$$

Hence, the quadratic singularity for  $\omega$  has been converted into a logarithmic singularity for  $\Omega$ . It can be assumed that a logarithmic singularity is numerically better to realize than a quadratic one. And hence, at first glance the substitution for  $\omega$  is promising. In detail at least two questions need to be answered:

- a) Are the ansatz functions for  $\omega$  better suited to approximate a function with logarithmic singularity than a function with quadratic singularity?
- b) How does the numerical error behave when comparing a quadrature rule for a logarithmic singularity to a quadratic singularity?

On the other hand, due to the substitution and transformation an additional source term appeared in (3.75) which needs to be discretized, namely

$$\int_D (\mu_l + \sigma_\omega \mu_t) \|\text{grad } \Omega\|_2^2 dx.$$

Because of (3.81) near a no slip wall we have

$$\|\text{grad } \Omega\|_2^2 = O\left(\frac{1}{h^2}\right).$$

Therefore, using the substitution  $\omega = e^\Omega$  converts the the quadratic singularity for  $\omega$  into a logarithmic for  $\Omega$ , on the other hand such behavior is shifted to another term. Naturally, a quadratic singularity is integrable in 3D, but one possible obvious advantage of the substitution is weakened. Finally, we want to shortly summarize the arguments of this paragraph:

- a) Equations for  $\mathcal{K}$  and  $\Omega$  are derived under the assumption that (3.72) is satisfied. As long as this assumption is not satisfied additional unknown error components are introduced.
- b) Due to solid wall boundary condition, the  $k$  substitution of  $\mathcal{K}$  cannot be realized equivalently.
- c) Quadratic singular behavior at a no-slip wall for  $\omega$  is converted to logarithmic singular behavior for  $\Omega$ . Then, the  $\text{grad } \Omega$  quadratic singular behavior needs to be realized.

Concluding, there is no obvious advantage to using variable substitution. Original problems are only shifted. The equivalence of the original system of equations and the system of equations obtained after variable substitution is at least questionable. Hence, before implementing this technique and use them on routine basis, care should be taken about the considerations presented here.

### 3.7 Discussion of SST blending function

We want to close this chapter with a small discussion of the blending functions  $F_2$  and  $\Phi$ , given in (3.11) and (3.13), required to formulate the SST-model. Function  $\Phi$  is introduced to realize a blending in the wake region of the boundary layer. The idea is to multiply a  $k\varepsilon$ -model by  $1 - F_1$ , and a  $k\omega$ -model by  $F_1$  and to add the equations of the models. Details are described in [18]. The function is designed with the following goal: "Starting from the surface, the function should be equal to one over a large portion of the boundary layer in order to preserve the desirable features of the  $k\omega$ -model, but go to zero at the boundary layer edge to ensure the freestream independence of the  $k\varepsilon$ -model." (see [18]). As a consequence, constants are blended with respect to (3.18a), (3.18b), and (3.20). From our perspective, there are several fallacies introduced by this blending.

In [30] and [19] the sensitivity of the  $k\omega$ -model to the freestream value of  $\omega_\infty$  is emphasized. Since (3.50) holds for the original  $k\omega$ -model, the  $k\omega$ -model of 2006 and the SST-model, with respect to the assumptions formulated, the decay behavior of  $\omega$  at infinity holds true for all these models. Hence, the analysis presented does not allow for a conclusion that such observed sensitivity is removed in the SST-model. Just because such sensitivity is observed in some examples discretized on given meshes, this does not allow for general conclusions.

Remark 3.4.3 indicates that in many applications the relation  $\mu_\infty^{\text{rat}} = \frac{\mu_{t,\infty}}{\mu_{l,\infty}}$  is some input parameter. Such input parameter makes sense only on a finite mesh, since in an infinite domain we have (3.55). To determine from  $\mu_\infty^{\text{rat}}$  values for  $k_\infty$  and  $\omega_\infty$ , a further condition is necessary. Let us assume that this further condition is the choice of  $k_\infty$  to determine

$$\omega_\infty = \frac{k_\infty}{\mu_\infty^{\text{rat}} \nu_{l,\infty}}.$$

Then, though  $\mu_\infty^{\text{rat}}$  and  $k_\infty$  are the given choices, one may get the impression that there is sensitivity with respect to  $\omega_\infty$ . But  $\omega_\infty$  is only a consequence of  $\mu_\infty^{\text{rat}}$  and  $k_\infty$ , and it is fully determined by these values. The interesting conjecture is now as follows. For the  $k\omega$ -model we have the decay behavior due to (3.53) of

$$\lim_{\|x\|_2 \rightarrow \infty} k(x) = O\left(\frac{1}{\|x\|_2^{6/5}}\right),$$

and for the SST-model roughly

$$\lim_{\|x\|_2 \rightarrow \infty} k(x) = O\left(\frac{1}{\|x\|_2^{1.086}}\right).$$

On a finite mesh, i.e., the farfield is only a few chord lengths away from the no-slip wall, the expected sensitivity of SST-model with respect to farfield values is even larger compared to the  $k\omega$ -model. At first glance the analysis contradicts the observations. But with a second glance, the lower decay rate allows for choosing larger values  $k_\infty$ . Determining sufficiently large values is necessary in case the discrete farfield is close to the no-slip wall, i.e., only a few chord lengths away. Hence, the observed insensitivity might only be a consequence due to the reduced decay behavior of  $k$  together with the possibility to allow for larger  $k_\infty$  values, which actually need to be guessed. And hence, it can be assumed that the introduced blending actually increases the sensitivity with respect to  $k_\infty$ . Nevertheless, analysis does not give a hint that sensitivity with respect to  $\omega_\infty$  is reduced or even removed.

Secondly, consider the modeling variable  $\omega$  represents a dissipation rate or length scale. Comparing  $k\omega$ -models with the one-equation model of Spalart-Allmaras [25, 1], one may conclude that the length scale is supplemented by the distance to the closest wall. From this viewpoint, one can argue that the differential equation modeling length scale has been decoupled by considering an algebraic magnitude. This concept becomes clear when one considers modeling distance to the closest wall by a further differential equation, namely the Eikonal equation [28]. From this author's viewpoint, it is misleading to follow on the one hand the idea to model length scale using a differential equation, i.e., the  $\omega$ -equation, and on the other hand to exploit in the formulation of the model an algebraic relation, namely distance to the closest wall. To state it directly, actually the SST-model is a three-equation model, and distance to the closest wall and  $\omega$  try to deal with the same effects. Moreover, introduction of distance to the closest wall into the blending function gives the impression one can determine in general a-priori the region where blending should happen, since it is mainly based on an algebraic quantity. Hence, when one considers that a one-equation model of Spalart-Allmaras [25, 1], which is based on distance to the closest wall, is not appropriate, one can conclude by more or less the same argumentation, that the SST-model is not appropriate, since it is based on similar assumptions.

Not to be misunderstood, this is not an argument for using the Spalart-Allmaras model. It is just noted that with respect to this design point both models seem to have similar properties and deficiencies.



## Chapter 4

# Differences of models: Menter-SST vs. Wilcox 2006

Before we go into details, we want to mention that there exists a number of two-equation turbulence models. An overview of a set of models, that are based on a  $k$ -equation, and a length scale equation for  $\omega$ , as well as their connection, is given in the report by Bredberg [5].

In this report we have only presented two of the most well known two-equation turbulence models. When one asks for the motivation to design so many turbulence models, the only obvious answer can be:

**Application of existing models is unsatisfactory.**

To the author's point of view a legitimate counter question is:

**Why does one think a modification of an existing model makes the situation more satisfactory?**

Throughout the literature it seems that much more effort has been put in modifying existing models than trying to understand the differences in all these modifications and their effects. Here, we roughly compare two frequently used two-equation models, the SST-model of Menter and the Wilcox model of 2006.

We only consider a comparison of these models in an analytical way. This has two simple reasons:

- a) In the code used we have only implemented the SST-Model of Menter and the original model of Wilcox from 1988. Thus, the Wilcox  $k\omega$ -model of 2006 has not been of the principal concern yet.
- b) It is the strong belief of this author, that an analytical understanding of the differences gives a much deeper insight and comprehension than a simple comparison of results. Moreover, an analytical investigation has much greater generality than examination of a small limited number of examples.

Nevertheless, to confirm the analytical investigations we give illustrations and plots of examples.

## 4.1 Difference in eddy viscosity

In the context of two-equation turbulence models using variables  $k$  and  $\omega$  there are three different definitions of eddy viscosity. The original definition is given in (3.5), which is replaced in the SST-model by either (3.10) or (3.22) and in the Wilcox model of 2006 by (3.8).

In summary, one can define a generalized eddy viscosity according to the original definition (3.5),

$$\mu_t = \rho \frac{k}{\tilde{\omega}}. \quad (4.1)$$

Depending on the definition of  $\tilde{\omega}$  we may generate the different approaches, for example,

$$\text{Wilcox 1988 and 1998: } \tilde{\omega} = \omega \quad (4.2)$$

$$\text{Wilcox 2006: } \tilde{\omega} = \max \left\{ \omega, C_{\text{lim}} \sqrt{\frac{2\Omega \otimes \Omega}{\beta^*}} \right\}, \quad (4.3)$$

$$\text{SST 1992: } \tilde{\omega} = \max \left\{ \omega, \frac{F_2 \sqrt{2\Omega \otimes \Omega}}{a_1} \right\}, \quad (4.4)$$

$$\text{SST 2003: } \tilde{\omega} = \max \left\{ \omega, \frac{F_2 \sqrt{2\mathcal{S} \otimes \mathcal{S}}}{a_1} \right\}. \quad (4.5)$$

According to (3.10) and (3.22), we have used for (4.4) the simple statement

$$\tilde{\omega} = \min \left\{ \frac{1}{\omega}, \frac{a_1}{F_2 \sqrt{2\Omega \otimes \Omega}} \right\} = \max \left\{ \omega, \frac{F_2 \sqrt{2\Omega \otimes \Omega}}{a_1} \right\} \quad (4.6)$$

and, in the same manner for (4.5)

$$\tilde{\omega} = \min \left\{ \frac{1}{\omega}, \frac{a_1}{F_2 \sqrt{2\mathcal{S} \otimes \mathcal{S}}} \right\} = \max \left\{ \omega, \frac{F_2 \sqrt{2\mathcal{S} \otimes \mathcal{S}}}{a_1} \right\}. \quad (4.7)$$

Comparing definitions (4.4) and (4.5) of SST-model and (4.3) of the Wilcox  $k\omega$ -model of 2006 we observe that their definitions are close. Inserting  $\beta^* = 9/100$  and using (4.3) we get for the Wilcox  $k\omega$ -model of 2006

$$\begin{aligned} \tilde{\omega} &= \max \left\{ \omega, C_{\text{lim}} \sqrt{\frac{2\Omega \otimes \Omega}{\beta^*}} \right\} = \max \left\{ \omega, C_{\text{lim}} \sqrt{\frac{2\Omega \otimes \Omega}{\frac{9}{100}}} \right\} \\ &= \max \left\{ \omega, C_{\text{lim}} \frac{10}{3} \sqrt{2\Omega \otimes \Omega} \right\}. \end{aligned} \quad (4.8)$$

Since the constant  $a_1$  for the SST-model was originally  $a_1 = 3/10$  and then changed to  $a_1 = 31/100$  (see Section 3.1.4), the only major difference in the formulation of the eddy viscosity of the 1992 version of the SST-model and Wilcox  $k\omega$ -model of 2006 is the factor  $C_{\text{lim}}$  and  $F_2$ . Supplementing those, the formulation for eddy viscosity of these models can be directly converted to one another. Hence, for a comparison of eddy viscosity of the Wilcox  $k\omega$ -model of 2006 (3.8) and the SST model we need to understand the difference of the function  $F_2$  given in (3.11) and the constant value  $C_{\text{lim}}$ . As a first step we need to solve the equation

$$F_2 = \tanh\left(\left(\max\{\Gamma_1, 2\Gamma_3\}\right)^2\right) = C_{\text{lim}}. \quad (4.9)$$

Using the definition of  $F_2$  and the representation of hyperbolic tangent,

$$\tanh(x) = 1 - \frac{2}{e^{2x} + 1},$$

we obtain

$$\begin{aligned} C_{\text{lim}} &= 1 - \frac{2}{e^{2x} + 1} \Leftrightarrow \frac{2}{1 - C_{\text{lim}}} - 1 = e^{2x} \\ x &= \frac{\ln\left(\frac{2}{1 - C_{\text{lim}}} - 1\right)}{2}. \end{aligned} \quad (4.10)$$

Choosing for example a value of  $C_{\text{lim}} = 0.95 = 19/20$ , the definition of eddy viscosity is in agreement when

$$\max\{\Gamma_1, 2\Gamma_3\} = \frac{\sqrt{\ln(39)}}{\sqrt{2}} \approx 1.35.$$

Naturally, in general we cannot give a closed solution of the equation (4.9). Such solution requires for example knowledge of  $k$  and  $\omega$ , which are solution of the system of RANS equations. Such remark shows also the dilemma of blending functions involved in the formulation of the turbulence models. Assumptions about solution behavior is introduced into the formulation of the equations without profunded theory that solutions will behave in the assumed range of expectations.

To understand the difference in formulation of eddy viscosity one needs to investigate the acting of function  $F_2$  defined in (3.11). This is general impossible, but, at least some qualitative behavior of the function  $F_2$  can be given. We separate the domain of interest into three regions:

- 1) Behavior of  $F_2$  near a no-slip wall.
- 2) Behavior of  $F_2$  in the farfield.
- 3) Behavior of  $F_2$  in the intermediate region.

To determine the behavior of  $F_2$  in a neighborhood of a no-slip wall we consider expression for  $\Gamma_1$  and  $\Gamma_3$ . Because of (3.41) and (3.42) we have for  $x \in \partial D_{\text{no-slip}}$

$$\lim_{h \rightarrow 0^+} \Gamma_1(x - hn(x)) = \lim_{h \rightarrow 0^+} \frac{C_{\Gamma_1} \nu_l(x - hn(x))}{h^2 \omega(x - hn(x))} = \frac{C_{\Gamma_1} \beta \nu_l(x)}{6 \nu_l(x)} = \frac{1}{6} C_{\Gamma_1} \beta, \quad (4.11)$$

$$\begin{aligned} \lim_{h \rightarrow 0^+} \Gamma_3(x - hn(x)) &= \lim_{h \rightarrow 0^+} \frac{\sqrt{k(x - hn(x))}}{\beta^* \omega(x - hn(x)) h} \\ &= \frac{\beta}{\beta^*} \lim_{h \rightarrow 0^+} \frac{h \sqrt{k(x - hn(x))}}{6 \nu_l(x)} = 0, \end{aligned} \quad (4.12)$$

that is the function  $\Gamma_1$  is bounded in a neighborhood of a no-slip wall and furthermore

$$\lim_{h \rightarrow 0^+} \max \{ \Gamma_1(x - hn(x)), 2\Gamma_3(x - hn(x)) \} = \frac{1}{6} C_{\Gamma_1} \beta. \quad (4.13)$$

Application of (4.13) gives the behavior for the function  $F_2$  in a neighborhood of a no-slip wall boundary

$$\lim_{h \rightarrow 0^+} F_2 = \tanh \left( \lim_{h \rightarrow 0^+} \Gamma_1^2 \right) = \tanh \left( \left( \frac{1}{6} C_{\Gamma_1} \beta \right)^2 \right) \approx 1. \quad (4.14)$$

Figure 4.1 demonstrates the behavior of  $\Gamma_1$  in a neighborhood of a no-slip wall. The picture on the left shows the behavior in a neighborhood of the leading edge, and the one on the right exhibits the behavior near the trailing edge. It is observed that  $\Gamma_1$  is bounded in a neighborhood of a no-slip wall. These examples demonstrate that in a neighborhood of a no-slip wall the predicted behavior indicated in (4.11) and (4.12) of  $\Gamma_1$  and  $\Gamma_3$  is maintained. Behavior of  $F_2$  is plotted in Figures 4.5, 4.6 and 4.7. The picture on the left of Figure 4.5 gives a global overview and on the right a zoom in the leading edge region and in Figure 4.6 on the left a zoom in the trailing edge region is given. As expected, the value is close to 1 near the no-slip wall and decays rapidly away from the no-slip wall.

To determine the behavior in the farfield we obtain using (3.50) and

$$\begin{aligned} \lim_{\|x\|_2 \rightarrow \infty} \Gamma_1 &= C_{\Gamma_1} \lim_{\|x\|_2 \rightarrow \infty} \frac{\nu_l}{\|x\|_2^2 \omega} = O \left( \frac{1}{\|x\|_2} \right), \\ \lim_{\|x\|_2 \rightarrow \infty} \Gamma_3 &= \frac{1}{\beta^*} \lim_{\|x\|_2 \rightarrow \infty} \frac{\sqrt{k}}{\|x\|_2^2 \omega} = O \left( \frac{1}{\|x\|_2^{\beta^*/(2\beta)}} \right). \end{aligned}$$

Hence, roughly speaking, we have at infinity

$$\lim_{\|x\|_2 \rightarrow \infty} \max \{ \Gamma_1, \Gamma_3 \} = \lim_{\|x\|_2 \rightarrow \infty} \Gamma_3.$$

For the intermediate region we need to determine when

$$\Gamma_1 \approx 2\Gamma_3 \quad \text{i.e.} \quad \frac{C_{\Gamma_1}\nu_l}{d^2\omega} \approx 2\frac{\sqrt{k}}{\beta^*\omega d},$$

hence

$$k \approx \frac{(C_{\Gamma_1}\beta^*)^2\nu_l^2}{4d^2} = \frac{2025\nu_l^2}{4d^2} \approx 500\frac{\nu_l^2}{d^2}.$$

This analysis shows that only in a neighborhood of a no-slip wall and the intermediate region we can expect that (4.10) is satisfied for some appropriate given value  $C_{\text{lim}}$ .

The analysis is still misleading, since it is so far only focused on  $C_{\text{lim}}$  and  $F_2$ . Due to (4.3), (4.4) and (4.5) these are only of relevance if

$$0 \leq \frac{\omega}{\tilde{\omega}} < 1,$$

otherwise, we obtain (4.2), and the eddy viscosity is computed as suggested in the original model of 1988. That is, the function  $F_2$  or constant  $C_{\text{lim}}$  are only of relevance if and only if conditions

$$\omega < \frac{F_2\sqrt{2\mathcal{S} \otimes \mathcal{S}}}{a_1} \quad \text{or} \quad \omega < \frac{F_2\sqrt{2\Omega \otimes \Omega}}{a_1} \quad \text{and} \quad \omega < C_{\text{lim}}\sqrt{\frac{2\Omega \otimes \Omega}{\beta^*}} \quad (4.15)$$

are satisfied. This means, as an additional complexity, one needs to understand the behavior of

$$\Omega \otimes \Omega \quad \text{or} \quad \mathcal{S} \otimes \mathcal{S}.$$

compared to behavior of  $\omega$ . Under the assumptions made at infinity all these terms vanish, i.e.

$$\lim_{\|x\|_2 \rightarrow \infty} \mathcal{S} \otimes \mathcal{S} = \lim_{\|x\|_2 \rightarrow \infty} \Omega \otimes \Omega = \lim_{\|x\|_2 \rightarrow \infty} \omega = 0,$$

and behavior (3.54) for eddy viscosity at infinity is recovered. Due to the no-slip wall boundary condition for velocity  $u$  and  $\omega$ , we expect that in a neighborhood of a no-slip wall all the expressions are large. However, as long as  $\mathcal{S} \otimes \mathcal{S}$  or  $\Omega \otimes \Omega$  do not grow faster than  $\omega$  near a no slip wall, eddy viscosity vanishes near a no-slip wall. Hence, behavior of the eddy viscosity at infinity in a neighborhood of a no-slip wall is not influenced replacing  $\omega$  by  $\tilde{\omega}$ , for example, in (4.3), (4.4) and (4.5).

So, such replacement of  $\omega$  by  $\tilde{\omega}$  might be only of relevance in an intermediate section away from the no-slip wall. An illustration of this argument is given in Figure 4.3, where a plot of  $\omega/\tilde{\omega}$  is given for two different test cases, which are described in Sections 6.1 and 6.2. Based on Figure 4.3 we may assume that  $\tilde{\omega}$  replaces  $\omega$  somewhere in the vicinity of the edge of the boundary layer. Moreover, quantitatively, we even notice

$$\frac{4}{5} \leq \frac{\omega}{\tilde{\omega}} \leq 1. \quad (4.16)$$

Notice, this conclusion is without any generality. Nevertheless, we simply get

$$\frac{4}{5}\tilde{\omega} \leq \omega \leq \tilde{\omega}.$$

Using definition (4.1) for the eddy viscosity, compared to its original definition we obtain that

$$\frac{5}{4}\rho\frac{k}{\tilde{\omega}} \leq \rho\frac{k}{\omega}.$$

Consequently, the original eddy viscosity is reduced by something between 0 and 20 percent in some region near the boundary layer edge compared to eddy viscosity of the original model of 1988.

Finally, we discuss our original intention, namely determining the difference between (4.3) and (4.4) or (4.5). This difference is illustrated, for example, in Figure 4.6 on the right. Here, the area where condition (4.15) is satisfied is bounded by a purple line. One can observe that for this test case near the trailing edge, where there is large flow separation, the function  $F_2$  varies between 0.8 and 1.0. Other areas are plotted in Figure 4.7. In these areas there is no separation and the value of  $F_2$  is in between 0.9 and 0.95.

This discussion and examples show that with respect to a solution obtained with the SST-model, in the region near the no-slip wall we roughly have  $F_2 \approx C_{\text{lim}}$ . Nevertheless, using  $F_2$  has impact on the eddy viscosity, and roughly speaking closer to the wall  $\tilde{\omega}^{\text{SST}}$  is larger and further away from the wall it is smaller when compared with  $\tilde{\omega}^{k\omega}$ . Hence, entering the shear layer the eddy viscosity for the SST-model is a little higher, and near the no-slip wall it is a little larger. The effect and difference on the overall solution is not clear and cannot be explicitly stated.

We started this section with the remark that at first glance there is an obvious difference in the formulation of eddy viscosity in the SST-model and the Wilcox model of 2006. On closer examination, these differences turn out to be only a small detail. Even with respect to the original model of 1988, there is a moderate lowering of something between 0 and 20 percent of the eddy viscosity at the boundary layer edge, which is only an estimate.

## 4.2 Production term of $\omega$ -equation

A further obvious difference in the class of  $k\omega$ -models of Wilcox when compared with the SST model of Menter is the limitation of the turbulence production term in the  $\omega$  equation. Since the SST-model uses the kinematic viscosity to formulate the production term for the  $\omega$ -equation, and therefore cancels out, one obtains

$$Pr_{\omega,\text{SST}} = 2\Phi_\gamma \bar{\mathcal{S}} \otimes \frac{du}{dx}. \quad (4.17)$$

To get an impression of the behavior of the expression  $\overline{\mathcal{S}} \otimes \frac{du}{dx}$  a plot of this function is given in Figure 4.8 for two examples. Note that the maximum of these functions is orders of magnitude larger than given in the scale. The scale is chosen to identify the behavior of the function. The expression  $\overline{\mathcal{S}} \otimes \frac{du}{dx}$  is in particular large in a neighborhood of solid wall, where one expects large velocity gradients.

The function  $\Phi_\gamma$  in the SST-model (see (3.20)) is given by

$$\Phi_\gamma = F_1\gamma_1 + (1 - F_1)\gamma_2 = \tanh((\Gamma_{F_1})^4) \gamma_1 + (1 - \tanh((\Gamma_{F_1})^4)) \gamma_2,$$

and function  $F_1$  is defined in (3.14). Since  $\Phi_\gamma$  is a convex combination of  $\gamma_1$  and  $\gamma_2$  the estimate

$$\frac{11}{25} \leq 0.44035 \approx \gamma_2 \leq \Phi_\gamma \leq \gamma_1 \approx 0.55317 \leq \frac{14}{25} \quad (4.18)$$

holds true. Inserting this into (4.17) and using (3.32) we get

$$\frac{22}{25} \overline{\mathcal{S}} \otimes \frac{du}{dx} \leq Pr_{\omega, \text{SST}} \leq \frac{28}{25} \overline{\mathcal{S}} \otimes \frac{du}{dx}.$$

For the original  $k\omega$ -model of 1988 we have

$$Pr_{\omega, (k, \omega)}^{(1988)} = \alpha \frac{\omega}{k} \tau \otimes \frac{du}{dx} = \frac{10}{9} \overline{\mathcal{S}} \otimes \frac{du}{dx}.$$

In the 2006 model of Wilcox one instead has

$$Pr_{\omega, (k, \omega)}^{(2006)} = \alpha \frac{\omega}{k} \tau \otimes \frac{du}{dx} = 2\alpha \frac{\omega}{k} \frac{k}{\tilde{\omega}} \overline{\mathcal{S}} \otimes \frac{du}{dx} = 2\alpha \frac{\omega}{\tilde{\omega}} \overline{\mathcal{S}} \otimes \frac{du}{dx},$$

and the ratio  $\omega/\tilde{\omega}$  is expressed by

$$\frac{\omega}{\tilde{\omega}} = \frac{\omega}{\max\left\{\omega, C_{\text{lim}} \sqrt{\frac{2\Omega \otimes \Omega}{\beta^*}}\right\}} = \begin{cases} 1, & \omega \geq C_{\text{lim}} \sqrt{\frac{2\Omega \otimes \Omega}{\beta^*}}, \\ \frac{\omega}{C_{\text{lim}} \sqrt{\frac{2\Omega \otimes \Omega}{\beta^*}}}, & \omega < C_{\text{lim}} \sqrt{\frac{2\Omega \otimes \Omega}{\beta^*}}. \end{cases}$$

Hence, such limitation generates a blending

$$\frac{\omega}{C_{\text{lim}} \sqrt{\frac{2\Omega \otimes \Omega}{\beta^*}}} \leq \frac{\omega}{\tilde{\omega}} \leq 1, \quad (4.19)$$

and multiplication of (4.19) with  $\alpha = 13/25$  yields,

$$\frac{13}{25} \frac{\omega}{C_{\text{lim}} \sqrt{\frac{2\Omega \otimes \Omega}{\beta^*}}} \leq \frac{13}{25} \frac{\omega}{\tilde{\omega}} \leq \frac{13}{25}. \quad (4.20)$$

Estimate (4.20) of the Wilcox model of 2006 plays the counterpart of (4.18) in the SST-model. Comparison of (4.20) and (4.18) show that on a qualitative level both

the  $k\omega$ -model of Wilcox (2006) and the SST-model of Menter introduce a similar limitation of the production term in the  $\omega$  equation. The limitation seems to be similar both qualitatively and quantitatively. In contrast to  $\Phi_\gamma$ , it is not possible to give an explicit lower bound for  $\omega/\tilde{\omega}$ , but illustration (4.3), which was already exploited in Section 4.1, gives a plot of  $\omega/\tilde{\omega}$ . Inserting (4.16) into (4.20), we obtain

$$0.416 = \frac{134}{25 \cdot 5} \leq \frac{13\omega}{25\tilde{\omega}} \leq \frac{13}{25} = 0.52. \quad (4.21)$$

This estimate is close to estimate (4.18) for the SST-model.

The argumentation of this paragraph shows that the turbulence production term is weighted

- 1) in the Wilcox model of 1988 by a factor  $f = 10/9 \approx 1.111$ ,
- 2) in the SST model by a factor  $0.88 = 22/25 \leq f \leq 28/25 = 1.12$ ,
- 3) in the Wilcox model of 2006 by a factor  $0.832 = 104/125 \leq f \leq 1.04$ .

To the author's point of view these differences are small. One may even ask the question, if one could not simply lower the factor of the original model of 1988 to, say  $f = 1$ , and one may expect in general a similar behavior. It turns out that the differences in limitation of turbulence production term in the  $\omega$ -equation are smaller than originally expected.

### 4.3 Diffusion source term

Contrary to the original model of 1988, both the Wilcox model of 2006 and the SST-model add an additional source term to the  $\omega$ -equation. For the Wilcox model of 2006 this term is given by (3.7),

$$Di_{\omega,(k,\omega)} = \sigma_d \frac{1}{\omega} \langle \text{grad } k, \text{grad } \omega \rangle$$

and for the SST-model by (3.19c),

$$Di_{\omega,\text{SST}} = 2(1 - F_1) \sigma_{\omega_2} \frac{1}{\omega} \langle \text{grad } k, \text{grad } \omega \rangle.$$

Obviously, both share the term

$$\frac{1}{\omega} \langle \text{grad } k, \text{grad } \omega \rangle,$$

and hence the difference is only due to weighting; that is, one needs to compare

$$\sigma_d = \begin{cases} 0, & \langle \text{grad } k, \text{grad } \omega \rangle \leq 0, \\ \frac{1}{8}, & \langle \text{grad } k, \text{grad } \omega \rangle > 0, \end{cases} \quad \text{and} \quad 2 \cdot 0.856(1 - F_1).$$

In a first step, we assume that in the boundary layer of smooth flow, that is near the no-slip wall, the derivatives of  $k$  and  $\omega$  are dominated with respect to the derivative in the  $y$ -direction, that is

$$\text{grad } k = \begin{pmatrix} \frac{\partial k}{\partial x} \\ \frac{\partial k}{\partial y} \\ \frac{\partial k}{\partial z} \end{pmatrix} \approx \begin{pmatrix} 0 \\ \frac{\partial k}{\partial y} \\ 0 \end{pmatrix}, \quad \text{grad } \omega = \begin{pmatrix} \frac{\partial \omega}{\partial x} \\ \frac{\partial \omega}{\partial y} \\ \frac{\partial \omega}{\partial z} \end{pmatrix} \approx \begin{pmatrix} 0 \\ \frac{\partial \omega}{\partial y} \\ 0 \end{pmatrix}.$$

Since  $\omega$  has a singularity (3.41) at the no-slip wall and  $\omega > 0$ , in a neighborhood of the no-slip wall  $\omega$  decreases. On the other hand  $k_{\partial D_{\text{no-slip}}} = 0$  and  $k > 0$ ,  $k$  is increasing in a neighborhood of the no-slip wall. Hence, in a neighborhood of a no-slip wall we have

$$\langle \text{grad } k, \text{grad } \omega \rangle \approx \frac{\partial k}{\partial y} \frac{\partial \omega}{\partial y} < 0. \quad (4.22)$$

Hence, in the neighborhood of the no-slip wall,  $\sigma_d = 0$  and the additional diffusion term in the Wilcox model of 2006 is not active.

For the SST-model, in a first step we conclude that due to (4.22)

$$C_D = \max \left\{ \frac{2\sigma_{\omega_2}\rho}{\omega} \langle \text{grad } k, \text{grad } \omega \rangle, \delta \right\} = \delta$$

in a neighborhood of the no-slip wall and therefore

$$\Gamma_2 = \frac{4\sigma_{\omega_2}\rho k}{d^2 C_D} = \frac{4\sigma_{\omega_2}\rho k}{d^2 \delta} \rightarrow \infty, \quad d \rightarrow 0.$$

Because of (4.11) and (4.12) we obtain in a neighborhood of no-slip wall

$$\Gamma_{F_1} = \min \{ \max \{ \Gamma_1, \Gamma_3 \}, \Gamma_2 \} \min \left\{ \frac{1}{6} C_{\Gamma_1}, \frac{4\sigma_{\omega_2}\rho k}{d^2 \delta} \right\} \approx \frac{1}{6} C_{\Gamma_1} \beta,$$

and therefore

$$F_1(\Gamma_{F_1}^4) \approx \tanh \left( \left( \frac{1}{6} C_{\Gamma_1} \right)^4 \right) \approx 1,$$

consequently

$$2 \cdot 0.856 (1 - F_1) \approx 0$$

in a neighborhood of a no-slip wall. That is, behavior near a no-slip wall is similar for both models. An example plot of function  $F_1$  is given in Figure 4.9. Moreover, Figure 4.4 demonstrates the behavior of  $\Gamma_3$  in a neighborhood of a no-slip wall. The picture on the left shows the behavior in a neighborhood of the leading edge, and on the right of the trailing edge. It is observed that  $\Gamma_3$  tends to zero in the near no-slip wall behavior. The function reaches its maximum isobar a short distance away from the no-slip wall.

At infinity we can assume that

$$\langle \text{grad } k, \text{grad } \omega \rangle \approx 0,$$

and so the diffusion term for both the Wilcox model of 2006 and the SST-model is negligible. It remains of interest to investigate function  $F_1$  for some intermediate region of the boundary layer.

Since  $k \geq 0$ ,  $k|_{\partial D_{\text{no-slip}}} = 0$  and  $k$  satisfies (3.53) we conclude that there may exist a region where

$$\langle \text{grad } k, \text{grad } \omega \rangle > 0, \quad (4.23)$$

and the value can be so large that

$$C_D = \frac{2\sigma_{\omega_2}\rho}{\omega} \langle \text{grad } k, \text{grad } \omega \rangle > \delta.$$

Note, it cannot be guaranteed that such a region exists. However, if such a region does not exist the argumentation above holds true and the additional diffusion source term is negligible. So, we now assume that (4.23) holds. Figure 4.10 gives a plot of the cross diffusion term in a neighborhood of a no-slip wall. The plot indicates the existence of such regions.

Actually, a prediction of (3.15) is in general impossible, since

$$\Gamma_{F_1} = \min \{ \max \{ \Gamma_1, \Gamma_3 \}, \Gamma_2 \}$$

depends on the solution of the full system of equations, which is impossible to predict for some inner region. However, at least quasi as a postprocessing step, we may evaluate and plot function  $F_1$  depending on (3.15). To this end we again refer to Figure 4.9. Clearly, there exists a small intermediate region where  $F_1$  drops to 0, and cross-correlated with Figure 4.10 the cross diffusion term is weighted in the SST-model with a factor of about

$$2 \cdot 0.856 = 1.712.$$

Compared to the Wilcox model the cross diffusion term is only weighted by

$$\frac{1}{8} = 0.125,$$

which is roughly about an order of magnitude smaller. Since the cross diffusion term itself is comparably small, the impact of this difference cannot be predicted. However, compared to the other differences in the model this difference seems to be comparably more significant.

## 4.4 Weighting of viscous flux terms

As the final difference to consider, notice that in the SST model the viscous flux term for  $k$ -equation is weighted by  $\Phi_k$  given in (3.18a) and for  $\omega$ -equation by  $\Phi_\omega$  given in (3.18b). Hence, following the discussion above we have

$$\begin{aligned} 0.85 &\leq \Phi_k \leq 1, \\ 0.5 &\leq \Phi_\omega \leq 0.856, \end{aligned}$$

and the distribution of the values follows the argumentation for function  $F_1$  discussed above. For the Wilcox model the values weighting viscous flux terms for  $k$ -equation and  $\omega$ -equation are fixed and given by

$$\sigma_k = 0.6, \quad \sigma_\omega = 0.5.$$

Hence, weighting of viscous flux terms represents some further difference of the models.

## 4.5 Strain rate and vorticity

One major change from the 1992 version of the SST-model compared to the 2003 version of the model is replacing the magnitude of vorticity  $\sqrt{2\Omega \otimes \Omega}$  by the magnitude of strain rate  $\sqrt{2S \otimes S}$  in the definition of eddy viscosity. That is, (3.10) was replaced by (3.22). The authors do not give an obvious explanation for this change in publication [22]. To better understand this change, straightforward computations give for the magnitude of strain rate

$$\begin{aligned} S \otimes S &= \frac{1}{4} \sum_{j=1}^3 \sum_{i=1}^3 \left( \frac{\partial u_i}{\partial x_j} + \frac{\partial u_j}{\partial x_i} \right) \left( \frac{\partial u_j}{\partial x_i} + \frac{\partial u_i}{\partial x_j} \right) \\ &= \frac{1}{4} \sum_{i,j=1}^3 \left( \frac{\partial u_i}{\partial x_j} + \frac{\partial u_j}{\partial x_i} \right)^2 \end{aligned}$$

and for the magnitude of vorticity

$$\begin{aligned} \Omega \otimes \Omega &= \frac{1}{4} \sum_{j=1}^3 \sum_{i=1}^3 \left( \frac{\partial u_i}{\partial x_j} - \frac{\partial u_j}{\partial x_i} \right) \left( \frac{\partial u_j}{\partial x_i} - \frac{\partial u_i}{\partial x_j} \right) \\ &= \frac{1}{4} \sum_{i,j=1, i \neq j}^3 \left( \frac{\partial u_i}{\partial x_j} - \frac{\partial u_j}{\partial x_i} \right)^2. \end{aligned}$$

An exchange of this term actually means that one has to understand the difference in maxima in (4.4) and (4.5), that is,

$$\begin{aligned}
S \otimes S - \Omega \otimes \Omega &= \frac{1}{4} \left( \sum_{i=1}^3 \left( 2 \frac{\partial u_i}{\partial x_i} \right)^2 \right) + \frac{1}{4} \left( \sum_{i,j=1, i \neq j}^3 \left( \frac{\partial u_i}{\partial x_j} + \frac{\partial u_j}{\partial x_i} \right)^2 \right) \\
&\quad - \frac{1}{4} \left( \sum_{i,j=1, i \neq j}^3 \left( \frac{\partial u_i}{\partial x_j} - \frac{\partial u_j}{\partial x_i} \right)^2 \right) \\
&= \sum_{i=1}^3 \left( \frac{\partial u_i}{\partial x_i} \right)^2 + \sum_{i,j=1, i \neq j}^3 \frac{\partial u_i}{\partial x_j} \frac{\partial u_j}{\partial x_i} \tag{4.24}
\end{aligned}$$

$$= \frac{du}{dx} \otimes \frac{du}{dx}. \tag{4.25}$$

Now, we need to ask at least the two following question:

- a) In what kind of solutions of the Navier-Stokes equations is (4.25) so large that it influences the definition of  $\tilde{\omega}$  in (4.5) compared to (4.4) significantly.
- b) Assume we have a solution of the Navier-Stokes equation where (4.25) is comparably large. In which way does the change of  $\tilde{\omega}$  influence solutions of the turbulence model; and then, conclusively, in which way does this influence the obtained eddy viscosity and a solution of the coupled system of mean flow and turbulence flow equations?

In general, it is impossible to assess the influence of one single term. The change of a single term influences the rest of equations in a nonlinear fashion. As long as no salient reasons are given for these changes, formulae determining the models appear to be arbitrary.

From the computations performed for this report and the results obtained we could not find any major difference for taking one of the formula, either  $\Omega \otimes \Omega$  or  $S \otimes S$  for  $\tilde{\omega}$ . Hence, these suggested changes seem to be a source for confusion.

## 4.6 Summary of differences

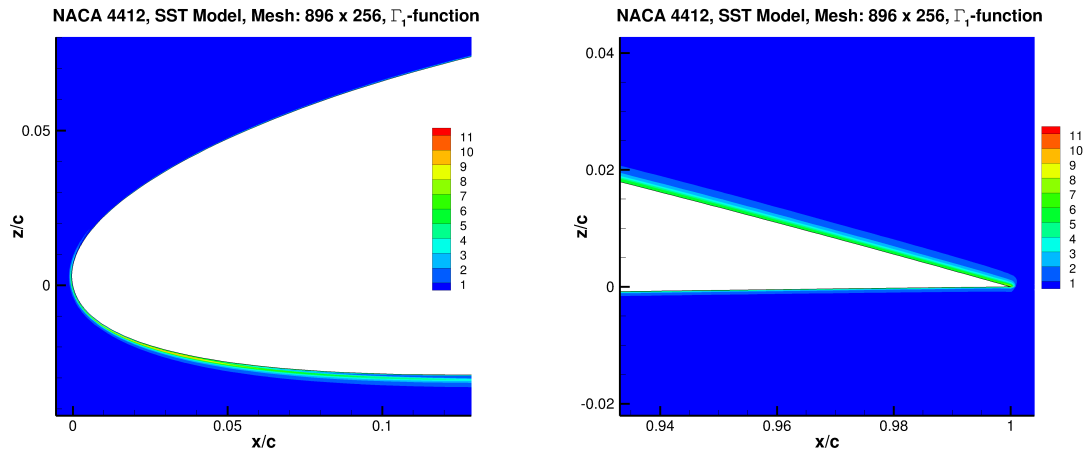
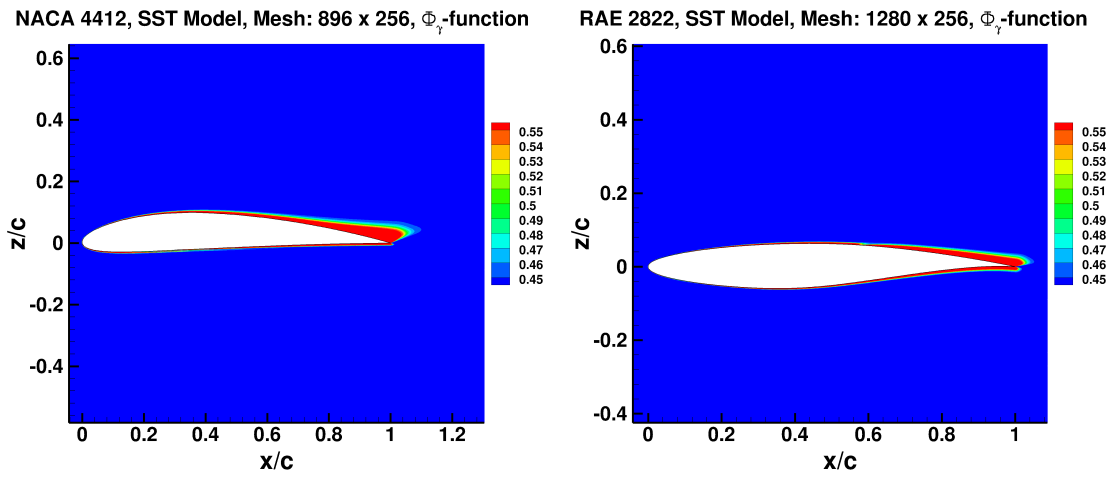
In this section an investigation has been performed considering differences in the type of  $k\omega$ -models considered. It turns out that several of the obvious differences are negligible and only details in formulation. Though, formally the SST-model is derived by combination of an  $k\omega$  and  $k\varepsilon$ -model its difference to a purely  $k\omega$ -type model is little.

One significant difference found is weighting of the cross diffusion source term. The impact of this difference in weighting is hard if not impossible to assess. Even

more, with all the reformulations and modifications done, one clearly has to state the question: What kinds of differences in the models are causing differences in the observed results?

And the final question stated is not only of importance for the different kinds of models, but also for example for the modifications which have been included into one type of problems, such as supplementing magnitude of vorticity by magnitude of strain rate.

The discussion about differences in the models is closed with the following remark. Along the lines of understanding of two-equation models all models suggested by Wilcox determine length scale, that is dissipation rate, by a differential equation only. The models of Wilcox do not use algebraic determined values. The SST-model of Menter requires additionally the closest distance to the no-slip wall. This can be viewed as a redundant information. Maybe usage of this algebraic magnitude is the major difference between the models. Considering distance to the closest wall modeled by the Eikonal equation, one can view the SST-model as a three-equation model where one equation can be solved independently. If this additional information cannot be exploited to advantage when compared with  $k\omega$ -models not including this information, to the author's point of view the question needs to be answered, why there is need for models constructed with this additional information.

Figure 4.1:  $\Gamma_1$  in a neighborhood of a no-slip wallFigure 4.2:  $\Phi_\gamma$  in a neighborhood of a no-slip wall

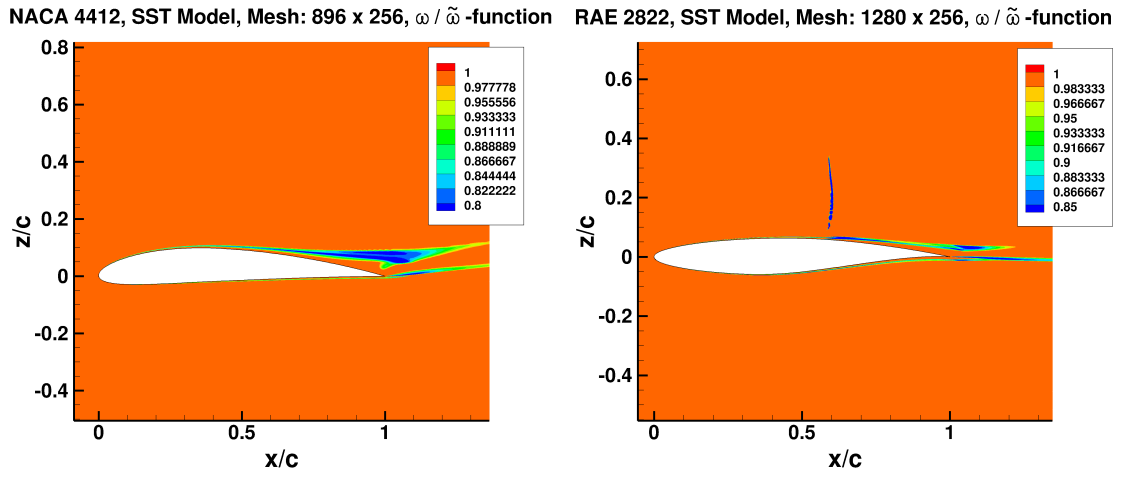


Figure 4.3: Function  $\omega/\tilde{\omega}$  in a neighborhood of a no-slip wall

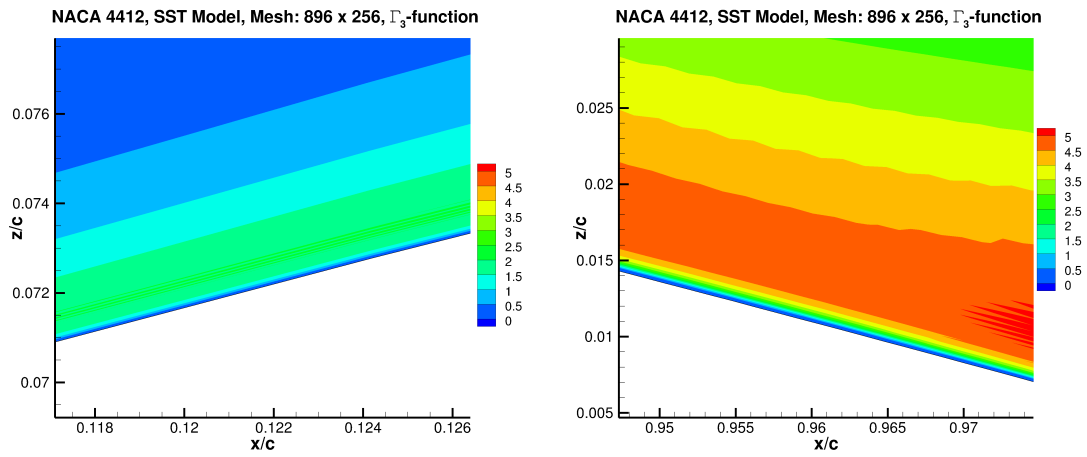


Figure 4.4:  $\Gamma_3$  in a neighborhood of a no-slip wall

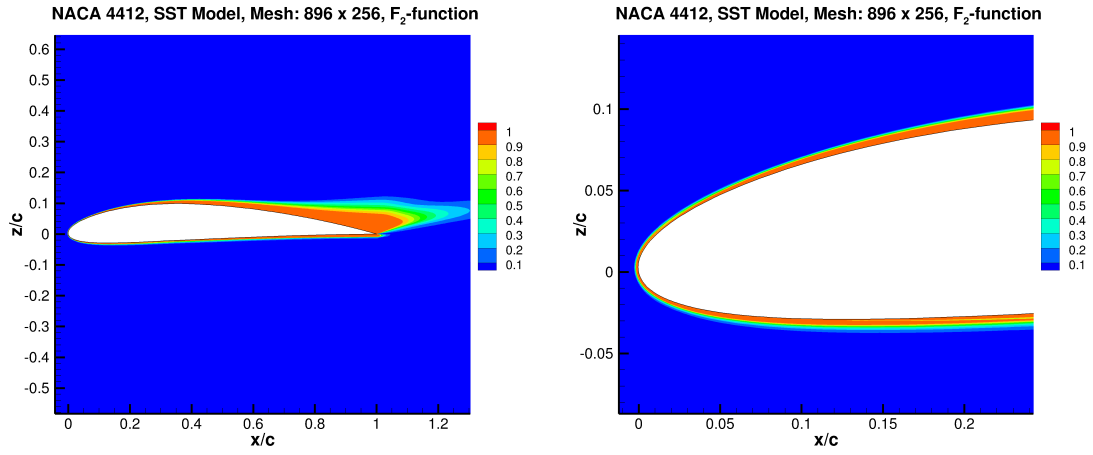


Figure 4.5: Left: Plot of  $F_2$  in a neighborhood of the airfoil. Right: Plot of  $F_2$  in a neighborhood of the leading edge

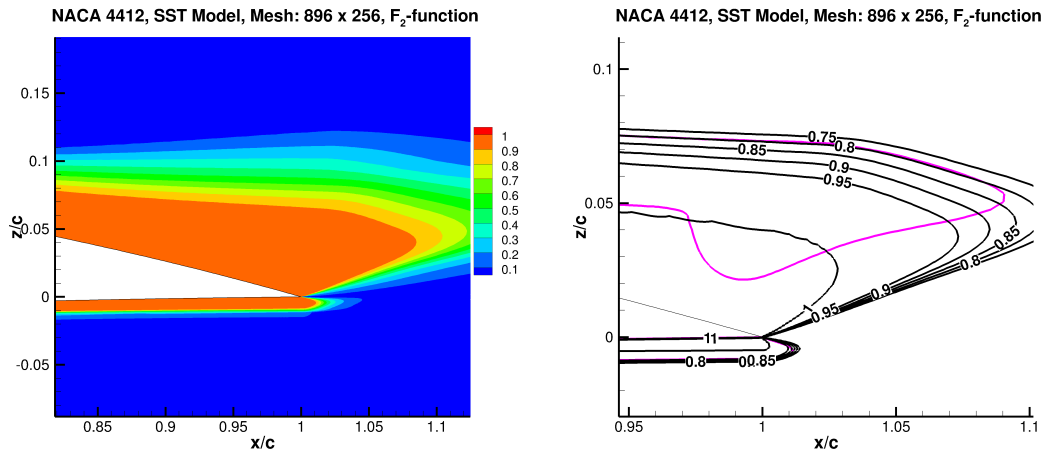


Figure 4.6: Left: Plot of  $F_2$  in a neighborhood of the trailing edge. Right: Plot of active region of  $F_2$ , i.e.  $\omega < \frac{F_2 \sqrt{2S \otimes S}}{a_1}$  marked by the purple line

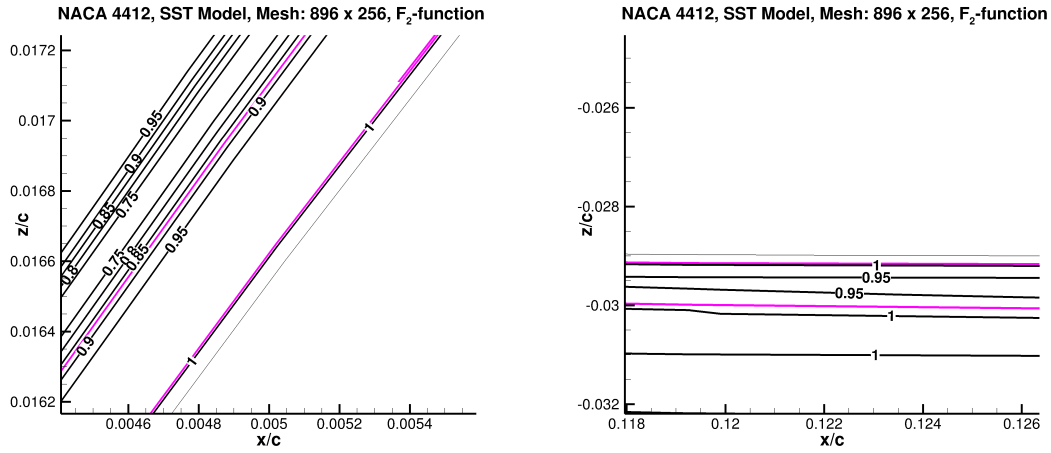


Figure 4.7: Left: Plot of active region  $F_2$  in a neighborhood of the leading edge. Right: Plot of active region of  $F_2$ , i.e.  $\omega < \frac{F_2 \sqrt{2S \otimes S}}{a_1}$  marked by the purple line

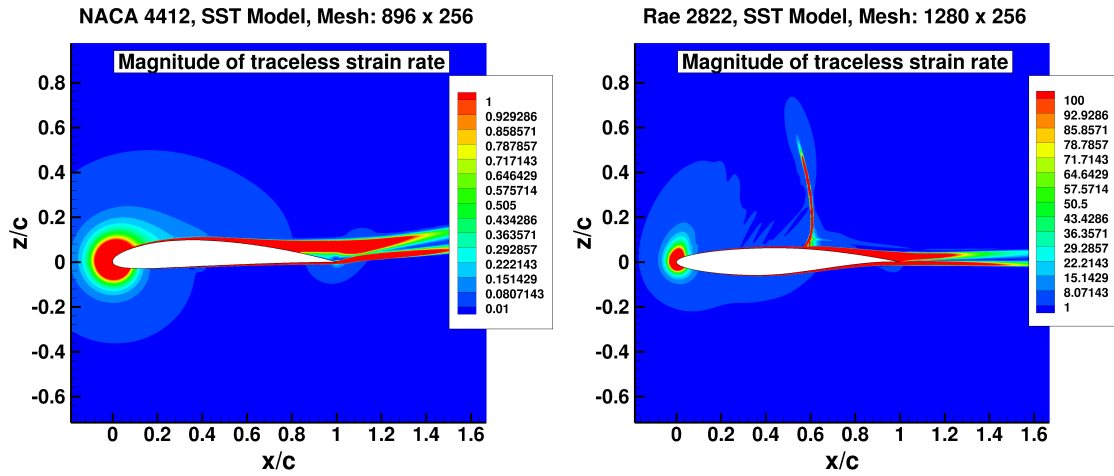
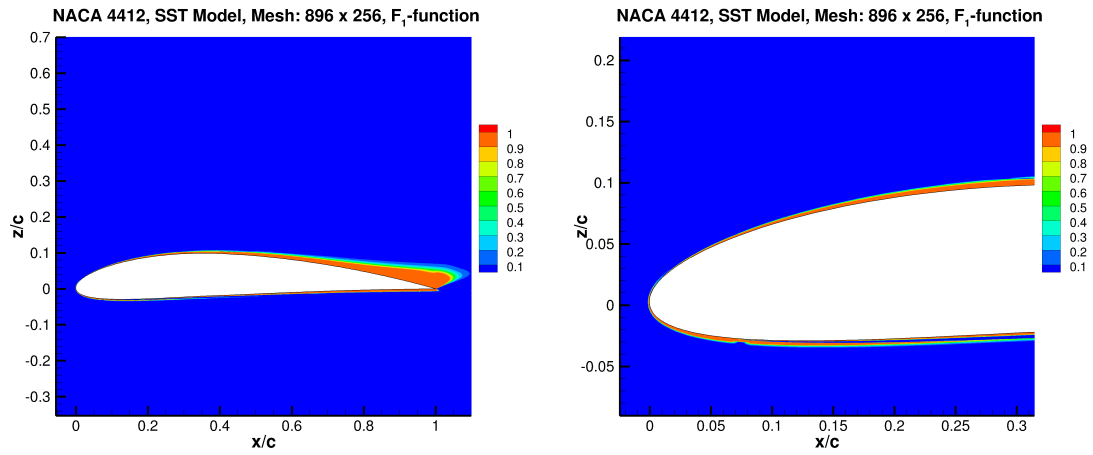
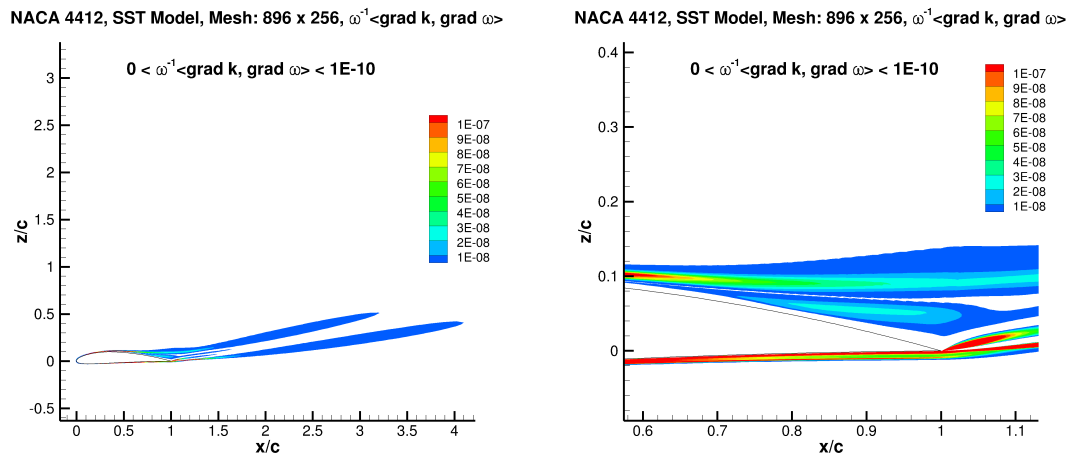


Figure 4.8: Magnitude of traceless strain rate in a neighborhood of a no-slip wall

Figure 4.9:  $F_1$  in a neighborhood of a no-slip wallFigure 4.10:  $\frac{1}{\omega} \langle \text{grad } k, \text{grad } \omega \rangle$  in a neighborhood of a no-slip wall

# Chapter 5

## Discretization strategy and solution algorithm

For a detailed presentation of discretization and solution algorithm we refer to the monologue [17].

### 5.1 Discretization

The discretization strategy followed employs a node centered, finite volume spatial discretization on meshes with mixed element types. The computational mesh, which is often called a dual mesh, is constructed by the primary grid in a preprocessing step. The dual grid forms the control volumes with the unknowns at vertices of the primary grid. Figure 5.1 shows a triangular grid and the generated computational mesh.

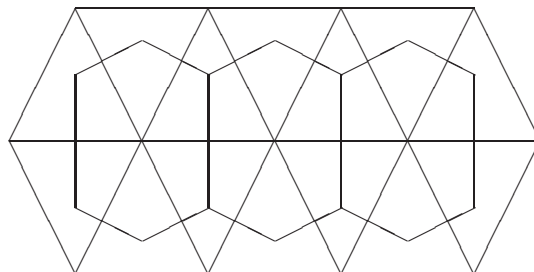


Figure 5.1: Example of a triangular primary grid and its dual grid

For the discretization the distinction between the primary and the dual grid is not necessary. It only emphasizes that the grid which is generated by a mesh generation tool might be different than the actual computational mesh. For the discretization strategy followed in this report the required geometric data of the given mesh are:

- a) the normal vector for each control surface,
- b) the surface area for each control surface,
- c) the barycenter for each control volume,
- d) the distance to the closest wall for each control volume.

Note, technically it does not matter whether this data was generated directly from a given primary mesh or by the introduction of a further intermediate step used to construct a computational mesh. On the other hand, with respect to accuracy, note that solutions obtained on these different computational meshes may differ significantly due to the different geometric data. This is in particular true for coarse grids, where an obtained solution might be far away from being mesh converged. In particular, the actual mesh geometry has to be considered for the formulation of the discretization of boundary conditions. The construction of the dual mesh yields so-called half-cells near the boundary, which directly results in an undesired jump in the metrics. An illustration of this issue as well as a discussion of the discretization strategies according to this property are given in [17].

To formulate the complete set of equations, we define the coefficient vector

$$\mathbf{W}_{\text{mean}}(t) := (W_1(t), \dots, W_{N_{\text{elem}}}(t))$$

to represent the ansatz for function for the mean flow equation. Considering a representation of the ansatz  $(k_h, \omega_h)$  we denote the corresponding coefficient vector by

$$\mathbf{W}_t(t) := ((k_1(t), \omega_1(t)), \dots, (k_{N_{\text{elem}}}(t), \omega_{N_{\text{elem}}}(t))).$$

Then, the discretization of the mean flow equations (2.1) together with the turbulent flow equations (3.36) or (3.37) yields the system of ordinary differential equations

$$\frac{d}{dt} \begin{pmatrix} \mathbf{W}(t) \\ \mathbf{W}_t(t) \end{pmatrix} = \begin{pmatrix} -\mathbf{M}_{\text{mean}}^{-1} \mathbf{R}_{\text{mean}}(\mathbf{W}(t), \mathbf{W}_t(t)) \\ -\mathbf{M}_{\text{turb}}^{-1} \mathbf{R}_{\text{turb}}(\mathbf{W}(t), \mathbf{W}_t(t)) \end{pmatrix}, \quad (5.1)$$

where

$$\begin{aligned} \mathbf{M}_{\text{mean}} &:= \text{diag}(\text{diag}(\text{vol}(\Omega_i))) \in \mathbb{R}^{5N_{\text{elem}} \times 5N_{\text{elem}}} \\ \mathbf{M}_{\text{turb}} &:= \text{diag}(\text{diag}(\text{vol}(\Omega_i))) \in \mathbb{R}^{2 \cdot N_{\text{elem}} \times 2 \cdot N_{\text{elem}}} \end{aligned}$$

denote the mass matrix for mean and turbulent flow equations. Depending on the actual mesh size, (5.1) represents a large scale, time dependent set of nonlinear

equations which need to be iterated in time. To approximately solve (5.1) we assume that the mean flow equations depend only on  $\mathbf{W}$  and  $\mathbf{W}_t$  acts only as a parameter here, whereas the turbulent flow equations depend only on  $\mathbf{W}_t$ , and  $\mathbf{W}$  acts as a parameter. Hence, we rewrite system (5.1) as

$$\frac{d}{dt}\mathbf{W}(t) = -\mathbf{M}_{\text{mean}}^{-1}\mathbf{R}_{\text{mean}}(\mathbf{W}(t); \mathbf{W}_t(t)) \quad (5.2a)$$

$$\frac{d}{dt}\mathbf{W}_t(t) = -\mathbf{M}_{\text{turb}}^{-1}\mathbf{R}_{\text{turb}}(\mathbf{W}_t(t); \mathbf{W}(t)). \quad (5.2b)$$

Equations (5.2a) and (5.2b) are then solved sequentially. It is not our goal to approximate time accurate solutions of (5.1), but our main interest is the robust approximation of a steady state solution. That is, we postulate that the left hand side of (5.1) vanishes, and that it satisfies

$$\frac{d}{dt}\mathbf{W}(t) = 0, \quad \frac{d}{dt}\mathbf{W}_t(t) = 0.$$

With respect to this assumption the system (5.2) simplifies to

$$0 = \mathbf{R}_{\text{mean}}(\mathbf{W}(t); \mathbf{W}_t(t)) \quad (5.3a)$$

$$0 = \mathbf{R}_{\text{turb}}(\mathbf{W}_t(t); \mathbf{W}(t)), \quad (5.3b)$$

which represents a nonlinear set of equations which needs to be solved. In principle, Newton's method is suggested to be the straightforward way to solve this set of equations.

## 5.2 Multistage implicit Runge-Kutta smoother

To approximately solve the algebraic system of equations (5.3) we apply a nonlinear multigrid method [27] called the Full Approximation Scheme (FAS). The approach to realize the multigrid components is based on the aggregation of the degrees of freedom. This procedure is realized by the agglomeration of control volumes. It is the advantage of such a procedure that the coarse grid problem can be constructed directly from the finest grid level data. To this end, in a first step, the construction of coarse grid levels needs to be defined. Second, the formulation of the nonlinear multigrid together with projection and interpolation operators to transfer the data from one grid level to the next are required. And, finally, an effective smoother needs to be derived. Note that a robust and efficient nonlinear multigrid algorithm can only be expected in cases where all these components are synchronized to each other. One cannot expect a robust and reliable algorithm if these components are developed independently of each other.

As a suitable smoother for nonlinear multigrid to solve the discretized flow equations (5.3a) and (5.3b), we consider the time dependent equations (5.2a) and (5.2b).

These are iterated in time using a multistage implicit Runge-Kutta smoother:

$$\begin{aligned}
\mathbf{W}^{(0)} &:= \mathbf{W}^{\text{T}_n} \\
\mathbf{W}^{(1)} &= \mathbf{W}^{(0)} - \alpha_{21} \Delta t \left[ \frac{dg_1(k^{(0)})}{dk} \right]^{-1} \mathbf{M}^{-1} \mathbf{R}(\mathbf{W}^{(0)}) \\
&\vdots \\
\mathbf{W}^{(s)} &= \mathbf{W}^{(0)} - \alpha_{s+1,s} \Delta t \left[ \frac{dg_s(k^{(0)})}{dk} \right]^{-1} \mathbf{M}^{-1} \mathbf{R}(\mathbf{W}^{(s-1)}) \\
\mathbf{W}^{\text{T}_{n+1}} &= \mathbf{W}^{(s)}.
\end{aligned} \tag{5.4}$$

Algorithm (5.4) indicates that for each stage the linear equation

$$\frac{dg_j(k^{(0)})}{dk} \mathbf{h}_j = \alpha_{j+1,j} \Delta t \mathbf{M}^{-1} \mathbf{R}(\mathbf{W}^{(j-1)})$$

needs to be solved. This can be equivalently formulated by

$$\left( (\Delta t)^{-1} \mathbf{M} + \alpha_{jj} \frac{d\mathbf{R}}{d\mathbf{W}}(\mathbf{W}^{(j-1)}) \right) \mathbf{h}_j = \alpha_{j+1,j} \mathbf{R}(\mathbf{W}^{(j-1)}). \tag{5.5}$$

In a general context, Algorithm (5.4) may be interpreted as a kind of Rosenbrock method (see e.g. [7]). However, within this report, we use this kind of method quite differently, namely to approximate steady-state solutions of (5.2a) and (5.2b) and to approximately solve (5.3a) and (5.3b). Although we are focused in this work on steady-state problems, such an algorithm can be incorporated into a dual time-stepping method, which solves for the unsteady solution by computing a sequence of steady-state solutions corresponding to each time step.

Additional acceleration techniques can be incorporated into the scheme. Here, we consider the following convergence acceleration techniques. First, for steady state computations the time step  $\Delta t$  in (5.5) is replaced (see also for example [16]) by some local time step  $\Delta T := \text{diag}(\text{diag}(\Delta t_i)) \in \mathbb{R}^{N_{\text{eq}} N \times N_{\text{eq}} N}$ . Here  $N_{\text{eq}} = 5$  for the mean flow equations and  $N_{\text{eq}} = 2$  for the turbulence flow equations. As local time step we choose an approximation to the spectral radius of the diagonal blocks of  $\frac{d\mathbf{R}}{d\mathbf{W}}$ , more exact

$$\begin{aligned}
\Delta t_i &:= \text{CFL} \cdot \text{vol}(D_i) \left[ \sum_{j \in \mathcal{N}(i)} \text{svol}(e_{ij}) \left( \rho \left( \frac{\partial \mathcal{H}^{1st, \text{Roe}}}{\partial W_i} \right) \right. \right. \\
&\quad \left. \left. + C_v \rho \left( \frac{\partial \langle f_v(W_i, W_j), n_{e_{ij}} \rangle}{\partial W_i} \right)^{\text{TSL}, \mu = \text{const}} \right) \right]^{-1}, \quad C_v := 8,
\end{aligned}$$

where

$$\begin{aligned} & \sum_{j \in \mathcal{N}(i)} \text{svol}(e_{ij}) \left( \rho \left( \frac{\partial \mathcal{H}^{1st, \text{Roe}}}{\partial W_i} \right) + \rho \left( \frac{\partial \langle f_v(W_i, W_j), n_{e_{ij}} \rangle}{\partial W_i} \right)^{\text{TSL}, \mu = \text{const}} \right) \\ &= \sum_{j \in \mathcal{N}(i)} \text{svol}(e_{ij}) \left( \lambda_{ij, \text{Roe}} + \frac{C_v \mu_{\text{eff}, e_{ij}}}{\text{dist}(e_{ij}) \rho_i} \max \left\{ \frac{4}{3}, \frac{\kappa_{\text{eff}, e_{ij}} (\gamma - 1)}{\mu_{\text{eff}, e_{ij}}} \right\} \right). \end{aligned}$$

As a further acceleration technique, to allow for over- and under-relaxation, we introduce a relaxation parameter  $\varepsilon$ , such that (5.5) is replaced by

$$\left( (\Delta T)^{-1} \mathbf{M} + \varepsilon \alpha_{jj} \frac{d\mathbf{R}}{d\mathbf{W}} (\mathbf{W}^{(j-1)}) \right) \mathbf{h}_j = \alpha_{j+1, j} \mathbf{R}(\mathbf{W}^{(j-1)}). \quad (5.6)$$

To shorten the notation, we define the linear operator for stage  $j$  by

$$\mathbf{P}_j = (\Delta T)^{-1} \mathbf{M} + \varepsilon \alpha_{jj} \frac{d\mathbf{R}}{d\mathbf{W}} (\mathbf{W}^{(j-1)}).$$

The linear equation (5.6) represents in general a large scale, ill-conditioned system and cannot be solved directly. Matrix-free Krylov subspace methods are therefore a natural choice to approximate a solution of (5.6) within a small number of steps. Instead of considering a variety of Krylov subspace methods we restrict ourselves to the Generalized Minimum Residual (GMRES) method preconditioned from the left; that is, we apply this method to obtain

$$\mathbf{Prec}_j^{-1} \mathbf{P}_j \mathbf{x} = \alpha_{j+1, j} \mathbf{Prec}_j^{-1} \mathbf{R}(\mathbf{W}^{(j-1)}). \quad (5.7)$$

Reducing the number of steps in the Krylov subspace to zero, only the first preconditioning step is left, i.e. Algorithm 5.4 reduces to approximate the solution of

$$\mathbf{Prec}_j \mathbf{h}_j = \alpha_{j+1, j} \mathbf{R}(\mathbf{W}^{(j-1)}). \quad (5.8)$$

As a consequence the Algorithm 5.4 simplifies to

$$\begin{aligned} \mathbf{W}^{(0)} &:= \mathbf{W}^n \\ \mathbf{W}^{(1)} &= \mathbf{W}^{(0)} - \alpha_{21} \mathbf{Prec}_1^{-1} \mathbf{R}(\mathbf{W}^{(0)}) \\ &\vdots \\ \mathbf{W}^{(s)} &= \mathbf{W}^{(0)} - \alpha_{s+1, s} \mathbf{Prec}_s^{-1} \mathbf{R}(\mathbf{W}^{(s-1)}) \\ \mathbf{W}^{n+1} &= \mathbf{W}^{(s)}. \end{aligned} \quad (5.9)$$

The Runge-Kutta iteration (5.9) depends on the construction of  $\mathbf{Prec}$  and the iterative linear solution method. A further, self-evident alternative of algorithm (5.9)

is the freezing of the preconditioner  $\mathbf{Prec}$  on the first stage, that is

$$\begin{aligned}
\mathbf{W}^{(0)} &:= \mathbf{W}^n \\
\mathbf{W}^{(1)} &= \mathbf{W}^{(0)} - \alpha_{21} \mathbf{Prec}_1^{-1} \mathbf{R}(\mathbf{W}^{(0)}) \\
&\vdots \\
\mathbf{W}^{(s)} &= \mathbf{W}^{(0)} - \alpha_{s+1,s} \mathbf{Prec}_1^{-1} \mathbf{R}(\mathbf{W}^{(s-1)}) \\
\mathbf{W}^{n+1} &= \mathbf{W}^{(s)}.
\end{aligned} \tag{5.10}$$

### 5.3 Construction of preconditioner

Instead of taking the exact residual  $\mathbf{R}$  for the Jacobian a simplification satisfying  $\tilde{\mathbf{R}} \approx \mathbf{R}$  is considered to construct the preconditioner for (5.7). Here, we consider a compact stencil approximating the extended stencil; that is, we choose  $\tilde{\mathbf{R}} = \mathbf{R}^{\text{comp}} \approx \mathbf{R}$ . Considering compact discretization for the derivative, the major advantage is that the stencil at point  $i$  relies only on next neighbor information. The associated Jacobian  $\frac{d\mathbf{R}^{\text{comp}}}{d\mathbf{W}}$  has several properties of interest, for example:

- a) It is much less memory intensive than the exact derivative  $\frac{d\mathbf{R}}{d\mathbf{W}}$ .
- b) It can be constructed by a loop over all edges corresponding to the design of the residual evaluation  $\mathbf{R}^{\text{comp}}$ .
- c) Assuming that  $\mathbf{R} \approx \mathbf{R}^{\text{comp}}$  holds, it can be assumed that  $\frac{d\mathbf{R}}{d\mathbf{W}} \approx \frac{d\mathbf{R}^{\text{comp}}}{d\mathbf{W}}$ .

We express such a residual by

$$\tilde{\mathbf{R}}_{\text{prec}}^{\text{comp}}(\mathbf{W}) = \tilde{\mathbf{R}}_{\left| \mathbf{A}_{ij}^{\text{Roe}} \right| = \text{const.}, \mu_{\text{eff}}, e_{ij} = \text{const.}}^{\text{comp}}(\mathbf{W}).$$

Using this notation and the corresponding approximate derivatives we need to include the stabilizing terms such that the final preconditioner is given by

$$\mathbf{Prec}_j := (\Delta T)^{-1} \mathbf{M} + \varepsilon \alpha_{jj} \frac{d\tilde{\mathbf{R}}_{\text{prec}}^{\text{comp}}}{d\mathbf{W}}(\mathbf{W}^{(j-1)}). \tag{5.11}$$

The preconditioner  $\mathbf{Prec}_{j,(k,\omega)}$  for the  $k\omega$ -turbulence model uses for the inviscid and viscous part the derivatives given in the monologue [17]. The derivatives of the source terms need to be modified. The diagonal terms of the derivatives of the destruction terms are neglected, that is

$$\frac{\partial D e_{k,(k,\omega)}}{\partial k_i} \quad \text{and} \quad \frac{\partial D e_{\omega,(k,\omega)}}{\partial \omega_i}$$

are left out in the preconditioner. The necessity for this modification is discussed in [17]. Corresponding to (5.11) the preconditioner for the  $k\omega$ -model is given by

$$\mathbf{Prec}_{j,(k,\omega)} = (\Delta T)^{-1} \mathbf{M} + \varepsilon \alpha_{jj} \frac{d\tilde{\mathbf{R}}_{\text{prec}}^{\text{comp},(k,\omega)}}{d\mathbf{W}}\left(\left((k,\omega)^{(j-1)}\right)\right). \tag{5.12}$$

## 5.4 Solving linear systems and truncation criteria

To implement a preconditioned GMRES method or to execute (5.9) for approximately solving (5.7) we need to efficiently find approximate solutions of large scale sparse linear systems

$$Ah = z.$$

In our applications we have for example

$$A = \mathbf{Prec}_j \quad \text{and} \quad z = -\alpha_{j+1,j} \mathbf{R}(\mathbf{W}^{(j-1)}).$$

An approximate solution is found using a symmetric Gauss-Seidel method accelerated using information of strongest coupling. Denoting the  $k$ th iterate by  $h^{(k)}$  and using as initial guess  $h^{(0)} = 0$ , we iterate until

$$\frac{\|z - Ah^{(k)}\|_2}{\|z\|_2} < \varepsilon, \quad \varepsilon = 10^{-2}.$$

The maximum number of iterations is set to  $k_{\max} = 250$ .

## 5.5 Positivity of $k$ and $\omega$

To deal with the problem of positivity of  $k$  and  $\omega$  we simply introduced a damping of the updates. For example, Algorithm (5.10) gives for the variables  $k_i$  and  $\omega_i$ ,  $i = 1, \dots, N_{elem}$ , the updates

$$k_i^{(j)} = k_i^{(0)} - \Delta k_i, \quad (5.13a)$$

$$\omega_i^{(j)} = \omega_i^{(0)} - \Delta \omega_i, \quad (5.13b)$$

where  $(\Delta k_i, \Delta \omega_i)$  denotes the symbol for  $i$ th entry of vector one obtains evaluating  $\alpha_{j+1,j} \mathbf{Prec}^{-1} \mathbf{R}(\mathbf{W}^{(j-1)})$ . The direct application of (5.13) often yield negative values in particular for  $k$ . Most often this was observed for the high-lift test cases, but almost all test cases showed up negative values for  $k$  and  $\omega$  at least during the starting phase of the iteration. Therefore, we replaced the update (5.13) by an application of Algorithm 1.

Algorithm 1 represents some kind of damped Newton method introducing a further effect of regularization. Expressed in formulae, Algorithm 1 realizes the following condition:

$$s_{n,i}^{(k)} = \min_{n \in \mathbb{N}_0} \left\{ \frac{1}{2^n} \right\} \quad \text{such that} \quad k_i^{\text{new}} > 0,$$

$$s_{n,i}^{(\omega)} = \min_{n \in \mathbb{N}_0} \left\{ \frac{1}{2^n} \right\} \quad \text{such that} \quad \omega_i^{\text{new}} > 0.$$

**Algorithm 1** Update for  $k\omega$ -model

---

```

1: procedure LOOP OVER ALL MESH POINTS TO UPDATE  $k$  AND  $\omega$ 
2:   for  $i = 1, \dots, N_{elem}$  do
3:      $s_n = 1$ 
4:     for  $n = 1, 2, \dots$  do
5:        $k_i^{new} = k_i^{(0)} - s_n \Delta k_i$ 
6:       if  $k_i^{new} > 0$  then
7:          $k_i^{(j)} = k_i^{new}$ 
8:         break
9:       else
10:         $s_{n+1} = \frac{s_n}{2}$ 
11:   for  $i = 1, \dots, N_{elem}$  do
12:      $s_n = 1$ 
13:     for  $n = 1, 2, \dots$  do
14:        $\omega_i^{new} = \omega_i^{(0)} - s_n \Delta \omega_i$ 
15:       if  $\omega_i^{new} > 0$  then
16:          $\omega_i^{(j)} = \omega_i^{new}$ 
17:         break
18:       else
19:         $s_{n+1} = \frac{s_n}{2}$ 

```

---

The undesired side effect is, that the updates may become arbitrary small yielding an overall convergence corruption. However, for none of the considered test cases stall of convergence has been observed so far. Compared with many others methods tried to ensure positivity of  $k$  and  $\omega$ , Algorithm 1 was within the author's implementation always superior. The simplicity is a further argument for Algorithm 1. But application of Algorithm 1 cannot guarantee convergence. Hence, future work needs to focus on other mechanisms to ensure positivity of  $k$  and  $\omega$  without reformulating the  $k\omega$ -model itself.

On the other hand, the damping of updates

$$\begin{aligned} k_i^{new} &= k_i^{(0)} - s_n \Delta k_i \\ \omega_i^{new} &= \omega_i^{(0)} - s_n \Delta \omega_i \end{aligned}$$

is also justified in the following sense. Using in general (5.4) and (5.5) to compute the updates we have

$$(\Delta k_i, \Delta \omega_i) = \alpha_{j+1,j} \left[ \left( (\Delta t)^{-1} \mathbf{M} + \alpha_{jj} \frac{d\mathbf{R}}{d\mathbf{W}} (\mathbf{W}^{(j-1)}) \right)^{-1,app} \mathbf{R}(\mathbf{W}^{(j-1)}) \right]_i.$$

A necessary criterion for convergence is  $\|\mathbf{R}(\mathbf{W}^{(j-1)})\| \rightarrow 0$ , that is in particular

$$(\mathbf{R}(\mathbf{W}^{(j-1)}))_i \rightarrow 0.$$

If the turbulence flow equations converge, at some iterate the updates  $\Delta k_i$  and  $\Delta \omega_i$  are so small, that additional damping is not necessary and at the same time positivity of  $k$  and  $\omega$  is ensured. Therefore, Algorithm 1 is not a severe restriction. In case this algorithm is active all over the iteration, the turbulence flow equations do not converge. Then one either needs to question the considered test case or the numerical method applied. In particular, if this is the case, it can be assumed that with the implemented solution method no positive function  $k$  and / or  $\omega$  can be computed.

To illustrate the mode of operation of Algorithm 1 a plot of the number of  $k$ -limitations and  $\omega$ -limitations is given in Figure 5.2 for the Wilcox model of 1988 and in Figure 5.3 for the the SST-model. To approximate a solution we performed for each multigrid cycle on the mean flow equations 20 subiterations on the turbulence flow equations. The number of multigrid cycles is plotted on the upper  $x$ -axis, the total number of subiterations on the lower  $x$ -axis. From Figure 5.2 (left) we can observe that not only the total number of limitations for  $k$  goes to zero, but also within each subiteration the number of limitations is significantly reduced. For the Wilcox model of 1988 no limitation of  $\omega$ -variable is required, which is obvious from Figure 5.2 (right).

For the considered example, the number of limitations required for the SST-model is significantly smaller. Moreover, Figure 5.3 (right) shows that for the SST-model also limitations for  $\omega$  are performed. As expected from consideration above, at some level in convergence the number of limitations for both  $k$  and  $\omega$  variable is 0. This means, that discrete positive solutions for  $k$  and  $\omega$  are obtained. This confirms numerically that the suggested limitation given by Algorithm 1 yields discrete solutions satisfying positivity (3.1) if convergence of the equations for  $k$  and  $\omega$  is observed. In case one of the functions for  $k$  or  $\omega$  is locally negative, the algorithm cannot converge.

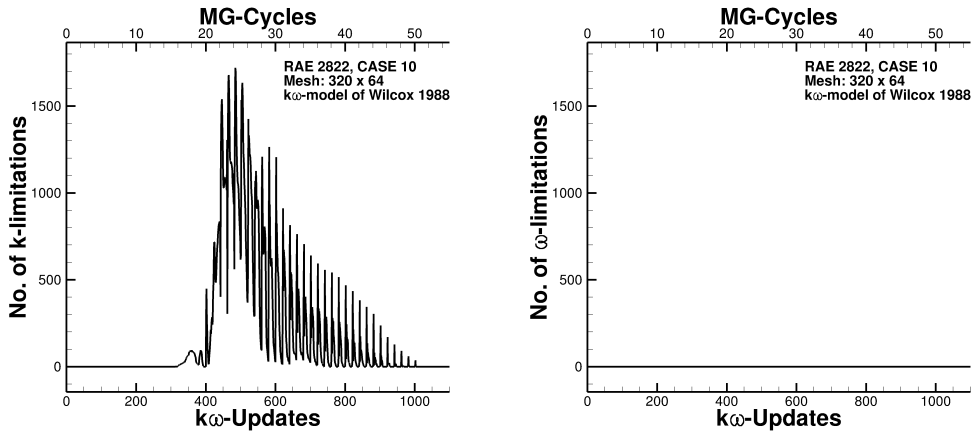


Figure 5.2: Number of limitations for the  $k\omega$ -model of 1988

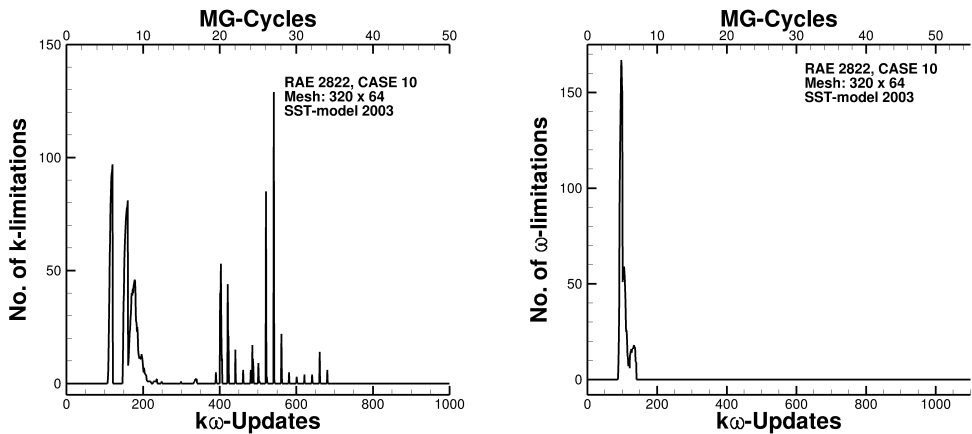


Figure 5.3: Number of limitations for the  $k\omega$ -model of 1988

# Chapter 6

## Numerical examples

To assess the suggested implementation of the Wilcox  $k\omega$ -model of 1988 and the SST model we investigate 2D and 3D examples. To avoid numerical errors for a given mesh we reduced the density residual to machine accuracy, that is, we stopped the iteration for the first iterate satisfying

$$\text{density residual}(n) < 10^{-14}. \quad (6.1)$$

For all test cases considered it was possible to fulfill (6.1), a requirement which importance has been formulated in Chapter 1.

To plot the convergence histories for density  $\rho$ ,  $k$  and  $\omega$  we applied the formulae

$$\text{density residual}(n) := \sqrt{\sum_{j=1}^{N_{elem}} \frac{(\mathbf{R}_{j,\text{mean},\rho}(\mathbf{W}^{T_n}))^2}{(\text{vol}(\Omega_j))^2}} / \sqrt{\sum_{j=1}^{N_{elem}} \frac{(\mathbf{R}_{j,\text{mean},\rho}(\mathbf{W}_\infty))^2}{(\text{vol}(\Omega_j))^2}},$$

and

$$k - \text{residual}(n) := \sqrt{\sum_{j=1}^{N_{elem}} \frac{(\mathbf{R}_{j,\text{turb},k}(k^{T_n}, \omega^{T_n}))^2}{(\text{vol}(\Omega_j))^2}} / \sqrt{\sum_{j=1}^{N_{elem}} \frac{(\mathbf{R}_{j,\text{turb},k}(k_\infty, \omega_\infty))^2}{(\text{vol}(\Omega_j))^2}},$$
$$\omega - \text{residual}(n) := \sqrt{\sum_{j=1}^{N_{elem}} \frac{(\mathbf{R}_{j,\text{turb},\omega}(k^{T_n}, \omega^{T_n}))^2}{(\text{vol}(\Omega_j))^2}} / \sqrt{\sum_{j=1}^{N_{elem}} \frac{(\mathbf{R}_{j,\text{turb},\omega}(k_\infty, \omega_\infty))^2}{(\text{vol}(\Omega_j))^2}}.$$

Using free stream variables to normalize the residuals of the turbulence flow equations, one may not observe such a decrease of the residual. This is because the free stream is often not a good initial guess, and hence in the initial phase of the iteration an increase of the residual for these equations is observed.

## 6.1 RAE 2822 Airfoil

The first examples considered correspond to the RAE 2822 airfoil. They have been chosen because they are frequently considered when attempting to validate turbulence models.

Cases	$M_\infty$	AoA	$Re$
Case 1	0.676	1.93°	$5.7 \cdot 10^6$
Case 9	0.73	2.79°	$6.5 \cdot 10^6$
Case 10	0.75	2.81°	$6.2 \cdot 10^6$

Table 6.1: Flow Conditions for RAE 2822 airfoil

	Coarse	Medium	Fine
Mesh size	$320 \times 64$	$640 \times 128$	$1280 \times 256$
No. of quadrilaterals	20480	81920	327680
No. of cells on the airfoil	256	512	1024

Table 6.2: Mesh data for RAE 2822 airfoil

We perform the computations on a sequence of C-type structured meshes described in Table 6.2. The meshes have a C-type topology. The finest mesh consists of 1280 cells around the airfoil (1024 cells on the airfoil) and 256 cells in normal direction. The normal mesh spacing at the surface of the finest mesh is approximately  $3 \cdot 10^{-6}$ , and the maximum surface cell aspect ratio is about 560.

Model	Grid	$C_L$	$C_D$	$(C_D)_p$	$(C_D)_v$
$k\omega$ -1988	$320 \times 64$	0.568334	0.01094482	0.00392265	0.00702217
$k\omega$ -1988	$640 \times 128$	0.571597	0.01076410	0.00386175	0.00690235
$k\omega$ -1988	$1280 \times 256$	0.569298	0.01093510	0.00391235	0.00702275

Table 6.3: Case 1: Computed lift and drag coefficients with  $k\omega$ -1988 model

Model	Grid	$C_L$	$C_D$	$(C_D)_p$	$(C_D)_v$
SST	$320 \times 64$	0.538247	0.01014596	0.00389907	0.00624689
SST	$640 \times 128$	0.547975	0.00975285	0.00375389	0.00599896
SST	$1280 \times 256$	0.560777	0.01024589	0.00381609	0.00642980

Table 6.4: Case 1: Computed lift and drag coefficients with SST model

Model	Grid	$C_L$	$C_D$	$(C_D)_p$	$(C_D)_v$
$k\omega$ -1988	$320 \times 64$	0.813847	0.0190240	0.0124897	0.0065343
$k\omega$ -1988	$640 \times 128$	0.818374	0.0189336	0.0125096	0.0064240
$k\omega$ -1988	$1280 \times 256$	0.814175	0.0188998	0.0123688	0.0065310

Table 6.5: Case 9: Computed lift and drag coefficients with  $k\omega$ -1988 model

Model	Grid	$C_L$	$C_D$	$(C_D)_p$	$(C_D)_v$
SST	$320 \times 64$	0.762732	0.0165200	0.0108057	0.0057143
SST	$640 \times 128$	0.774292	0.0163844	0.0108964	0.0054880
SST	$1280 \times 256$	0.773810	0.0164611	0.0109026	0.0055585

Table 6.6: Case 9: Computed lift and drag coefficients with SST model

Model	Grid	$C_L$	$C_D$	$(C_D)_p$	$(C_D)_v$
$k\omega$ -1988	$320 \times 64$	0.822756	0.0301132	0.0237356	0.0063776
$k\omega$ -1988	$640 \times 128$	0.829374	0.0302744	0.0239849	0.0062895
$k\omega$ -1988	$1280 \times 256$	0.824434	0.0300871	0.0236905	0.0063966

Table 6.7: Case 10: Computed lift and drag coefficients with  $k\omega$ -1988 model

Model	Grid	$C_L$	$C_D$	$(C_D)_p$	$(C_D)_v$
SST	$320 \times 64$	0.722263	0.0241748	0.0187140	0.0054608
SST	$640 \times 128$	0.742187	0.0246749	0.0194276	0.0052473
SST	$1280 \times 256$	0.743644	0.0248062	0.0194821	0.0053241

Table 6.8: Case 10: Computed lift and drag coefficients with SST model

Convergence histories for Case 1, Case 9 and Case 10 for the  $k\omega$ -model of 1988 are shown in Figures 6.9, 6.11 and 6.13, for the SST-model they are plotted in Figures 6.10, 6.12 and 6.14. Note that we have plotted the convergence histories for  $k$ - and  $\omega$ -equation on logarithmic scale. The reason is that initial values in particular for  $k$ -equation are so inappropriate, that during the first iterations an increase of residual of about four orders of magnitude is observed. After such initial increase is reached, residual drops and has expected behavior. And such increase in residual needs to be considered as value for normalization. Nevertheless, it seems to be in particular the  $k$ -equation, which is responsible for slowdown in convergence, and in particular the inappropriate choice of initial guess seems to be a major contribution for such behavior.

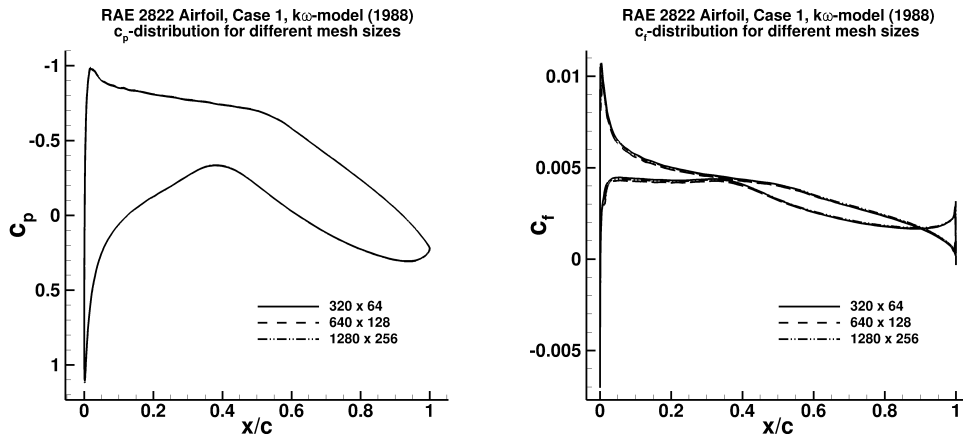


Figure 6.1: Computed  $C_p$ - and  $C_f$ - distribution for Case 1 using  $k\omega$ -model of Wilcox (1988)

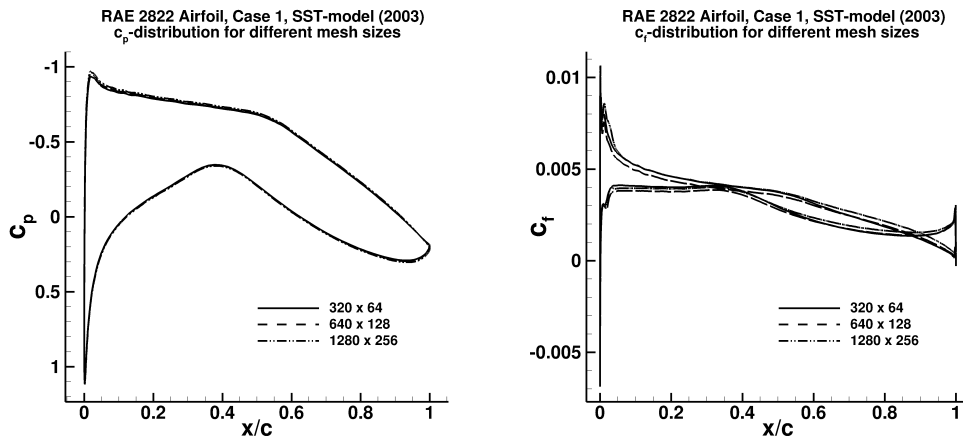


Figure 6.2: Computed  $C_p$ - and  $C_f$ - distribution for Case 1 using SST-model (2003)

### 6.1.1 Necessity of production limiter

Formulae (3.33a) and (3.33b) introduced a limiter for the production term in the  $k$ -equation. The limiter is constructed such that the value of production does not exceed a multiple of destruction. The necessity of such limitation is demonstrated in the following two examples based on Case 9 and Case 10 documented above.

Figure 6.15 shows computed eddy viscosity for Case 9 on the  $320 \times 64$  mesh. Note, both results correspond to fully converged solutions, and the corresponding convergence history is given in Figure 6.17. The solution without production limiter shows an exceed in eddy viscosity in a neighborhood where the shock interacts with free shear flow. Such effect is suppressed when using the production limiter, shown

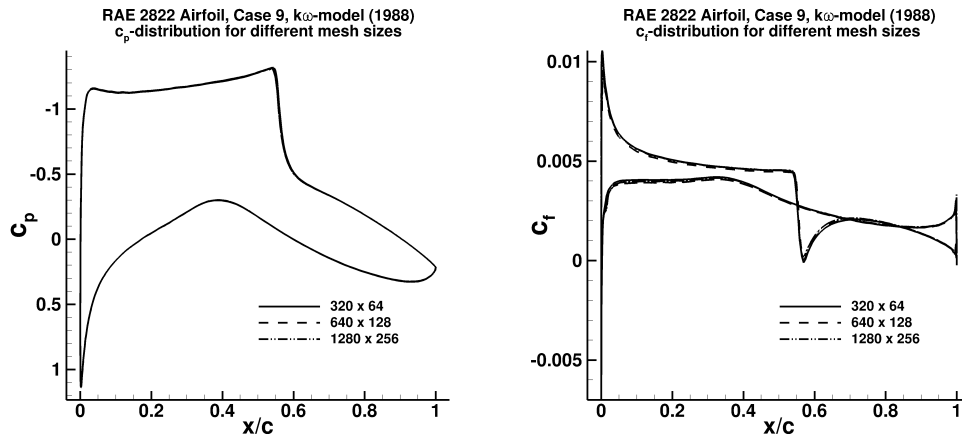


Figure 6.3: Computed  $C_p$ - and  $C_f$ - distribution for Case 9 using  $k\omega$ -model of Wilcox (1988)

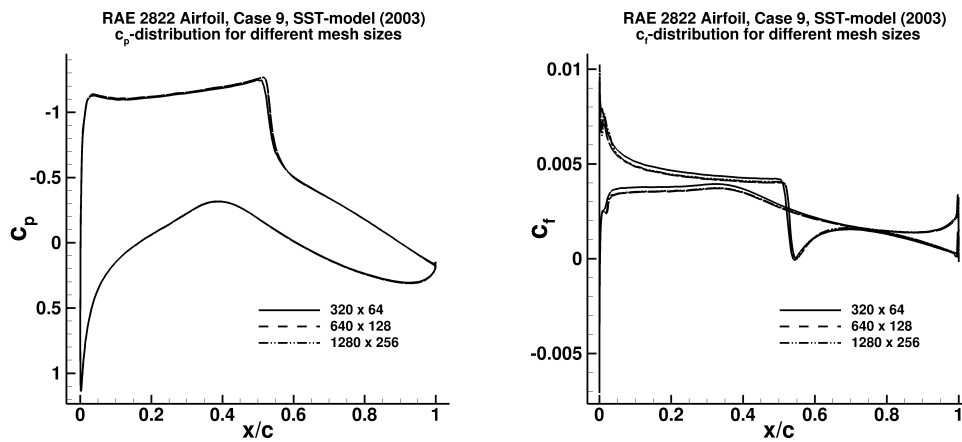


Figure 6.4: Computed  $C_p$ - and  $C_f$ - distribution for Case 9 using SST-model (2003)

in Figure 6.15 (right).

The same observation is true for Case 10 on the  $320 \times 64$  mesh. Given two fully converged solutions (see Figure 6.17 (right)), the one with production limiter shows an excess in eddy viscosity in a neighborhood where the shock interacts with free shear flow, which vanishes when the production limiter is used.

Most disturbing about the different solutions for eddy viscosity is the fact, that these differences have approximately no impact on computed  $C_p$ -distribution and  $C_f$ -distribution. A plot of such distributions is given in Figure 6.18 for Case 9 and Figure 6.19 for Case 10. Obviously, though the eddy viscosity with and without production limiter 3.33a is significantly different its impact on computed  $C_p$ -

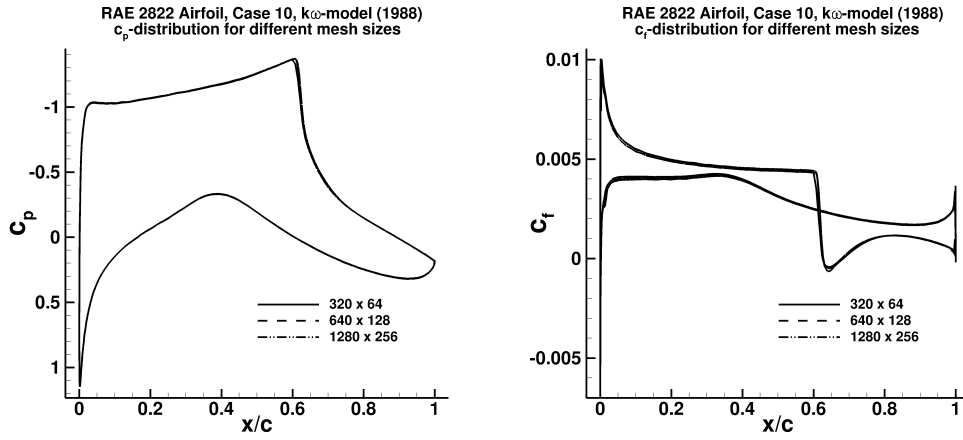


Figure 6.5: Computed  $C_p$ - and  $C_f$ - distribution for Case 10 using  $k\omega$ -model of Wilcox (1988)

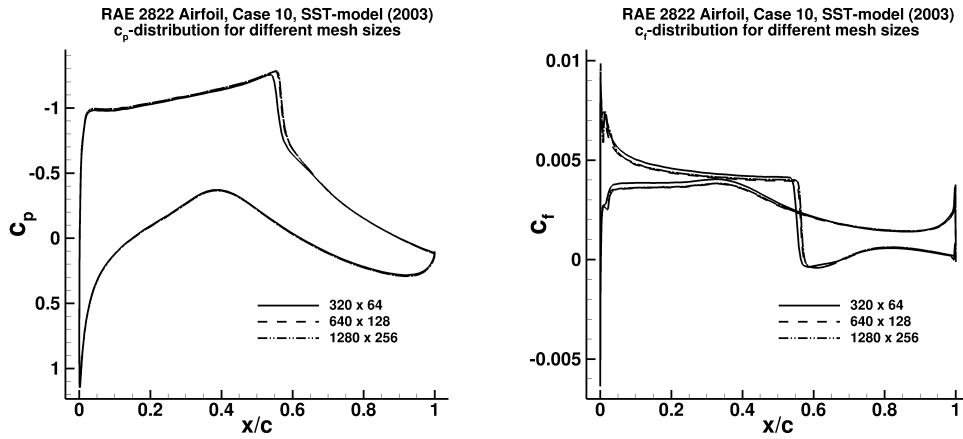


Figure 6.6: Computed  $C_p$ - and  $C_f$ - distribution for Case 10 using SST-model (2003)

distribution and  $C_f$ -distribution is not noticeably.

With respect to mesh refinement the situation becomes different. Figures 6.20 and 6.21 show convergence histories for Case 9 and Case 10 with and with production limiter for mesh size  $640 \times 128$ . In our code framework without production limiter it was not possible to get a converged solution. It may be possible that the disturbances in eddy viscosity are so large, that convergence is not possible on this mesh size.

Concluding, we summarize that this short investigation shows that introduction of production limiter can have significant impact on the computed eddy viscosity. Its

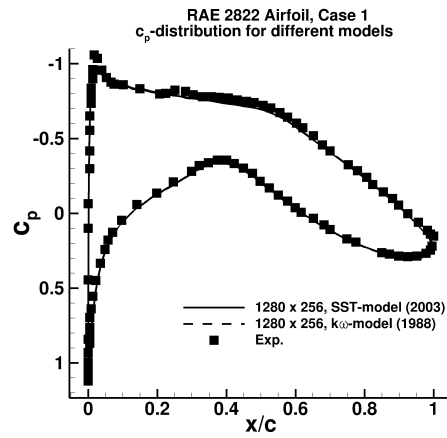


Figure 6.7: Computed  $C_p$ -distribution for Case 1 and comparison with experimental data

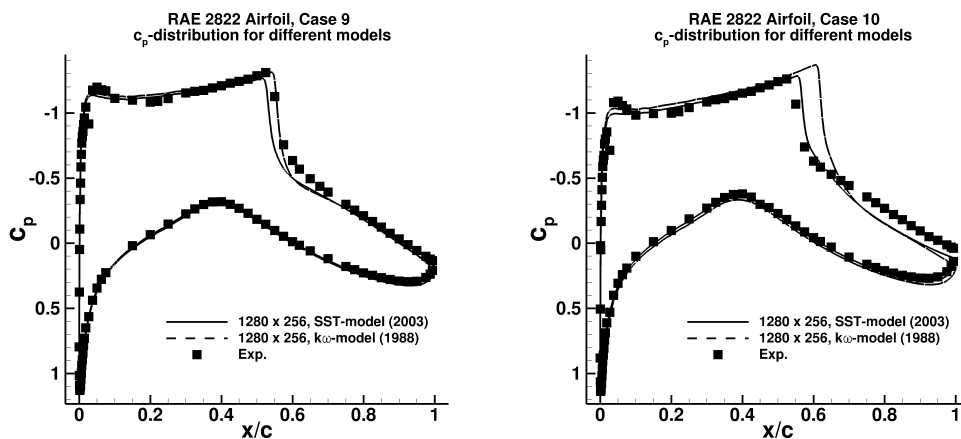


Figure 6.8: Computed  $C_p$ -distribution for Case 9 and Case 10 and comparison with experimental data

impact can be so severe that without usage of the limiter convergence is not possible. On the other hand, at least for these two examples, and where a fully converged solution was possible, a significant change in the computed eddy viscosity, did not yield to significant changes in  $C_p$ -distribution and  $C_f$ -distribution. Such observation can be interpreted in both directions.

- a) The influence of computed eddy viscosity is so weak, that if a fully converged solution is possible, no noticeably change in the final solution of mean flow equations can be found.
- b) Vice versa, it is interesting to notice that significant change in the computed

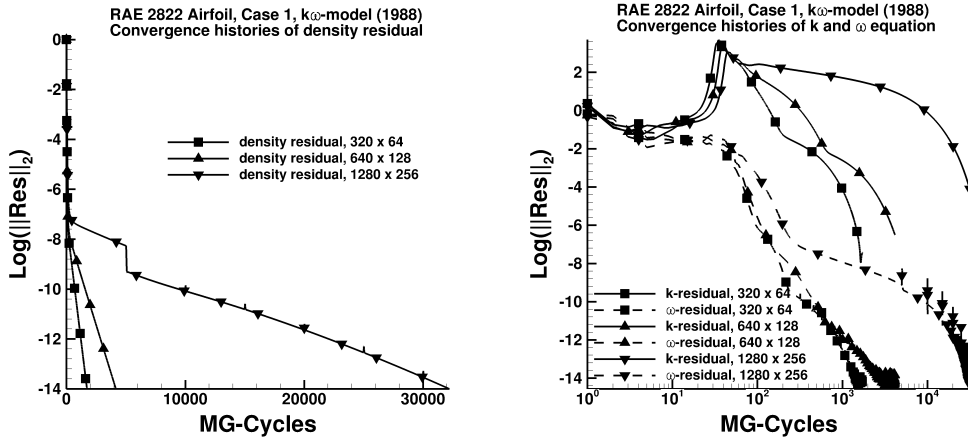


Figure 6.9: Convergence histories for Case 1 (left density residual, right  $k$  and  $\omega$  residual) on sequence of meshes,  $k\omega$ -model 1988

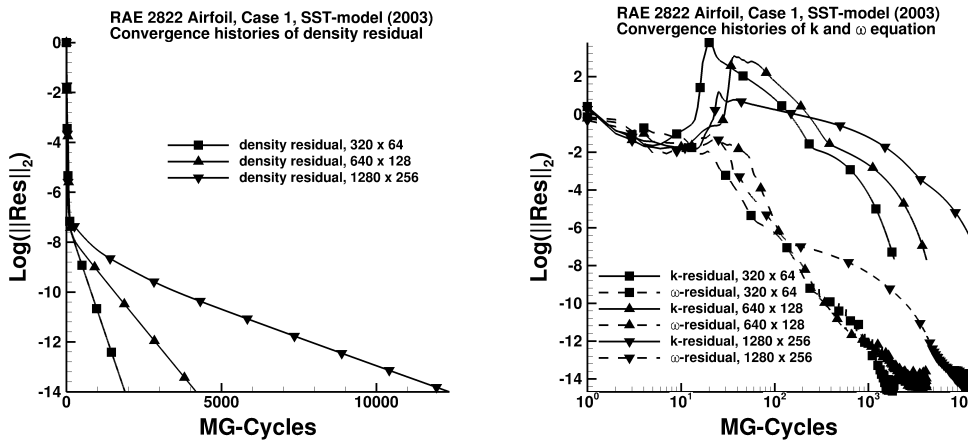


Figure 6.10: Convergence histories for Case 1 (left density residual, right  $k$  and  $\omega$  residual) on sequence of meshes, SST-model 2003

eddy viscosity does not yield significant difference in  $C_p$ -distribution and  $C_f$ -distribution. Such observation gives rise to the question, in which way eddy viscosity needs to be changed such that it influences the solution of mean flow equations.

As final remark for this topic we mention that in formulae (3.33a) and (3.33b) a factor of 20 was introduced for limitation. However, throughout the literature one finds other factors such as 10 or 5 for limitation of production compared to destruction. With respect to our findings such factors might be negligible, when one compares for fully converged solutions obtained  $C_p$ -distribution and  $C_f$ -distribution.

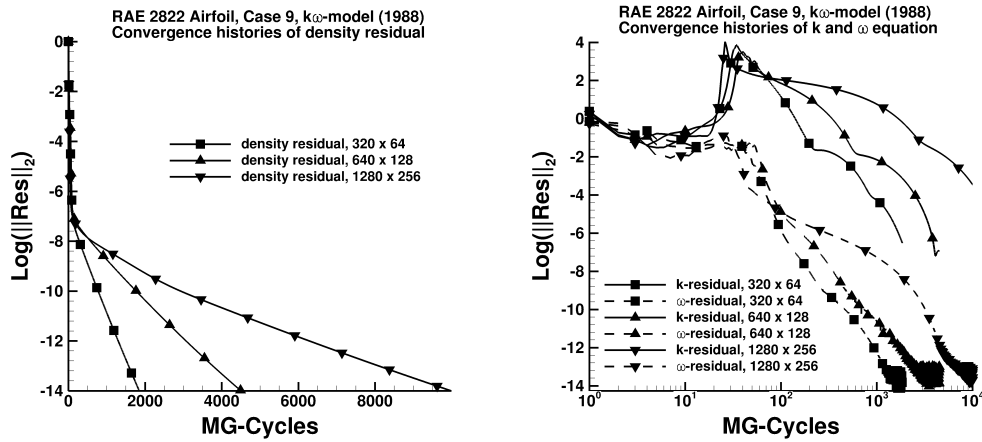


Figure 6.11: Convergence histories for Case 9 (left density residual, right  $k$  and  $\omega$  residual) on sequence of meshes,  $k\omega$ -model 1988

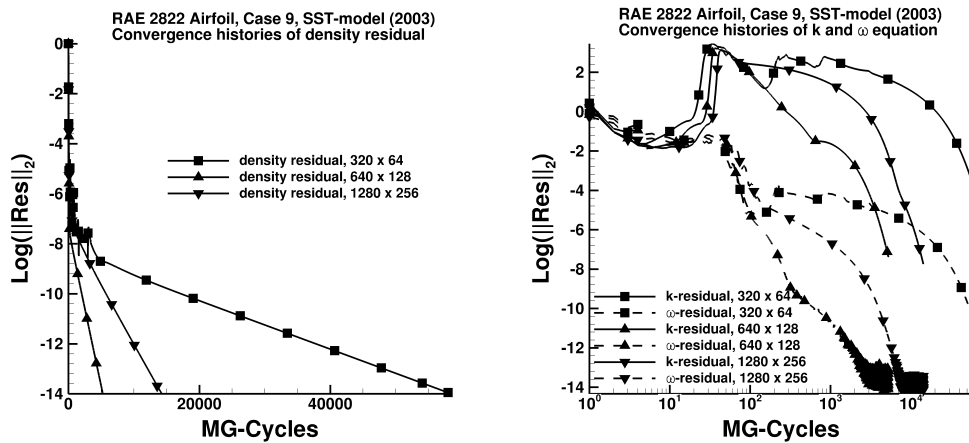


Figure 6.12: Convergence histories for Case 9 (left density residual, right  $k$  and  $\omega$  residual) on sequence of meshes, SST-model 2003

One may find differences only in obtained eddy viscosity, that is solutions of the  $k\omega$ -model itself.

## 6.2 NACA 4412 airfoil flow

We consider the low-speed flow over the NACA 4412 airfoil at high angle of attack. The flow conditions are:

- Geometry: NACA 4412 airfoil

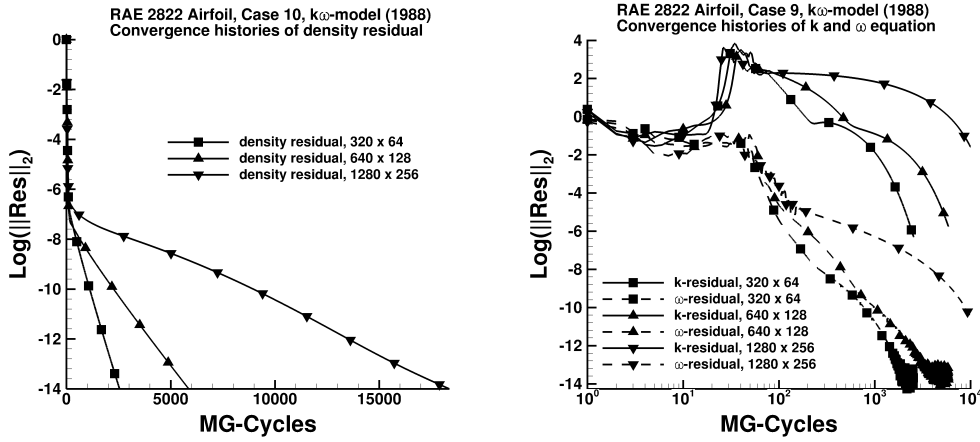


Figure 6.13: Convergence histories for Case 10 (left density residual, right  $k$  and  $\omega$  residual) on sequence of meshes,  $k\omega$ -model 1988

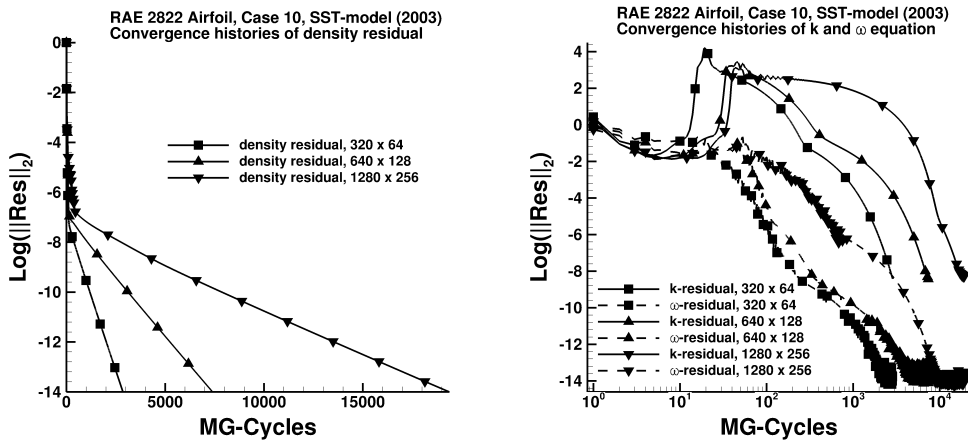


Figure 6.14: Convergence histories for Case 10 (left density residual, right  $k$  and  $\omega$  residual) on sequence of meshes, SST-model 2003

- Reynolds number:  $Re = 1.52 \cdot 10^6$
- Inflow Mach number:  $M_\infty = 0.09$
- Angle of attack:  $AoA = 13.87^\circ$ .

The grids used for the calculations are from the NASA Turbulence Modeling Resource website [9], and they consist of  $112 \times 32$ ,  $224 \times 64$ ,  $448 \times 128$ ,  $896 \times 256$  and  $1792 \times 512$  cells with the outer boundary located at 100 chords. Experimental data for this flow are reported by Coles and Wadcock [6].

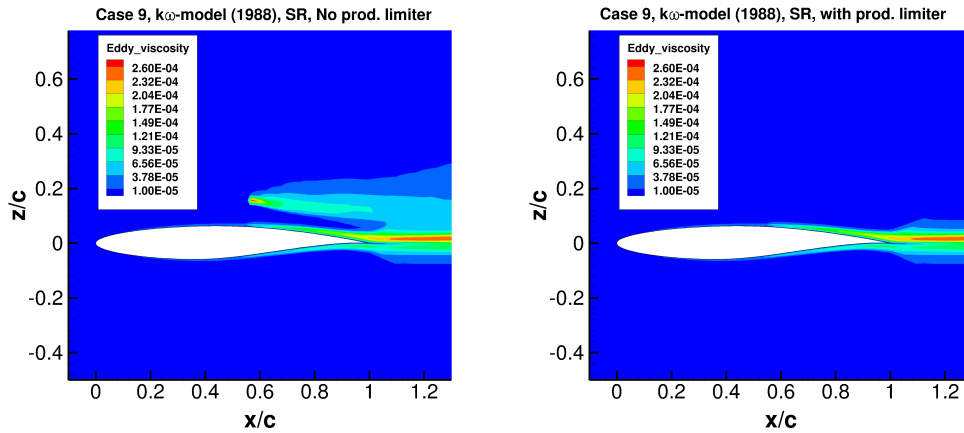


Figure 6.15: Computed eddy viscosity for Case 9 without (left) and with (right) production limiter for  $320 \times 64$  mesh

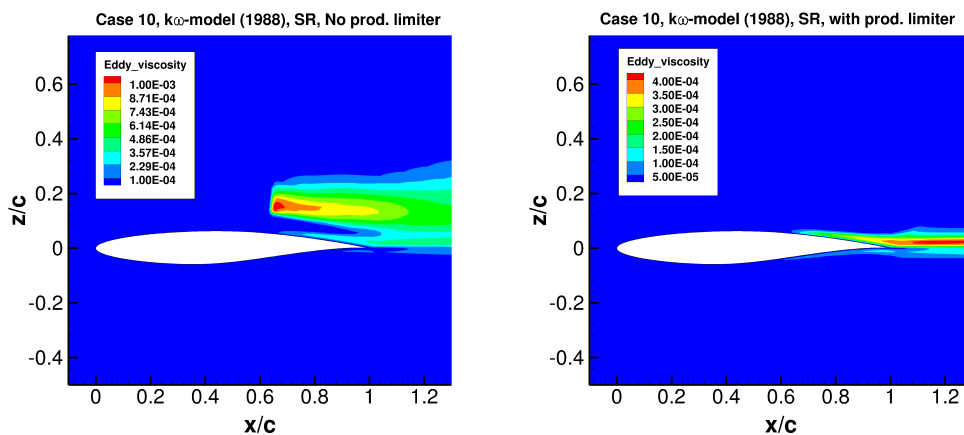


Figure 6.16: Computed eddy viscosity for Case 10 without (left) and with (right) production limiter for  $320 \times 64$  mesh

### 6.2.1 Motivation for NACA 4412 airfoil flow

An investigation of this test case was chosen because of several reasons:

- a) Often convergence difficulties are reported for high lifting airfoil flows. It can be assumed that large separations at the trailing edge of the airfoil are the main reason that several flow solvers show up convergence problems.
- b) To correctly predict the onset and amount of separation in adverse pressure gradient flows is an ongoing task in the development and assessment of models and computer codes trying to approximate solutions of high Reynolds number

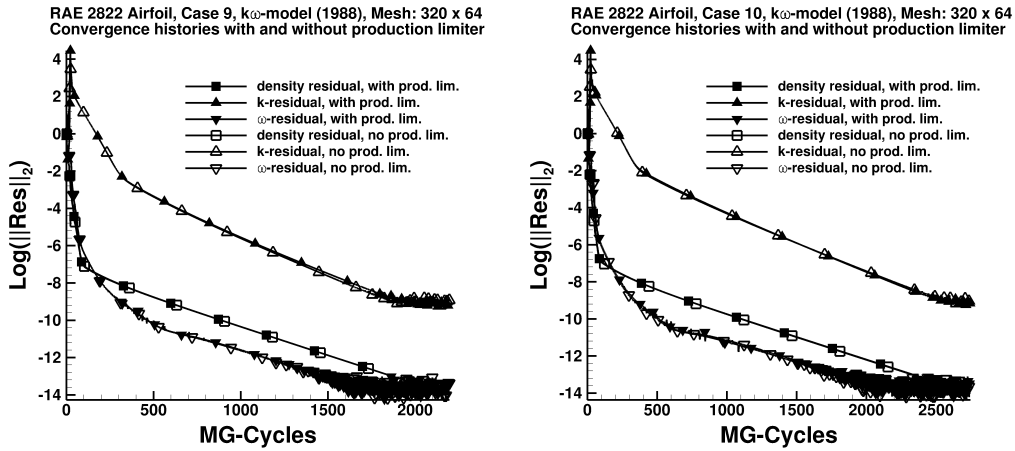


Figure 6.17: Convergence histories for Case 9 (left) and Case 10 (right) on the  $320 \times 64$  mesh with and without usage of production limiter

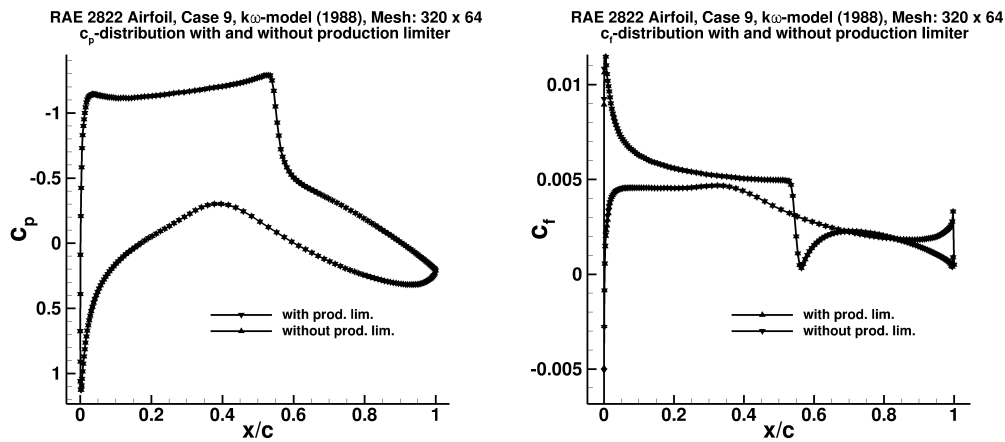


Figure 6.18: Computed  $C_p$  (left) and  $C_f$  (right) distribution for Case 9 using production limiter for  $320 \times 64$  mesh

turbulent flows.

- c) In the literature it has been reported that the Menter Shear Stress Transport Two-Equation turbulence model shows improved results compared with other turbulence models.

The presented results in this report have been obtained without a specified transition location.

Historically, this test case was considered by Rogers et al. in 1993 [24]. These authors made computations on a mesh with size  $241 \times 63$ . For their computations

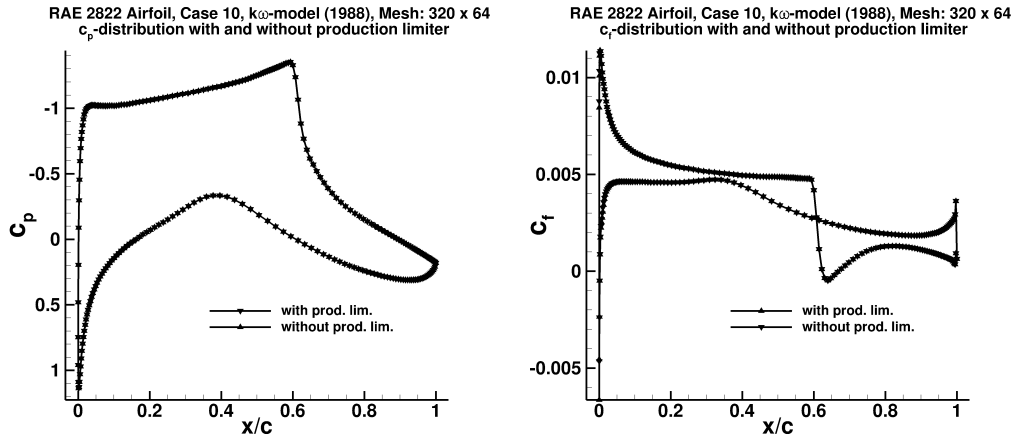


Figure 6.19: Computed  $C_p$  (left) and  $C_f$  (right) distribution for Case 10 using production limiter for  $320 \times 64$  mesh

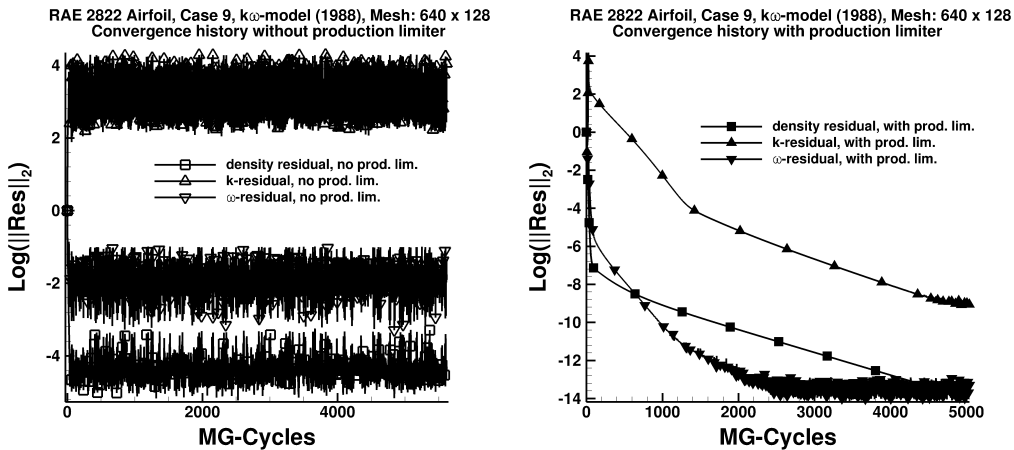


Figure 6.20: Convergence histories for Case 9 on the  $640 \times 128$  mesh with (left) and without (right) usage of production limiter

they used both the Baldwin-Barth [3] and the Baldwin-Lomax [2] turbulence model. Roughly speaking, the numerical results did not match the measured velocity profiles in the trailing edge region. The measurements indicate a large separation whereas the computation only predict a tiny separation. The Baldwin-Barth-model showed an improvement when compared with the Baldwin-Lomax-model. Naturally, a specifically chosen turbulence model is always only one possible explanation to explain differences when comparing measurements with computational data. For example, missing wind-tunnel effects in the computations may also influence computational data significantly.

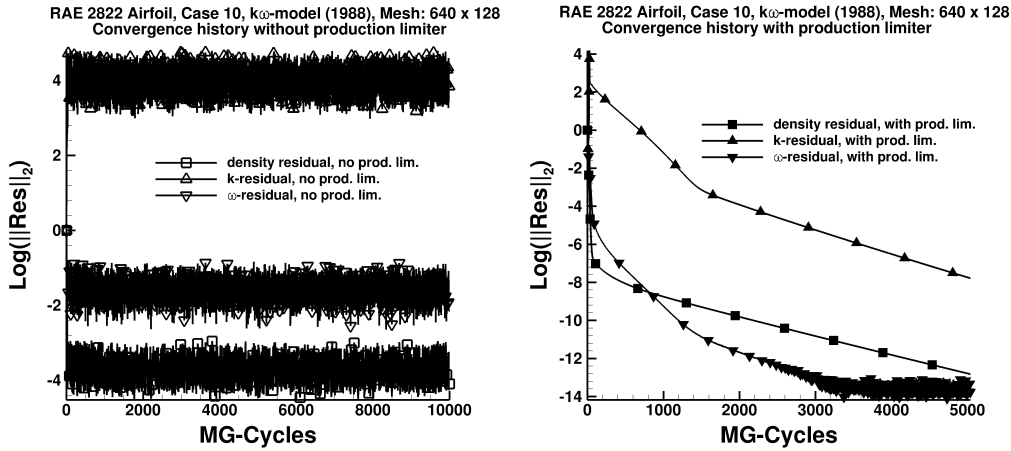


Figure 6.21: Convergence histories for Case 9 on the  $640 \times 128$  mesh with (left) and without (right) usage of production limiter

From our perspective it is important to emphasize, that the authors of [24] were not able to converge the considered test case in their numerical setup. A look at Figure 6 in [24] shows that neither with both considered turbulence models nor with respect to inclusion of transitional effects, the authors were in a position to reduce the residual more than 7 orders of magnitude. Second, the computations were restricted to one mesh size of  $241 \times 63$  and no convergence study has been performed. Hence, with respect to this limited number of data carrying many uncertainties, it prohibits to conclude about certain properties of (approximate) solutions of the governing equations of interest.

Doubts about such results are mentioned here, since the results shown by Menter [18] are based upon the same Code named INS3D, which seems to have been extended for the work in [18] by several two-equation  $k\omega$ -type models. Though Menter mentions that his grid was of size  $241 \times 61$  personally made available by Rogers, we assume that it is the same grid used in [24]. Figure 21 in [18] shows very good agreement of results obtained with the INS3D code in combination with the SST-model for the velocity profiles, whereas the agreement of computational results of pressure distribution compared with experimental data is not as good as one may expect from the velocity profiles. The author does neither show or discuss convergence histories nor mesh refinement studies for this test case. Since the flow solver used to obtain such results was not even able to converge for the Baldwin-Barth or the Baldwin-Lomax model, and convergence is generally much harder for a two-equation model to obtain, the data presented can be categorized as less sustainable and conclusions about certain properties of approximate solutions are maybe misleading.

### 6.2.2 Discussion of results for NACA 4412 airfoil flow

To be in agreement with the presentation of this test case in [18], we performed the computations with the original SST-model of 1992. The computations are performed on a sequence of C-type structured meshes described in Table 6.9. The meshes have a C-type topology. The finest mesh consists of 1792 cells around the airfoil (1024 cells on the airfoil) and 512 cells in normal direction

	Grid 1	Grid 2	Grid 3	Grid 4	Grid 5
Mesh size	$112 \times 32$	$224 \times 64$	$448 \times 128$	$896 \times 256$	$1792 \times 512$
No. of quadrilaterals	3584	14336	57344	229376	917504
No. of cells on the airfoil	64	128	256	512	1024

Table 6.9: Mesh data for NACA 4412 airfoil

The convergence histories of the computations are given in Figures 6.22, 6.23 and 6.24. For all five meshes it was possible to get fully converged results. To compare with other results, additionally the convergence history for a computation with the Spalart-Allmaras turbulence is shown in Figure 6.24, for the finest mesh only.

This is a test case with low inflow Mach number, hence it is recommended to apply techniques taking care of low Mach number effects. To this end, in a first step the influence of a low Mach number modified scheme is compared with a non modified scheme. Figures 6.25 and 6.26 show the results obtained in a neighborhood of the trailing edge region. The qualitative behavior of the results is significantly different. Whereas the non modified scheme shows a large separation with an induced smaller separation, the low Mach modified scheme shows several interacting separations, that is we observe four different interacting vortices. Comparing with Figures 6.27 and 6.28 we conclude that the solutions computed on the meshes of dimension  $112 \times 32$  and  $224 \times 64$  are already qualitatively wrong. The solutions on the finer meshes Grid 3, Grid 4, and Grid 5 only exhibit one large separation. As indicated in Figure 6.27 for Grid 3, that is mesh size  $448 \times 128$ , both solutions show the same qualitative behavior with only one large trailing edge separation which is also observed in Figure 6.28 for the finer meshes of size  $896 \times 256$  and  $1792 \times 512$ . As a consequence, we conclude that for the computation with the SST-model the meshes of dimension  $112 \times 32$  and  $224 \times 64$  are too coarse with respect to the discretization scheme applied and the results are useless.

To confirm that results for Grid 3 are close for the low Mach modified and non low Mach modified discretization the  $C_p$ - and  $C_f$ -distribution are plotted in Figure 6.29. Significant differences are not noticeably. Additionally, Figure 6.30 shows the  $C_f$ -distribution over the airfoil with respect to mesh refinement. Roughly speaking the plotted distributions do not differ significantly. Nevertheless, with respect to mesh

refinement is observed that the separation point moves slightly downstream from about  $x/c = 0.73$  for the mesh of dimension  $448 \times 128$  to  $x/c = 0.775$  for the mesh of dimension  $1792 \times 512$ .

Figure 6.31 presents the computed  $C_p$ -distribution for the finest mesh  $1792 \times 512$  and compares the results with available measurements. The predicted  $C_p$  values are close to the measurements but in particular at the trailing edge region where the separation is observed a larger offset is noticed. It is interesting to observe that the results obtained with the Spalart-Allmaras model and the  $k\omega$ -model of 1988 are a bit closer to the measurements, in particular on the upper surface of the airfoil. Therefore, with respect to assessment of the  $C_p$ -distribution no clear advantage of the SST-model compared to the  $k\omega$ -model of 1988 and the Spalart-Allmaras model is apparent.

Foundation for possibly improved accuracy shown in [18] is a comparison of velocity profiles for different two equation models. To repeat such investigation we consider the measurements of Coles and Wadcock [6] and compare the normalized  $U$  and  $V$  velocity profiles. Figures 6.32 and 6.33 demonstrate these profiles for mesh size  $224 \times 64$ . From the discussion above we already know that these results are stigmatized as useless, since the qualitative behavior of the computed solution is wrong. Nevertheless, in particular for the non low-Mach modified scheme the qualitative behavior of the  $U$  velocity profiles looks usable, whereas all other three plots present large offsets to the experimental data.

For Grid 3, that is dimension  $448 \times 128$ , the plot of  $U$  velocity is given in Figure 6.34 and of  $V$  velocity in Figure 6.35. Comparing with experimental data one can observe that low Mach modification yields slight improvements in accuracy of the computed data. For a direct lineup the  $U$  and  $V$  velocity with and without low Mach modification are shown in Figure 6.36. This argumentation again justifies the use of a low Mach modified upwinding for this nearly incompressible flow.

The influence of mesh refinement is observed in Figures 6.37 and 6.38. Though there is significant offset with respect to computed and measured data for the velocity profiles further downstream, in particular the first distribution at position  $x/c = 0.6753$  moves with respect to mesh refinement towards the measurements. Hence, with respect to implemented techniques we see that there is significant influence of the mesh resolution, that is the number of degrees of freedom, on the obtained results. And even for a 2D computation going from a mesh of dimension  $896 \times 256$  to  $1792 \times 512$  influence the results significantly. It is important to emphasize that such difference in the results are not obvious for  $C_p$ - and  $C_f$ -distribution (see for example Figure 6.30), but the differences become visible for example for velocity profiles.

Such investigation indicates that a full picture of computed results and an assessment of numerical errors due to discretization can only be obtained when sys-

tematic mesh refinement studies are performed and other error sources such as non-converged solutions can be excluded.

To finish this discussion about this test case we need to compare the results for the SST-model with results simulated with other turbulence models. Besides the  $k\omega$ -model of 1988 we additionally consider the model of Spalart and Allmaras in its version from 2012 [25, 1]. As already discussed above, for both the  $k\omega$ -model of 1988 and the Spalart and Allmaras model the  $C_p$ -distribution is slightly closer to the measurements when compared with the SST-model. This is illustrated in Figure 6.31. Qualitatively when comparing the separation at the trailing edge region for the SST-model given in Figure 6.28 with the separation regions for the  $k\omega$ -model of 1988 and the model of Spalart and Allmaras given in Figure 6.40 we observe a significant smaller region of separation for the latter two models. This qualitative difference has impact on the velocity profiles. For both the Spalart-Allmaras model and the  $k\omega$ -model of 1988 the  $U$  and  $V$  velocity profiles given in Figures 6.41 and 6.42 have a significant larger offset to the measurements than the results obtained with the SST-model.

Model	Grid	$C_L$	$C_D$	$(C_D)_p$	$(C_D)_v$
SST (1992)	$112 \times 32$	1.115302	0.05924011	0.05248218	0.006757927
SST (1992)	$224 \times 64$	1.407756	0.04225768	0.03545256	0.006805121
SST (1992)	$448 \times 128$	1.546775	0.03612658	0.02923285	0.006893731
SST (1992)	$896 \times 256$	1.581805	0.03470805	0.02773761	0.006970441
SST (1992)	$1792 \times 512$	1.592374	0.03419930	0.02720273	0.006996579
SA (2012)	$112 \times 32$	1.325708	0.05248384	0.04581902	0.006664820
SA (2012)	$224 \times 64$	1.600099	0.03403803	0.02704957	0.006988457
SA (2012)	$448 \times 128$	1.667591	0.03196258	0.02485611	0.007106468
SA (2012)	$896 \times 256$	1.693518	0.03132716	0.02416555	0.007161606
SA (2012)	$1792 \times 512$	1.704360	0.03111185	0.02392695	0.007184901
$k\omega$ -1988	$112 \times 32$	1.451475	0.04314109	0.03506584	0.008075255
$k\omega$ -1988	$224 \times 64$	1.645732	0.03379649	0.02541849	0.008377999
$k\omega$ -1988	$448 \times 128$	1.716063	0.03017178	0.02201703	0.008154748
$k\omega$ -1988	$896 \times 256$	1.719199	0.03057190	0.02225611	0.008315793
$k\omega$ -1988	$1792 \times 512$	1.714416	0.03098995	0.02263542	0.008354530

Table 6.10: Computed lift and drag coefficients for NACA 4412 airfoil

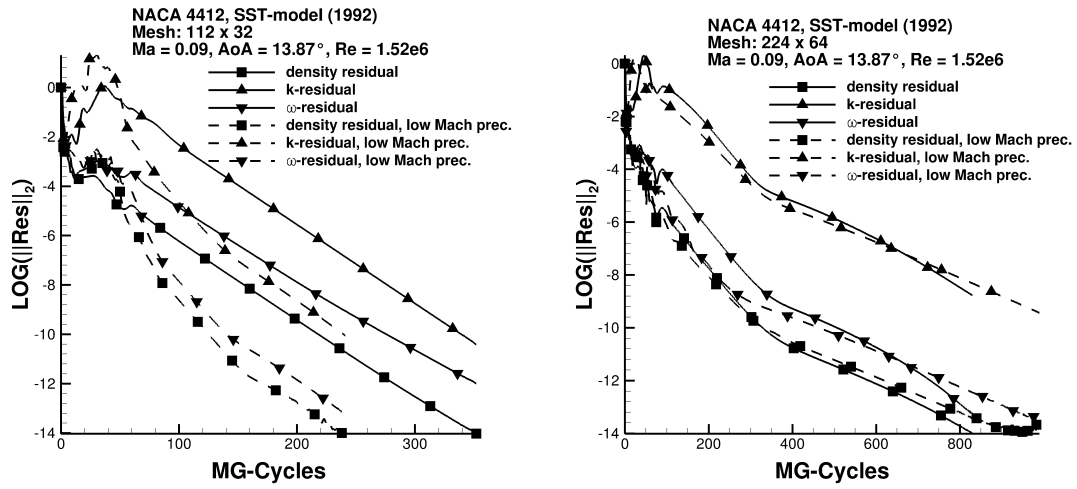


Figure 6.22: NACA4412 computations: Convergence histories for meshes  $112 \times 32$  and  $224 \times 64$

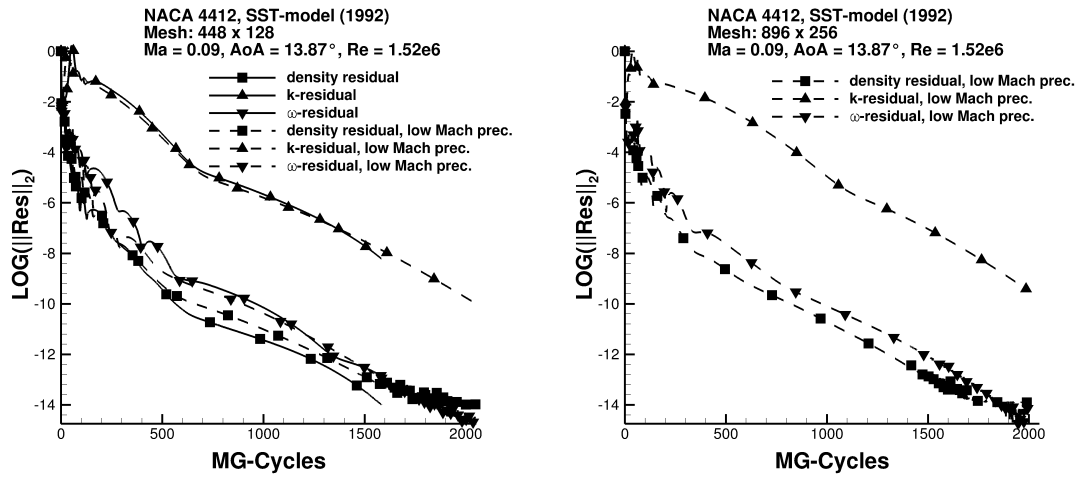
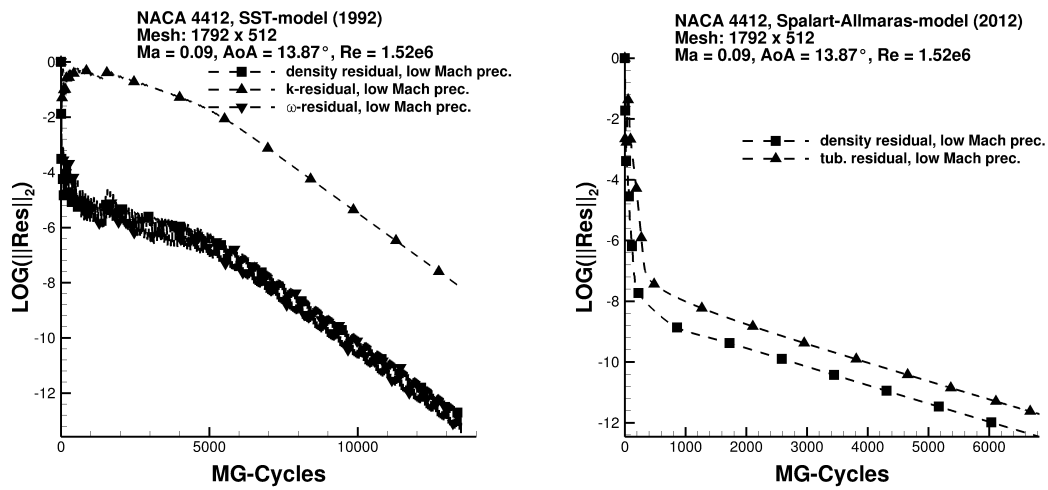
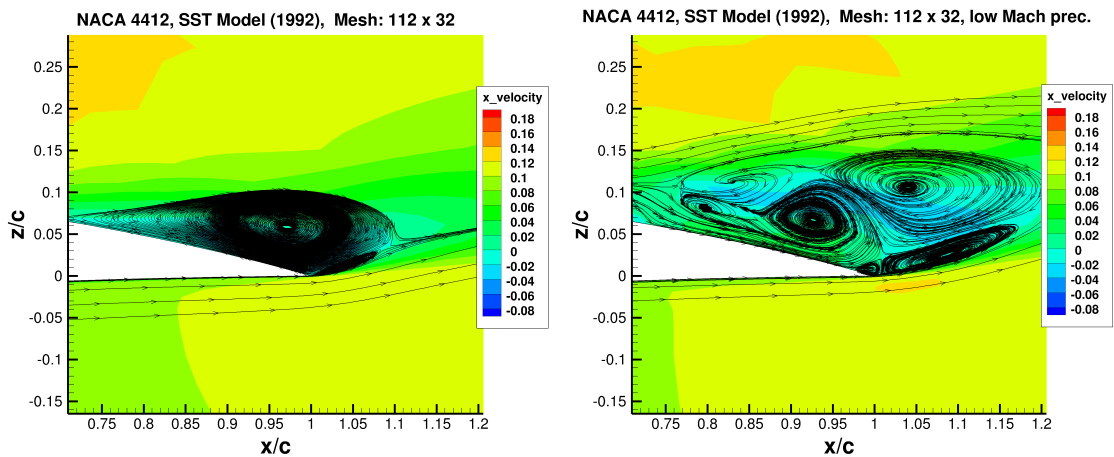


Figure 6.23: NACA4412 computations: Convergence histories for meshes  $448 \times 128$  and  $896 \times 256$

Figure 6.24: NACA4412 computations: Convergence history for mesh  $1792 \times 512$ Figure 6.25: Blow-up of trailing edge region on underresolved mesh  $112 \times 32$ , left without and right with low speed preconditioning

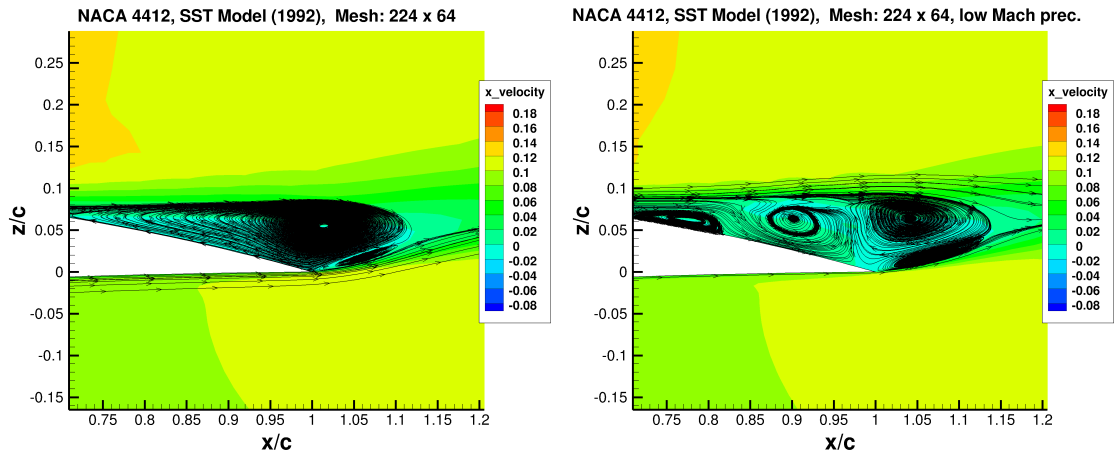


Figure 6.26: Blow-up of trailing edge region on underresolved meshes  $224 \times 64$ , left without and right with low speed preconditioning

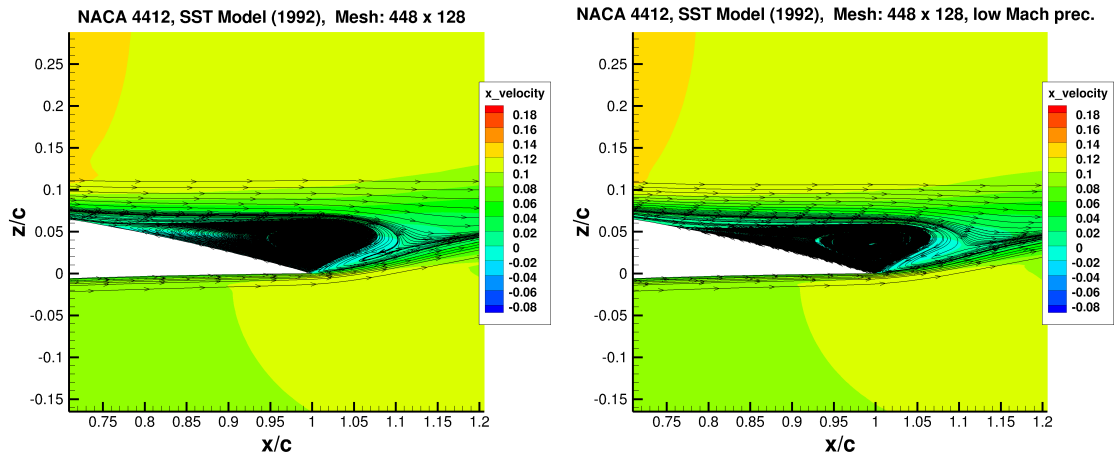


Figure 6.27: Blow-up of trailing edge region on mesh  $448 \times 128$ , left without and right with low speed preconditioning

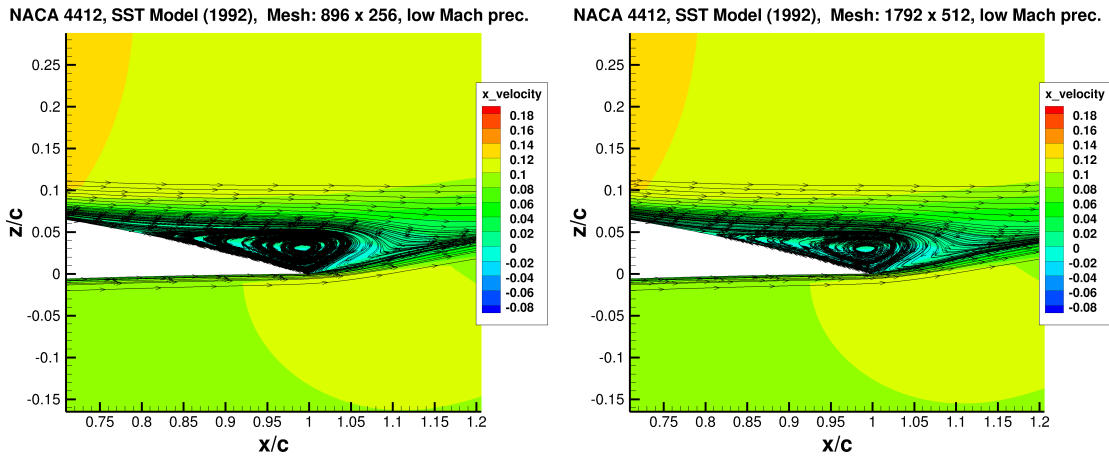


Figure 6.28: Blow-up of trailing edge region on meshes  $896 \times 256$  (left) and  $1792 \times 512$  (right) using low speed preconditioning

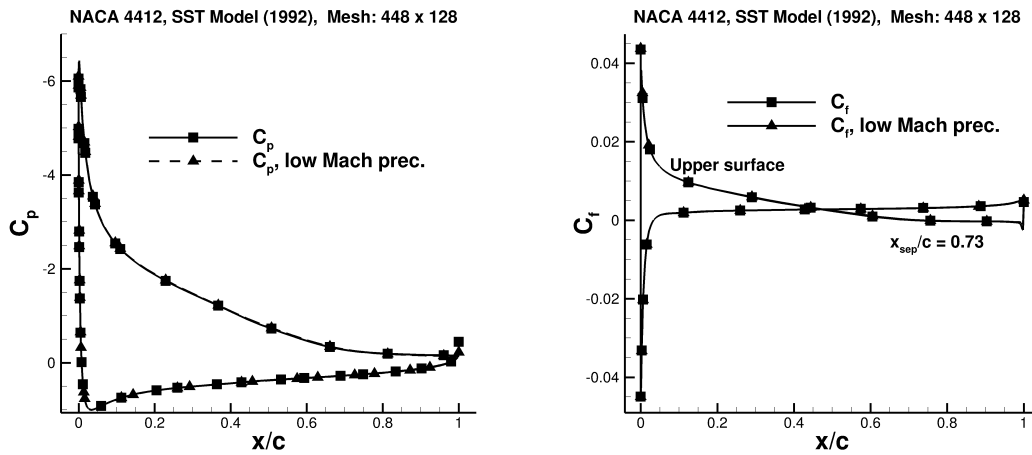


Figure 6.29:  $C_p$ - and  $C_f$ -distribution on mesh  $448 \times 128$

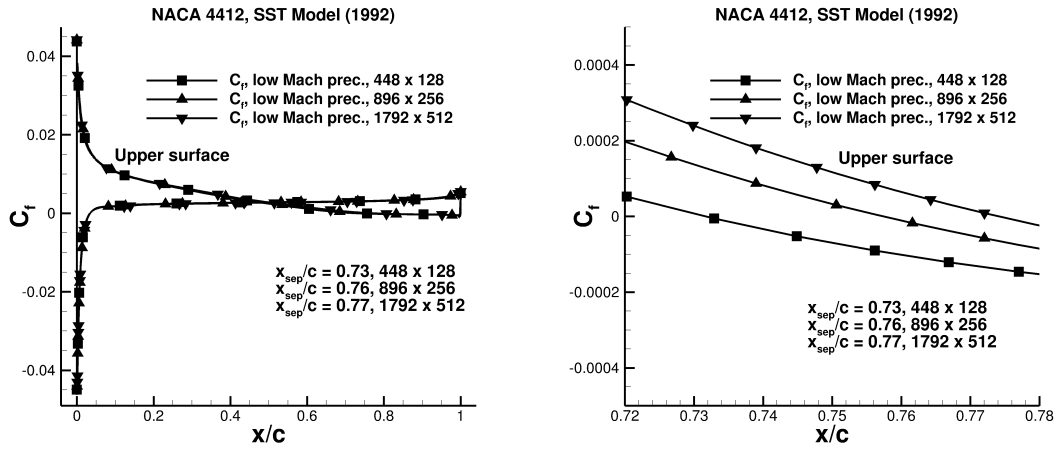


Figure 6.30: Comparison of  $C_f$  for meshes  $448 \times 128$ ,  $896 \times 256$ , and  $1792 \times 512$

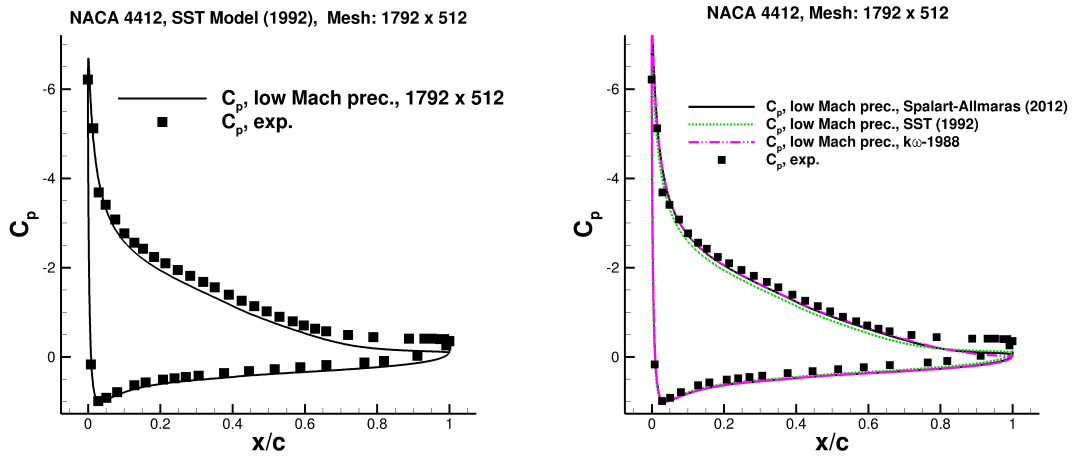


Figure 6.31:  $C_p$ -distribution on mesh  $1792 \times 256$  and comparison with other turbulence models

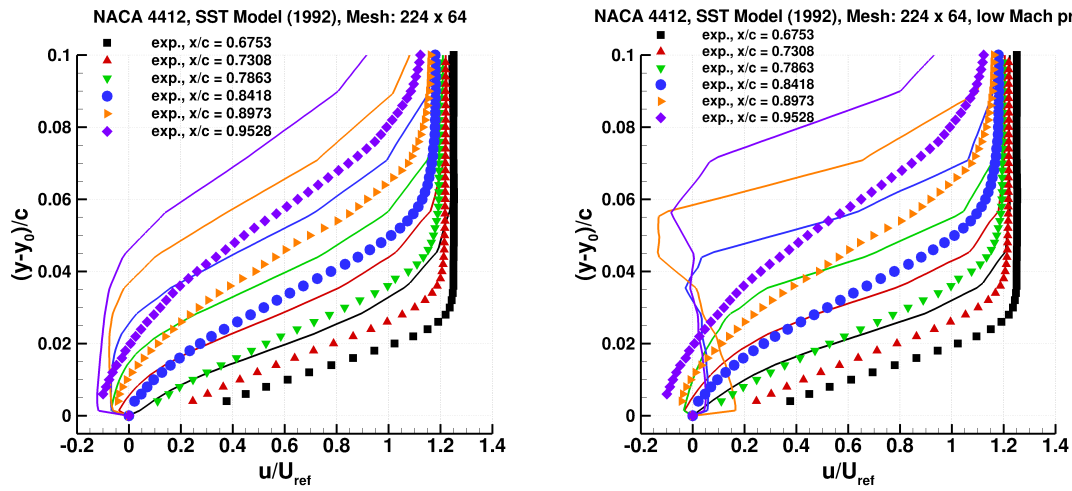


Figure 6.32:  $U$  velocity distributions at six streamwise locations on underresolved mesh  $224 \times 64$ , left without and right with low speed preconditioning

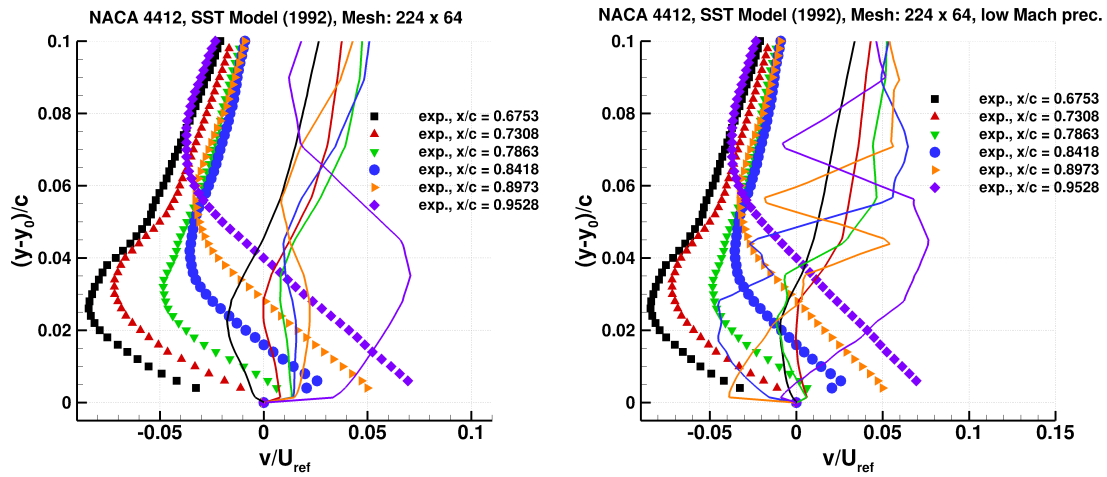


Figure 6.33:  $V$  velocity distributions at six streamwise locations on underresolved mesh  $225 \times 65$ , left without and right with low speed preconditioning

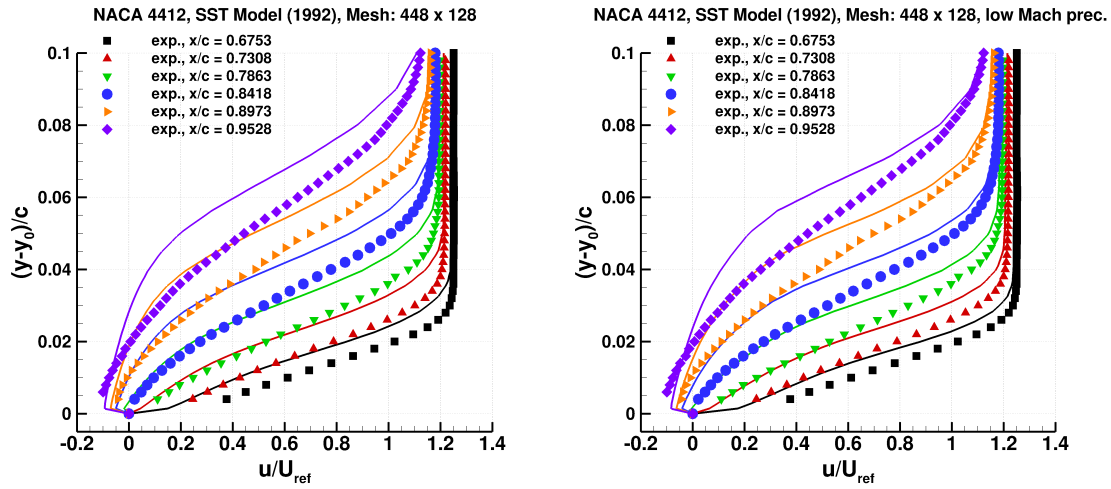


Figure 6.34:  $U$  velocity distributions at six streamwise locations on mesh  $448 \times 128$ , left without and right with low speed preconditioning

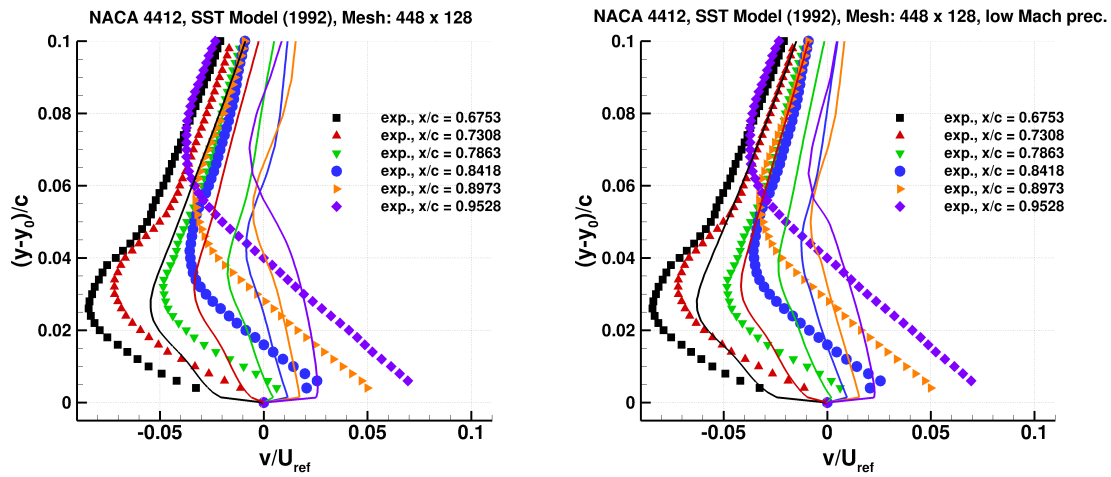


Figure 6.35:  $V$  velocity distributions at six streamwise locations on mesh  $448 \times 128$ , left without and right with low speed preconditioning

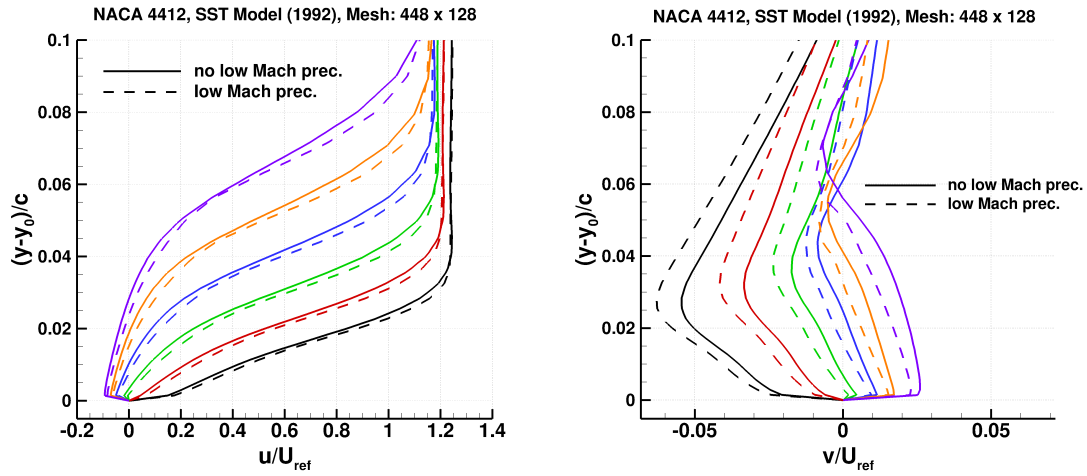


Figure 6.36: Comparison of  $U$  and  $V$  velocity distributions at six streamwise locations on mesh  $448 \times 128$  without and with low speed preconditioning

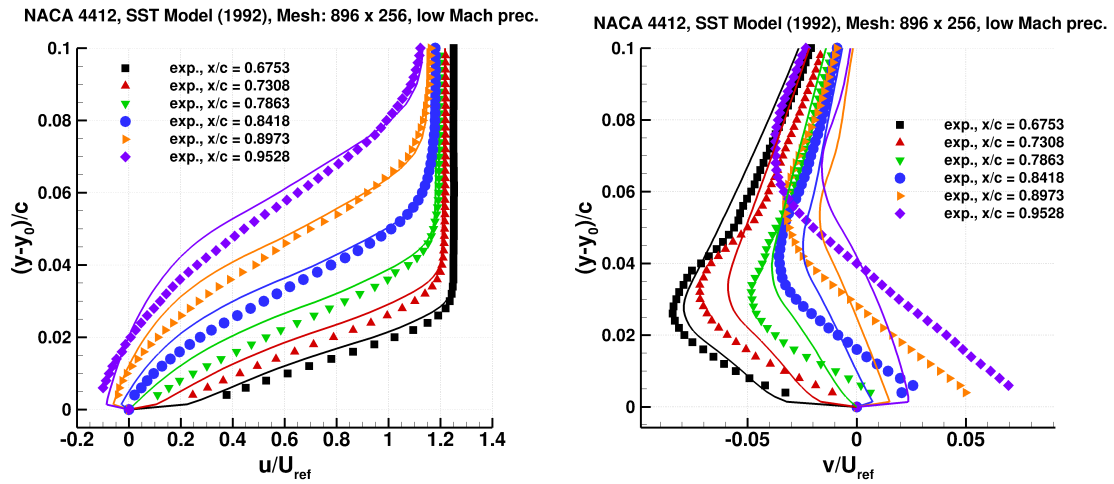


Figure 6.37:  $U$  and  $V$  velocity distributions at six streamwise locations on mesh  $896 \times 256$  using low speed preconditioning

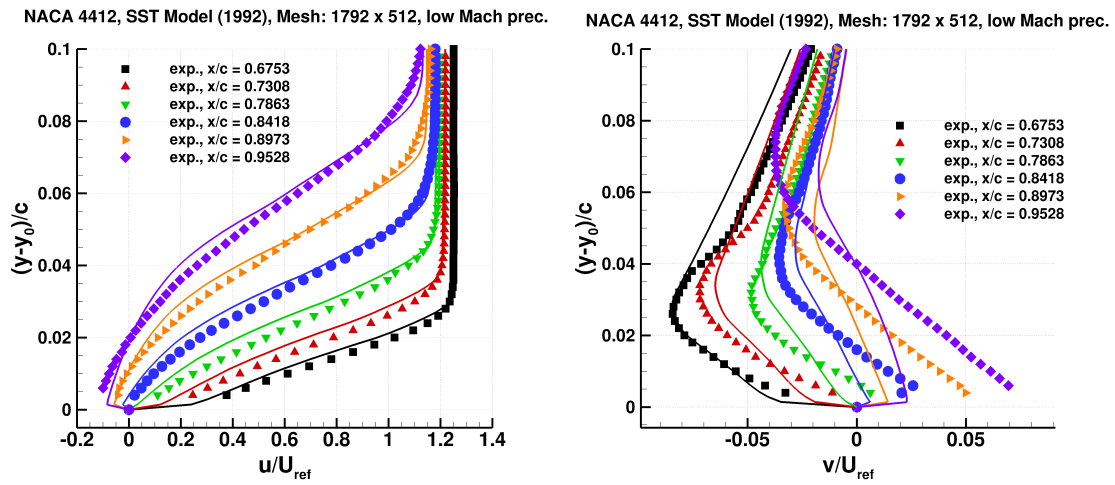


Figure 6.38:  $U$  and  $V$  velocity distributions at six streamwise locations on mesh  $1792 \times 512$  using low speed preconditioning

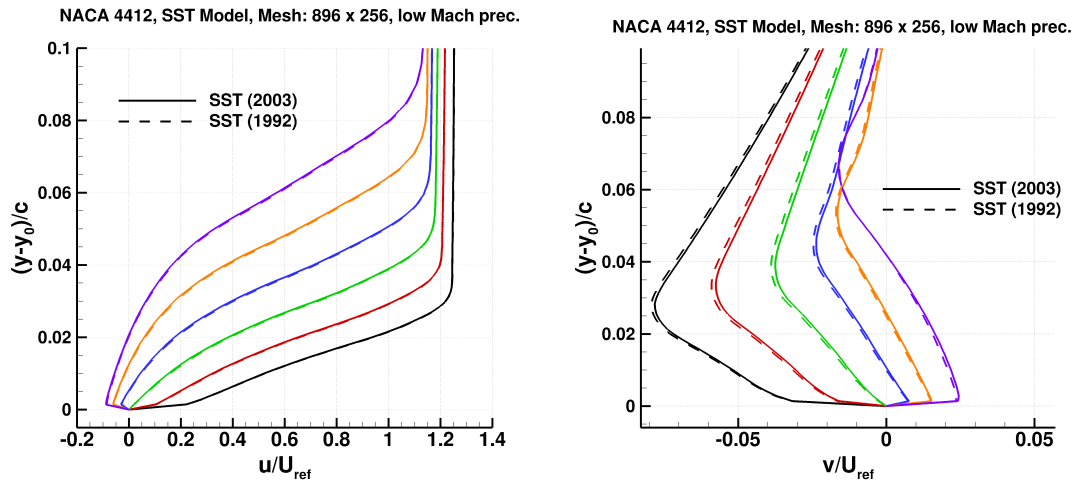


Figure 6.39:  $U$  and  $V$  velocity distributions at six streamwise locations on mesh  $896 \times 256$  using low speed preconditioning

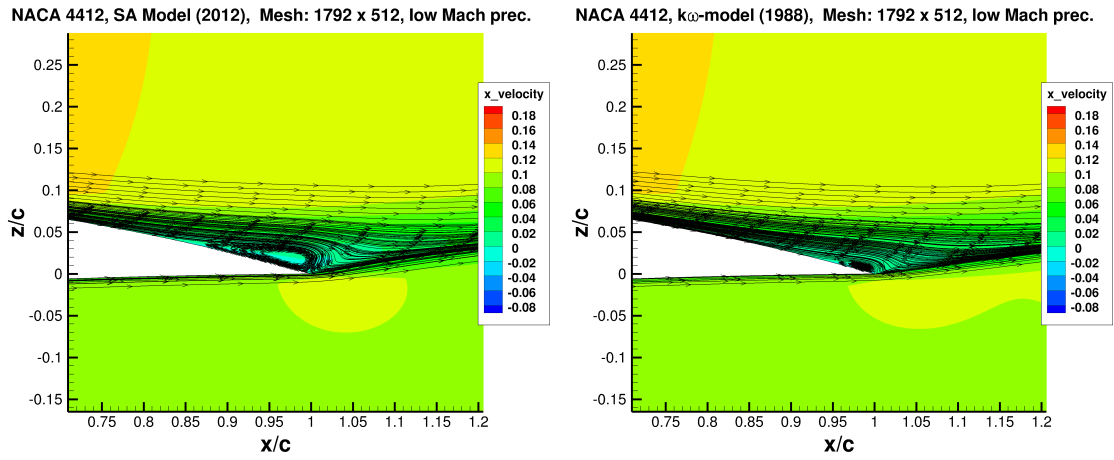


Figure 6.40:  $C_p$ -distribution on mesh  $1792 \times 256$  and comparison with other turbulence models

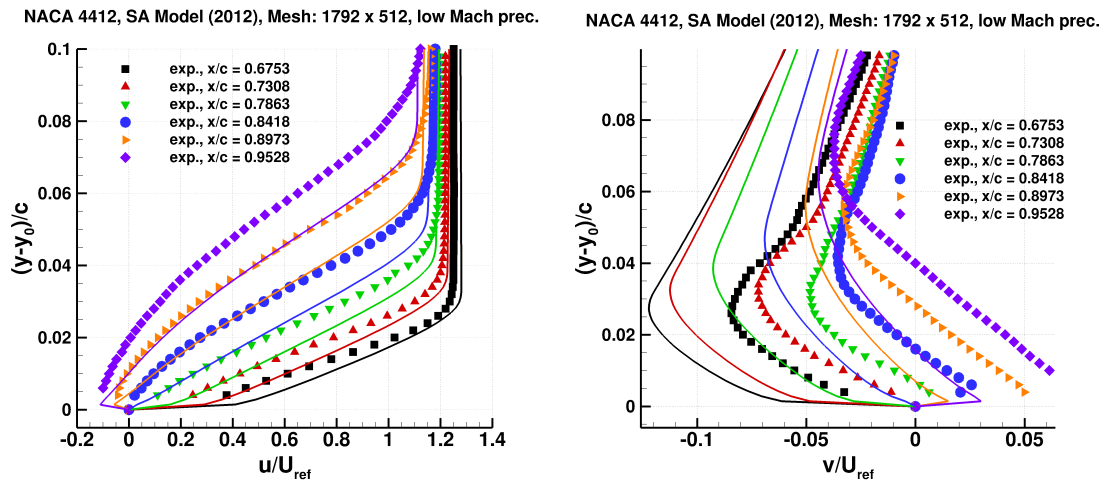


Figure 6.41:  $U$  and  $V$  velocity distributions at six streamwise locations on mesh  $1792 \times 512$  using low speed preconditioning

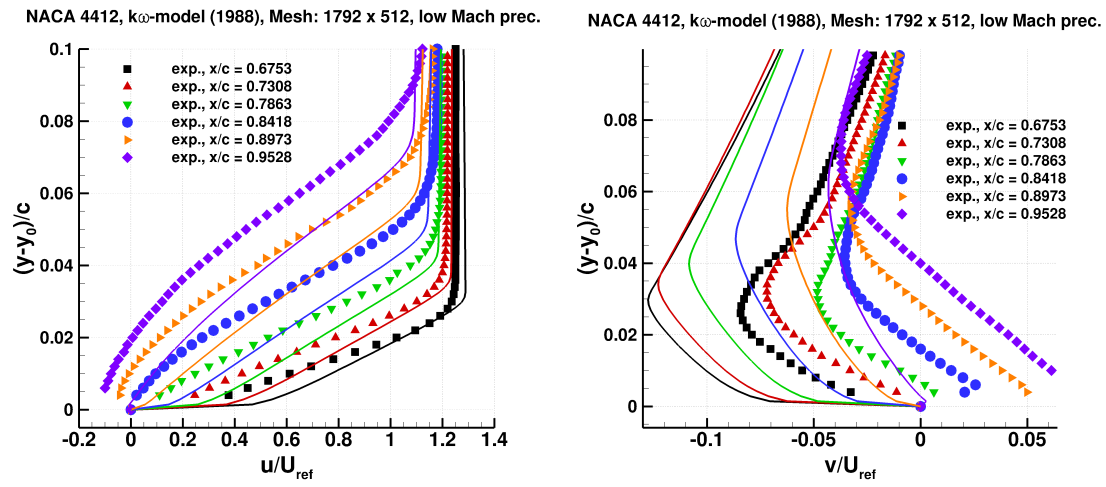


Figure 6.42:  $U$  and  $V$  velocity distributions at six streamwise locations on mesh  $1792 \times 512$  using low speed preconditioning

### 6.3 Transonic turbulent flow over a common research model

Level	Hybrid meshes		Hexahedral meshes	No. of points
	No. of Tetrahedra	No. of Prisms	No. of Hexahedrons	
L1	2555904	425984	638976	660177
L2	8626176	1437696	2156544	2204089
L3	20766720	3301376	5111808	5196193
L4	69728256	11261952	17252352	17441905

Table 6.11: Mesh data for DPW5 CRM

The final presented test case in this report is turbulent flow over a common research model. This test case was considered at the fifth AIAA Drag Prediction Workshop. The considered original meshes are block-structured. A sequence of hybrid meshes were generated from the pure hexahedral meshes. A detailed description of the meshes can be found in [29]. The relevant physical conditions are:

- Geometry: Wing-body configuration, fifth AIAA Drag Prediction Workshop
- Reynolds number:  $Re = 5.0 \cdot 10^6$
- Inflow Mach number:  $M_\infty = 0.85$
- Angle of attack  $2.15^\circ$

Compared to the other test cases, we do not consider a detailed discussion of the results. To the author's impression throughout the literature there exist only very few reports, if not even none, where systematic mesh refinement studies together with the SST-model are shown for 3D turbulent flows and fully converged solutions are obtained. Hence, the result shown here is not a validation of accuracy. This has been done in detail for the latter two examples in Sections 6.1 and 6.2.

This example serves this purpose to demonstrate the applicability of the solution algorithm discussed in Chapter 5 to 3D turbulent flows for two equation turbulence models. Figure 6.43 shows the convergence histories for the sequence of meshes for the considered test case. Application of the algorithm presented in Chapter 5 made it possible to reach fully converged results for both the hexahedral and hybrid sequence of meshes in only a few hundred multigrid cycles.

6.3. TRANSONIC TURBULENT FLOW OVER A COMMON RESEARCH MODEL 107

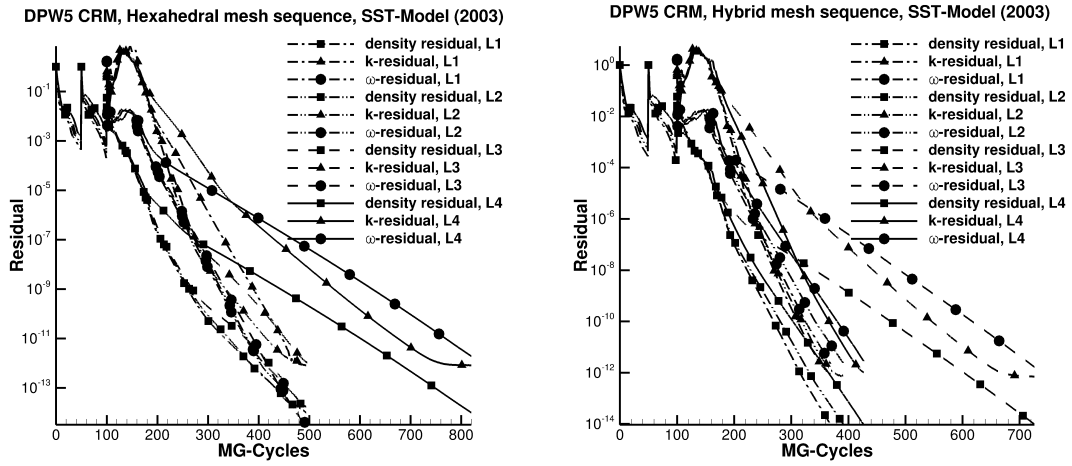


Figure 6.43: Convergence histories for DPW5 CRM and SST-model



# Chapter 7

## Conclusion and Discussion

### 7.1 Discussion of solution algorithm

Several years ago it was possible to successfully apply implicit solution algorithms to the Reynolds averaged Navier-Stokes equation in combination with a one-equation turbulence model of Spalart and Allmaras in the context of a 3D finite-volume code designed to deal with hybrid meshes. It turned out that a straightforward transfer of the ideas to two-equation turbulence models was impossible.

This observation goes hand in hand with an analysis of the literature published for two equation models. In the fewest cases even the authors publishing turbulence models show convergence histories nor are implementation details discussed. Though not explicitly stated in these publications, a lack of missing information gives cause for suspicion that application of suggested methodologies does not work so well as the presented results make it appear. In the Introduction in Section 1.2 we already gave a short discussion about several strategies one finds in implementations to deal with two-equation turbulence models. Such modifications directly yield to the question: How resilient are results computed with two-equation turbulence models and are they reproducible?

To deal with this question a necessary demand is to create an environment which has the potential to compute for a large number of different problems

- a) machine accurate solutions for given number of degrees of freedom,
- b) mesh converged results,

without a need to change from problem to problem the discretization strategy. In the words of the Introduction, a reliable solution algorithm is required.

To realize an algorithm for approximately solving the transport equations for two-equation turbulence models, from the perspective of this author, one key ingredient, if not the key ingredient, was to get rid off limitations of the turbulence variables  $k$

and  $\omega$ . A hard limitation of these values based on some fixed values has not led to a generally feasible approach. Instead, the approach discussed in Section 5.4 turned out to be crucial for the success. A further key element is the implicit treatment of the source terms. Here not all source terms could be considered, but only a selection. Unfortunately, within our framework it was also not possible to apply multigrid to two-equation turbulence models. This must be viewed as one critical issue, which needs to be addressed in future.

Compared to solution algorithms for the Spalart-Allmaras model of 2012, one needs to admit with big share disappointment, that the algorithmical reliability reached for this turbulence model could not be reached for two-equation models. Even more, the algorithmical reliability of the  $k\omega$ -model of 1988 is larger when compared with the SST-model. From all considered models implemented the SST-model is the one which makes the greatest challenges for reliable numerical simulations.

Having this thought in mind, and if one additionally considers the extra effort required for solving for two-equation transport models, naturally the following questions arise:

- With respect to accuracy, what is the gain one has when using two-equation turbulence models compared to the one-equation model of Spalart-Allmaras?
- Is the scientific and algorithmical work justified for making progress in this area?

## 7.2 Discussion of accuracy

With the establishment of solutions algorithms which have at least the potential to solve some basic flow cases, we have the obligation to validate the results computed and to compare with results from other models. It is content of this report to deal with this topic in two ways.

- a) Compare several of the models in an analytic way.
- b) Compare results of at least some (representative) test cases.

Already discussed above, to compare models based on possibly representative test cases gives, to the author's point of view, only limited insight. Even if differences can be observed and identified, these are then test case specific and a generalization of such findings is not possible. Moreover, experimental data has also error components and instead of a direct comparison statistical error bars should be included. Unfortunately we do not have such error components available. Moreover, a sustainable assessment of the models could only be performed if a complete uncertainty analysis is performed. That is, for both the errors and uncertainties in measurements as well as uncertainties in modeling parameters are available. Due

to the complexity of this question, this author's opinion is, that too less information and data is given to provide for a consistent uncertainty analysis. Hence, all conclusions made are uncertain and not sustainable. Being aware of this fact, we retreat ourselves to a discussion for the the data available.

In a first step we want to discuss if at least for the example presented in this report some assertions about accuracy can be made. For the RAE2822 test case Case1, which is subsonic, the results for the  $k\omega$ -model of 1988 and the SST-model are close. From the author's point of view this test case is not suitable to justify the additional effort for the SST-model.

The situation is more interesting for Case 9 and Case 10. Figure 6.8 is maybe the indicator to discuss the differences. For both Case 9 and Case 10, as a consequence of the application of the SST-model the predicted shock location moves upstream compared with the  $k\omega$ -model of 1988. For Case 9, where the  $k\omega$ -model of 1988 has good agreement with measurements, the SST-model impairs the predictions. On the other hand, for Case 10, where the  $k\omega$ -model predicts the shock position too far downstream, an application of the SST-model improves the predictions when compared with measurements. Retreat to this observation, an effect, which is desired for one given test case, is undesired for another test case. Hence, for these test cases even such superficial comparisons of numerical data does not allow for a clear statement. It can be assumed that the inclusion of an uncertainty analysis may blurres the overall view additionally.

Maybe, from our point of view even more interesting, is the low speed flow around the NACA 4412 airfoil. First of all note, our results show again two different trends. Figure 6.31 shows that the  $C_p$ -distribution is predicted slightly better for the SA-model and the  $k\omega$ -model of 1988. On the other hand, the velocity profiles are significantly better reproduced using the SST-model. Qualitatively speaking, the effect of using the SST-model is the prediction of a significantly larger separation at the trailing edge of the airfoil.

How careful one needs to be when one tries to conclude something from comparing computed results and measurements is emphasized in the following paragraph. In [24] one finds the following: "In the experiment the flow separated at approximately 85% of chord. Trip-strips were employed in the experiment on the suction and pressure surfaces at chord locations of  $x/c$  of 0.023 and 0.1, respectively." In the computations performed for this report no transition points were set and transitional effects were not investigated. This goes along with [18] (see p. 23): "Computations have been performed with and without a specified transition location and differences between computations are small. Results are given here for the case were transition was not specified, so that the models picked their own transition location."

Having all these differences in mind, and considering additionally that for the computations wind tunnel effects were totally neglected, it is actually highly ques-

tionable to compare experimental data with the computed values, at least without mentioning all the uncertainties going hand in hand with these comparisons. Hence, even though the SST-model results show improved velocity profiles, with respect to all these considerations this might be viewed to happen accidentally rather than to conclude an improved prediction.

To furthermore emphasize the difficulty of this test case, we quote from [9], 2018-12-17, where SST-results with two well-known NASA codes, CFL3D and FUN3D are shown: "Note that for this particular case the SST model does not converge readily to a steady-state result when using either of the two codes. However, the solutions are reasonable steady (quasi-steady) with only very small oscillations in drag coefficient." This quote emphasizes again the difficulty to obtain fully converged results for this test case when applied with the SST-model. Without having erased numerical errors a clear assessment of the effect of turbulence model is impossible.

Moreover, this honest remark from [9] also shows that even within well established codes implementing RANS equations and two-equation turbulence models, it is not straightforward to solve these equations, not even for such a basic 2D test case.

Hence, when considering all the error components together with their interaction one has to be very careful to conclude for the test cases presented an evaluation of the suggested models. Having this in mind, from the author's point of view, none of the presented models crystallizes as superior to the others, at least for the test cases considered in this report.

Such observation is possibly of no big surprise. Considering the analysis comparing differences in the models shown in Chapter 4 the overall observation is that differences in the models are small and the impact of these differences is hard to predict. Moreover, the models only interact with the mean flow equations using the eddy viscosity. This means, roughly speaking, that these models decrease locally the Reynolds number. Hence, compared to the laminar Navier-Stokes equations, locally the RANS equations weight the viscous terms higher. Such weighting must be so large, that the RANS equations allow for a steady state solution. Such weighting influences the solution of a system of nonlinear equations and this solution influences the solution of two additional nonlinear transport equations for turbulence. To predict this complex interaction of these two systems of nonlinear equations appears almost impossible, in particular considering that such prediction needs to work for a variety of problems, such that these problems allow for a steady state solution without blurring the main characteristics of the simulated flow of interest.

### 7.3 Boundary value problems

To this author's impression almost all turbulence models follow the strategy to include for turbulence effects in the equations only. This is interesting from the

point of view that a main driver for solutions are the boundary values. Roughly speaking, the prediction cannot become better than the boundary values enforced.

In Chapter 3 the classical boundary values for two-equation models were presented. Additionally, the assumptions were formulated to derive these boundary conditions. It is questionable and highly unlikely that the assumptions used to derive the boundary conditions are satisfied for any general situation. Just as an example, when one considers flows with adverse pressure gradient it may be inappropriate to assume constant pressure near a no-slip wall. Since, in particular, near the no-slip wall, that is inside the boundary layer, the solution will depend significantly on the boundary values, to this author's assumption, an improved prediction can only be obtained by considering problem appropriate boundary values.

It was shown and discussed that determination of boundary values for  $\omega$  for both no-slip wall and farfield determine the behavior at the boundaries for  $k$  significantly. Consequently, the behavior of eddy viscosity  $\mu_t$  in the boundary layer is determined to a large extent by the no-slip boundary condition for  $\omega$ . With respect to this knowledge it can be assumed that reformulation and manipulation of the equations for the turbulence models itself, will only have limited influence.

In this sense, an improvement of turbulence models might only be possible when significantly better understanding of the complete boundary value problem is available. Any model including an equation for dissipation rate  $\omega$  is restricted to the shortcomings which are inherent to this equation and its boundary values.

Furthermore, discussed in Section 3.6 there does not exist a mathematical sleight of hand to get rid off the singular behavior near the no-slip wall for  $\omega$ . Inclusion of a variable substitution gives rise to many more questions than answered. If in some implementations a variable substitution is possibly the only way to solve the system of RANS equations together with a two-equation model, then this may serve as a further indicator that these equations are in general not straightforward to use. As mentioned above, this should lead to the fundamental question if these models satisfy properties such that they can be used on routine basis in industrial processes. As long as questions, for example, about equivalence of the substituted equations, additional dissipative effects due to the substitution as well as additional unknown error components are not satisfactorily answered, to this author's opinion these substitutions should only be included into computer codes with utmost caution and spread with the warning there exist many unexplained theoretical questions. Instead, one may view the logarithmic reformulated equations as some new kind of model, totally neglecting the viewpoint that these reformulated models are or need to be equivalent to the original set of equations. Then, for these "new" models, one has to perform validation for a number of basic test cases to make sure, that these "new" models predict flows in the range of expectations.

Finally and conclusively, techniques presented in this report for solving the RANS equations in combination with two-equation  $k\omega$ -type turbulence models do not suf-

face the demands formulated in the Introduction of this report. From a perspective point of view it is not clear what methodologies and techniques need to be developed to reach such a goal. This gives rise to the question if it makes sense at the time to put further effort into this activity. And this statement is not restricted to two-equation  $k\omega$ -type models, but also for the one-equation model of Spalart and Allmaras the situation is not much better.

# Bibliography

- [1] S. R. ALLMARAS, F. T. JOHNSON, AND P. R. SPALART, *Modifications and Clarifications for the Implementation of the Spalart-Allmaras Turbulence Model*, in International Conference on Computational Fluid Dynamics 7, Hawaii, no. ICCFD7-1902 in Conference Proceeding Series, 2012.
- [2] B. BALDWIN AND H. LOMAX, *Thin layer approximation and algebraic model for separated turbulent flows*, AIAA Journal 78-257, (1978).
- [3] B. S. BALDWIN AND T. J. BARTH, *A one-equation turbulence transport model for high reynolds number wall-bounded flows*, NASA Technical Memorandum 102847, 1990.
- [4] F. BASSI, A. CRIVELLINI, S. REBAY, AND M. SAVINI, *Discontinuous Galerkin solution of the Reynolds-averaged NavierStokes and  $k - \omega$  turbulence model equations*, Computers & Fluids, 34 (2005), pp. 507 – 540. Residual Distribution Schemes, Discontinuous Galerkin Schemes and Adaptation.
- [5] J. BREDBERG, *On Two-equation Eddy-Viscosity Models*, Internal report, Department of Thermo and Fluid Dynamics, Chalmers University of Technology, Göteborg, Sweden, 2001.
- [6] D. COLES AND A. WADCOCK, *Flying-Hot-wire Study of Flow Past an NACA 4412 Airfoil at Maximum Lift*, AIAA Journal, 17 (1979), pp. 321 – 329.
- [7] E. HAIRER, S. P. NORSETT, AND G. WANNER, *Solving Ordinary Differential Equations II. Stiff and Differential-Algebraic Problems*, Springer, New York, 1992.
- [8] R. HARTMANN, J. HELD, AND T. LEICHT, *Adjoint-based error estimation and adaptive mesh refinement for the RANS and  $k-\omega$  turbulence model equations*, J. Comput. Phys., 230 (2011), pp. 4268–4284.
- [9] [HTTP://TURBMODELS.LARC.NASA.GOV](http://TURBMODELS.LARC.NASA.GOV), *Turbulence modeling resource website*, 2013.

- [10] F. ILINCA, J.-F. HETU, AND D. PELLETIER, *A unified finite element algorithm for two-equation models of turbulence*, Computers & Fluids, 27 (1998), pp. 291–310.
- [11] W. P. JONES AND B. E. LAUNDER, *The prediction of laminarization with a two-equation model of turbulence*, International Journal of Heat and Mass Transfer, 15 (1972), pp. 301–314.
- [12] G. KALITZIN, G. MEDIC, G. IACCARINO, AND P. DURBIN, *Near-wall Behavior of RANS Turbulence Models and Implications for Wall Functions*, Journal of Computational Physics, 204 (2005), pp. 265–291.
- [13] A. N. KOLMOGOROV, *The local structure of turbulence in incompressible viscous fluid for very large Reynolds numbers*, Dokl. Akad. Nauk., SSSR, 30 (1941), pp. 299–303.
- [14] ———, *Equations of turbulent motion in incompressible viscous fluids for very large Reynolds numbers*, Izvestia Academy of Sciences, USSR, 6 (1942), pp. 56–58.
- [15] N. KROLL, M. ABU-ZURAYK, D. DIMITROV, T. FRANZ, T. FÜHRER, T. GERHOLD, S. GÖRTZ, R. HEINRICH, C. ILIC, J. JEPSEN, J. JÄGERSKÜPPER, M. KRUSE, A. KRUMBEIN, S. LANGER, D. LIU, R. LIEPELT, L. REIMER, M. RITTER, A. SCHWÖPPE, J. SCHERER, F. SPIERING, R. THORMANN, V. TOGITI, D. VOLLMER, AND J.-H. WENDISCH, *DLR project Digital-X: towards virtual aircraft design and flight testing based on high-fidelity methods*, CEAS Aeronautical Journal, 7 (2016), pp. 3–27.
- [16] S. LANGER, *Hierarchy of Preconditioning Techniques for the solution of the Navier-Stokes equations discretized by 2nd order unstructured finite volume methods*, in ECCOMAS 2012 CONFERENCE, Conference Proceeding Series, Sept. 2012.
- [17] ———, *Preconditioned newton methods to approximate solutions of the reynolds averaged navier-stokes equations*, tech. rep., Institut für Aerodynamik und Strömungstechnik, June 2018.
- [18] F. R. MENTER, *Improved Two-Equation  $k-\omega$  Turbulence Models for Aerodynamic Flows*, tech. rep., NASA, 1992.
- [19] ———, *Influence of freestream values on  $k-\omega$  turbulence model predictions*, AIAA Journal, 30 (1992), pp. 1657–1659.
- [20] ———, *Zonal Two Equation  $k - \omega$  Turbulence Models for Aerodynamic Flows*, tech. rep., NASA, 1993.

- [21] —, *Two-Equation Eddy-Viscosity Turbulence Models for Engineering Applications*, Aiaa Journal, 32 (1994), pp. 1598–1605.
- [22] F. R. MENTER, M. KUNTZ, AND R. LANGTRY, *Ten years of industrial experience with the SST turbulence model*, Turbulence, Heat and Mass Transfer, 4 (2003).
- [23] W. RODI AND D. B. SPALDING, *A two-parameter model of turbulence, and its application to free jets*, Wärme und Stoffübertragung, 3 (1970), pp. 85–95.
- [24] S. P. ROGERS, N. L. WILTBERGER, AND D. KWAK, *Efficient simulation of incompressible viscous flow over single and multielement airfoils*, Journal of Aircraft, 30 (1993), pp. 736–743.
- [25] P. R. SPALART AND S. R. ALLMARAS, *A One-Equation Turbulence Model for Aerodynamic Flows*, in AIAA Computational Fluid Dynamics Conference, no. 1992-439 in Conference Proceeding Series, AIAA, 1992.
- [26] D. L. STEFANSKI, R. S. GLASBY, J. T. ERWIN, S. R. ALLMARAS, J. G. CODER, AND N. K. BURGESS, *A Modified  $k - \omega$  Turbulence Model for Finite-Element CFD*, in AIAA Computational Fluid Dynamics Conference, no. 2018-4041 in Conference Proceeding Series, AIAA, 2018.
- [27] U. TROTTENBERG, C. W. OOSTERLEE, AND A. SCHULLER, *Multigrid*, Academic Press, Inc., Orlando, FL, USA, 2001.
- [28] P. G. TUCKER, C. L. RUMSEY, P. R. SPALART, R. B. BARTELS, AND R. T. BIEDRON, *Computations of Wall Distances Based on Differential Equations*, AIAA Journal, 43 (2005), pp. 539–549.
- [29] J. C. VASSBERG, *A Unified Baseline Grid about the Common Research Model Wing-Body for the Fifth AIAA CFD Drag Prediction Workshop*, in Proc. 29th AIAA Applied Aerodynamics Conference, Honolulu, HI, June 2011, no. 2011-3508 in Conference Proceeding Series, AIAA, 2011.
- [30] D. C. WILCOX, *A half century historical review of the  $k - \omega$  model*.
- [31] —, *Reassessment of the Scale-Determining Equation for Advanced Turbulence Models*, AIAA Journal, 26 (1988), pp. 1299–1310.
- [32] —, *Turbulence Modeling for CFD*, DCW Industries, Incorporated, 1994.
- [33] —, *Turbulence Modeling for CFD (Third Edition) (Hardcover)*, DCW Industries, Incorporated, 11 2006.
- [34] —, *Formulation of the  $k-w$  turbulence model revisited*, AIAA Journal, 46 (2008), pp. 2823–2838.



**DLR-IB-AS-BS-2019-120**

**An initial investigation of solving RANS equations in  
combination with two-equation turbulence models**

**Stefan Langer**

Verteiler:

Institutsbibliothek	1 Exemplar
Verfasser	5 Exemplare
Institutsleitung	1 Exemplar
Abteilungsleiter	1 Exemplar
Deutsche Bibliothek in Frankfurt/Main	2 Exemplare
Niedersächsische Landesbibliothek Hannover	1 Exemplar
Techn. Informationsbibliothek Hannover	1 Exemplar
Zentralbibliothek BS	2 Exemplare
Zentralarchiv GÖ	1 Exemplar
Reserve	5 Exemplare